2017

# Estimate freeway travel time reliability under recurring and nonrecurring congestion

Chaoru Lu
*Iowa State University*

# Estimate freeway travel time reliability under recurring and nonrecurring congestion

by

**Chaoru Lu**

A dissertation submitted to the graduate faculty

in partial fulfillment of the requirements for the degree of

DOCTOR OF PHILOSOPHY

Major: Civil Engineering (Transportation Engineering)

Program of Study Committee:
Jing Dong, Major Professor
Anuj Sharma
Peter Savolainen
Alice Alipour
Sigurdur Olafsson

The student author, whose presentation of the scholarship herein was approved by the program of study committee, is solely responsible for the content of this dissertation. The Graduate College will ensure this dissertation is globally accessible and will not permit alterations after a degree is conferred.

Iowa State University
Ames, Iowa
2017

# DEDICATION

To my wife, my daughters and my parents who give me unconditional love.

# TABLE OF CONTENTS

Page

LIST OF FIGURES ..... v

LIST OF TABLES ..... vii

ACKNOWLEDGEMENTS ..... viii

ABSTRACT ..... ix

CHAPTER 1. INTRODUCTION ..... 1
1.1 Background ..... 1
1.2 Research Overview ..... 3
1.2.1 Research question 1: How to precisely estimate corridor-level travel time and its reliability? ..... 4
1.2.2 Research question 2: How to consider stochastic nature of driver behavior into the travel time reliability analysis? ..... 5
1.2.3 Research question 3: How to estimate work zone travel time reliability? ..... 7
1.3 Dissertation Structure ..... 8

CHAPTER 2. LITERATURE REVEW ..... 9
2.1 Estimation Methods of Travel Time and Its Reliability ..... 9
2.2 Effects of Stochastic Driver Behavior Parameter on Travel Time Reliability ..... 11
2.3 Impact of Work Zone on Travel Time Reliability ..... 13

CHAPTER 3. ESTIMATE FREEWAY CORRIDOR-LEVEL TRAVEL TIME AND ITS RELIABILITY ..... 17
3.1 Introduction ..... 17
3.2 Data Description ..... 18
3.2.1 Probe Vehicle Data ..... 18
3.2.2 Radar Sensor Data ..... 19
3.3 Methodology ..... 24
3.3.1 Spatial Correlation of Link Travel Times ..... 24
3.3.2 Travel Time Estimation ..... 25
3.3.3 Travel Time Distribution ..... 31
3.4 Results ..... 32
3.4.1 Travel Time Calculation ..... 33
3.4.2 Travel Time Distribution ..... 38
3.5 Summary ..... 46

CHAPTER 4. ESTIMATE TRAVEL TIME RELIABILITY MEASURES BY CONSIDERING THE STOCHASTIC NATURE OF DRIVER BEHAVIOR PARAMETERS ..... 47
4.1 Introduction ..... 47

4.2 Methodology ..... 48
4.2.1 Two-component travel time distribution ..... 48
4.2.2 Stochastic Headways and Standstill Distances ..... 53
4.2.3 Steady-State Car-Following Behavior ..... 55
4.2.4 Travel time reliability based on steady-state car-following models ..... 60
4.2.5 Travel time reliability based on VISSIM ..... 62
4.3 Results ..... 63
4.3.1 Time Headway and Standstill Distance Distribution ..... 63
4.3.2 Speed-Density Relationship ..... 69
4.3.3 Comparison of stochastic Pipes car-following model and VISSIM simulation ..... 73
4.3.4 Comparison of vehicle type-specific distribution input mode results and field data ..... 75
4.3.5 Travel time reliability ..... 77
4.4 Summary ..... 81

CHAPTER 5. TRAVEL TIME RELIABILITY IN URBAN FREEWAY WORK ZONES ..... 83
5.1 Introduction ..... 83
5.2 Data Description ..... 83
5.3 Methodology ..... 87
5.3.1 Work Zone Capacity ..... 88
5.3.2 Work Zone Travel Time and Its Reliability Estimation ..... 93
5.4 Result ..... 95
5.4.1 Speed-Volume-Density Relationship ..... 95
5.4.2 Performance Evaluation of Capacity Prediction Framework ..... 101
5.4.3 Work Zone Travel Time and Its Reliability Estimation ..... 107
5.5 Summary ..... 109

CHAPTER 6. CONCLUSIONS AND FUTURE RESEARCH ..... 111
6.1 Research Highlights ..... 111
6.1.1 Estimating Corridor-Level Travel Time Reliability Using Radar Sensor Data ..... 111
6.1.2 Incorporating Standstill Distance and Time Headway Distributions in Car Following Models to Estimate Travel Time Reliability ..... 112
6.1.3 Travel Time Reliability of Urban Freeway Work Zones ..... 112
6.2 Summary of Contributions ..... 113
6.3 Future Research ..... 114

REFERENCES ..... 116

APPENDIX A. DERIVATION OF FIRST AND SECOND CONDITION ..... 130

APPENDIX B. DERIVATION OF INFLECTION POINT EQUATION ..... 136

# LIST OF FIGURES

Figure 1.1 The Sources of Congestion National Summary (Cambridge Systematics and Texas Transportation Institute, 2005) ..... 2

Figure 3.1 Sensor Locations (source: ©2015 Google) ..... 20

Figure 3.2 Flow Chart for Handling Missing Data ..... 22

Figure 3.3 Availability of INRIX and Sensor Data ..... 23

Figure 3.4 Heat Map of Correlations between Links of the I-235 Corridor ..... 24

Figure 3.5 Node-link Representation ..... 25

Figure 3.6 Study Corridor and Sensor Locations (source: ©2015 Google) ..... 33

Figure 3.7 Comparison of Model-based Travel Time Index, Vanajakshi et al. (2009) Travel Time Index, Naïve-approach Based Travel Time Index and INRIX Travel Time Index ..... 36

Figure 3.8 Speed Contour of Sensors ..... 37

Figure 3.9 Probability Density Distributions of Peak 15-minute Travel Times ..... 42

Figure 3.10 Cumulative Density Distributions of Peak 15-minute Travel Times ..... 44

Figure 4.1 Two-component Travel Time Model ..... 50

Figure 4.2 Corridor-level Travel Time Reliability Measure Estimation Framework ..... 53

Figure 4.3 Histograms of vehicle type–specific and all vehicle–type time headways ..... 64

Figure 4.4 Histograms of vehicle type–specific and overall standstill distances ..... 67

Figure 4.5 Speed-Density Plots Generated Using Pipes Car-following Model ..... 71

Figure 4.6 Speed-Density Plots Generated Using INTEGRATION Car-following Model ..... 72

Figure 4.7 Simulated Speed-Density Plots Using VISSIM with Varying CC0 Parameters, Compared with Speed-Density Region Generated Using Stochastic Pipes Car-following Model ..... 74

Figure 4.8 Simulated Speed-Density Plots Using VISSIM with Varying CC1 Parameters, Compared with Speed-Density Region Generated Using Stochastic Pipes Car-following Model ..... 75

Figure 4.9 Field Data Compared with Speed-Density Region Generated Using Stochastic Pipes Car-Following Model ..... 76

Figure 4.10 Study Freeway Segment (Google 2017) ..... 77

Figure 5.1 Work Zone Layouts. ..... 85

Figure 5.2 Comparison of Typical Speed-volume Relationship of Non-work Zone and Work Zone. ..... 98

Figure 5.3 Comparison of Typical Speed-density Relationship of Non-work Zone and Work Zone. ..... 99

Figure 5.4 Diagnostic Plots of Speed-density Relationships of Typical Non-work Zone and Work Zone. ..... 101

Figure 5.5 Speed-volume Relationships Before and During Work Zone ..... 103

Figure 5.6 Speed-density Relationships Before and During Work Zone ..... 104

Figure 5.7 Diagnostic Plots of Speed-density Relationships Before-and During Work Zone .. 105

Figure 5.8 Comparison of Estimated Capacity and Existing Literatures ..... 107

Figure 5.9 Comparison of Model-based and INRIX Travel Time Index ..... 108

# LIST OF TABLES

Table 3.1 Outlier Identification Rules for Radar Sensor Data (Vanajakshi, 2005) ..... 21

Table 3.2 Plausible Function Forms of Travel Time Distribution ..... 32

Table 3.3 Performance Measures of Different Methods ..... 38

Table 3.4 Performance Measure of Different Data Aggregation Level ..... 39

Table 3.5 Model Selection Based on Log-likelihood ..... 40

Table 3.6 The Variance of Reliability Indices of INRIX Travel Time and SCTTE Model-based Travel Time ..... 45

Table 4.1 Plausible Function Forms of Time Headway and Standstill Distance Distributions ..... 55

Table 4.2 Summary Statistics of Time Headways ..... 65

Table 4.3 Log-likelihood Ratio Test Statistic of Headway Models ..... 65

Table 4.4 Estimated Parameters of Time Headway Distributions ..... 66

Table 4.5 Summary Statistics of Standstill Distances ..... 68

Table 4.6 Log-likelihood Ratio Test Statistic of Standstill Distance Models ..... 68

Table 4.7 Estimated Parameters for Standstill Distance Distributions ..... 69

Table 4.8 Traffic Volumes in Congested and Uncongested Conditions ..... 78

Table 4.9 Comparison of Travel Time Reliability Measures Calculated Using Different Methods ..... 81

Table 5.1 Summary of Work Zone Configurations ..... 86

Table 5.2 Parameters of Logistic Speed-Density Models ..... 95

Table 5.3 Capacities from Proposed Method, HCM, WorkZoneQ and Maximum 15-min Flow Rate ..... 106

Table 5.4 The Reliability Indices of INRIX Travel Time and HCM Model-based Travel Time ..... 109

# ACKNOWLEDGEMENTS

I would like to express my sincerest gratitude to my advisor, Dr. Jing Dong, for her encouragement, tremendous patience, support and guidance throughout my Ph.D. study. Her strong work ethics and commitment to excellence always inspire me to be a better researcher. Her enthusiastic encouragement and intelligent guidance have worked as a lighthouse during my tough times. Without Dr. Dong's guidance and support, I would have never been able to accomplish this dissertation. I would like to thank Dr. Anuj Sharma, Dr. Peter Savolainen, Dr. Alice Alipour and Dr. Sigurdur Olafsson for their supports and helps through this research. Their valuable comments and suggestions to my initial work directly contribute to the completion of my dissertation.

Fortunately, I am able to work with a great team during my study in Iowa State University. I particularly acknowledge Dr. Bo Wang for his help and guidance during the beginning of my doctoral study. Moreover, I am grateful to my colleague and friends, Luning Zhang, Liang Hu, Chenhui Liu, Tingting Huang, and Skylar Knickerbocker for providing helpful supports along the ways. My research would not have been possible without their helps.

Special thanks to Dr. Haibo Lü for his encouragement, guidance and inspiration through my life.

Finally, I would like to express my heartfelt gratitude to my families for their endless encourage, support, and unconditional love.

# ABSTRACT

Travel time and its reliability are considered as intuitive measure of service quality by transportation agencies. Moreover, highly reliable travel times allow for arriving at work or other destinations on time in the context of personal travel and facilitate just-in-time logistics services in freight operations. Travel times are the result of the traffic congestion. By considering different impact factors and shortcoming of the sensing technologies, this dissertation proposed methods for travel time and its reliability estimation.

First of all, this dissertation presented a method to estimate corridor-level travel times based on data collected from roadside radar sensors, considering spatially correlated traffic conditions. Link-level and corridor-level travel time distributions are estimated using these travel time estimates and compared with the ones estimated based on probe vehicle data. The maximum likelihood estimation is used to estimate the parameters of Weibull, gamma, normal, and lognormal distributions. According to the log likelihood values, lognormal distribution is the best fit among all the tested distributions. Corridor-level travel time reliability measures are extracted from the travel time distributions. The proposed travel time estimation model can well capture the temporal pattern of travel time and its distribution.

Second, a travel time reliability measure estimation method is proposed by incorporating standstill distance and time headway distributions in car-following models. The method is based on simplified two-component travel time distribution. By using Monte Carlo simulation, the speed-density region under congested condition and the travel time reliability measures can be generated. The results shows that the speed-density region derived from the steady-state Pipes model encloses most of the field data. Moreover, the proposed method estimate travel time reliability measures more precisely and faster, compared with using VISSIM simulation.

Finally, a work zone travel time estimation approach is proposed in this dissertation. First, the impact of work zone on capacity is investigated. For the work zone capacity prediction framework, the predicted upper bound of capacity is close to the maximum 15-min flow rate. Moreover, based on the predicted capacity, density at capacity and free flow speed, work zone travel times are estimated by using the modified segment speed estimation model from the study of Newman. The estimated travel times roughly followed the pattern of the INRIX travel times. Moreover, the travel time reliability indices are estimated directly from the estimated travel times. The result shows that the travel time reliability indices based on estimated travel times are close to the indices based on INRIX travel times.

# CHAPTER 1. INTRODUCTION

## 1.1 Background

Many metropolitan areas are facing traffic congestion problems due to the increasing of travel demand and the limited funding for road network expansion. Therefore, Intelligent Transportation System (ITS) technologies, such as Advanced Transportation Management Systems (ATMS) and Advanced Traveler Information Systems (ATIS), are widely deployed to improve the travel experience of individuals and the operational performance of existing transportation systems.

Travelers can benefit from the information provided by ATIS, such as travel time, to make better travel decision in terms of route, mode and departure time choices. Highly reliable travel times allow for arriving at work or other destinations on time in the context of personal travel and facilitate just-in-time logistics services in freight operations, while highly variable travel times indicate unpredictable trip times and low quality of transportation services (Turochy and Smith, 2002). Moreover, from transportation agencies' point of view, travel time and its reliability are considered as more intuitive measure of service quality, compared to the levels of service defined in the highway capacity manual (Chen et al., 2003). Travel time and its reliability can also be used for cost-benefit analysis of drivers and major road schemes (Peer et al., 2012; Mackie et al., 2001). The accuracy of travel time and its reliability information provided by ATIS affects both travelers' and transportation agencies' decisions. Therefore, engineers and researchers continually search for effective ways to provide robust and accurate method to estimation travel time and its reliability.

Travel times are the result of the traffic congestion. In order to estimate travel time reliability under recurring and nonrecurring congestion, it is important to understand the causes

affecting variability. Seven root causes of traffic congestion have been defined by Federal Highway Administration (FHWA). They are traffic incidents, work zones, weather, fluctuations in normal traffic, special events, traffic control devices and physical bottlenecks (Cambridge Systematics and Texas Transportation Institute, 2005). As shown in Figure 1.1, among the seven root causes, physical bottlenecks, which causes recurring congestion, contribute 40% of the travel delay on road network. Work zones, which cause nonrecurring congestion, contribute to 10% of the travel delay on road networks. Moreover, driver behavior, such as time headways, affects the capacity of freeways. And, the capacity of freeways has been widely considered as an important parameter in delay-volume function to estimate travel time. Consequently, by affecting the capacity of freeways, driver behavior affects the travel times of freeways. Therefore, by studying physical bottlenecks, work zone and driver behavior (e.g. time headways and standstill distances), travel time and its reliability on freeways can be well understood and estimated.

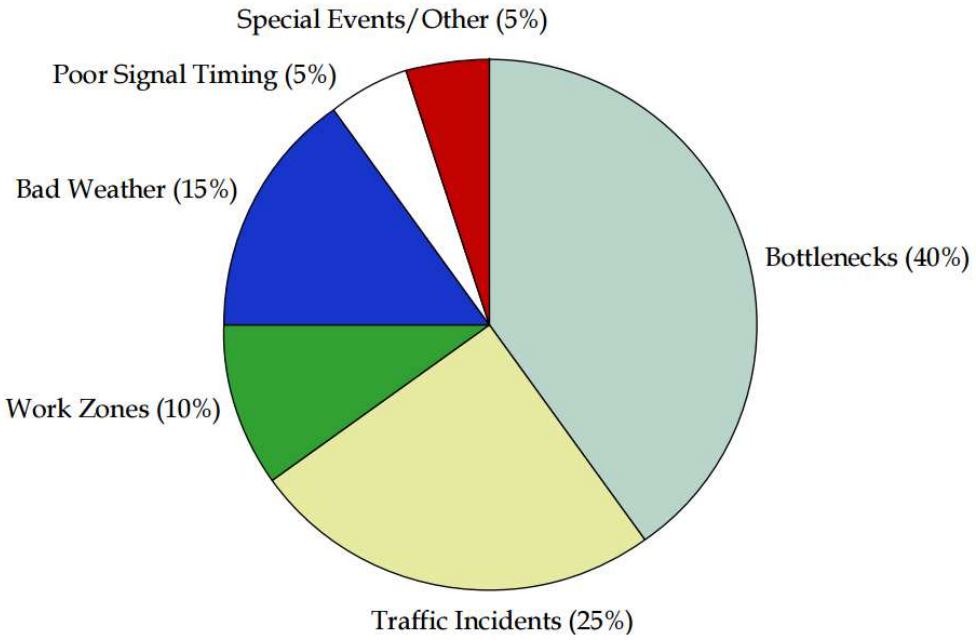


**Figure 1.1 The Sources of Congestion National Summary (Cambridge Systematics and Texas Transportation Institute, 2005)**

Travel time and its reliability can be collected or estimated based on various advanced technologies. Travel times can be estimated from traffic data (e.g. flow rate, speed and density) or collected directly. Several technologies, such as point detectors (e.g. Radar sensor and loop detector), probe vehicle technologies and license plate matching, are widely used to measure travel times. Different technology has different advantages and disadvantages. For example, the accuracy of probe vehicle technology is highly depend on the sample size and may cause concerns over citizen privacy. License plate matching is less practical for high-speed traffic or long road sections with low through traffic. Point-detectors only provide point speed, which is difficult to be used to estimate accurate travel time directly (Vanajakshi et al., 2009). As a result, it is desired to develop a proper method, which considers the shortcoming of the technology, to precisely estimate travel time and its reliability.

With the advances in sensing technologies for intelligent transportation systems, more information, such as road surface condition, event data and traffic data, can be extracted from different sources. This information makes it possible to estimate the travel time and its reliability under recurring and nonrecurring congestion.

The objective of this dissertation is to develop travel time and its reliability estimation methods, considering different impact factors and shortcoming of the sensing technologies. In particular, this research addresses the impact of physical bottlenecks, driver behavior (e.g. time headways and standstill distances) and work zone on travel time reliability.

## 1.2 Research Overview

This study aims at developing the estimation and prediction methods of travel time reliability on urban freeways. Data-driven and simulation-based methods are two major methods utilized to estimate travel time and its reliability. Moreover, travel time reliability of work zones

is investigated in this study. Three research questions are discussed in details in the following sections.

### 1.2.1 Research question 1: How to precisely estimate corridor-level travel time and its reliability?

Travel time reliability is considered as one of the key performance measures of road networks and corridors (Van Lint et al., 2008; Van Lint and Van Zuylen, 2005). Recently, travel time reliability attracted significant attention due to the influence of travel time variability on route, departure time, and mode choices. Operating agencies pay more attentions to monitor the reliability of transportation systems through various data sources (e.g. Wavetronix sensor and probe vehicle). Moreover, the impact of traffic incidents and bad weather on travel time is uncovered by collecting event and weather data. Consequently, the traveler information system can provide reliability-related information that enables travelers to meet their on-time arrival goals. Moreover, traffic network design problems have also incorporated travel time reliability as a factor (Chootinan et al., 2005; Sumalee et al., 2006)

Although extensive research has been done on travel time reliability, several challenges still need to be addressed. One of these challenges is how to address spatial and temporal correlations in estimating travel time and its reliability. Although travel times can be easily integrated across time (successive time frames constituting a trip) and space (adjacent links constituting a path), travel time distributions are generally non-additive because of the spatial and temporal correlations. In this study, spatial correlation is considered in travel time estimation model. Considering the correlation among multiple bottlenecks along a freeway corridor, the travel time along a stretch of freeway can be computed as the sum of a set of correlated link travel times.

Accordingly, the corridor-level travel time distributions, as well as various travel time reliability measures, can be estimated.

The first objective is to quantify segment- and corridor-level reliability measures on urban freeways. By analyzing urban freeway traffic data and probe vehicle data, a corridor-level travel-time reliability measure estimation model was developed. Because probe vehicles directly collect travel-time data, segment-level and corridor-level travel-time distributions can be easily estimated. In the absence of the direct measurement of travel times, point measurements of traffic conditions obtained from loop detectors or roadside sensors were used to estimate travel time and reliability measures along a stretch of urban freeway. In particular, the flow rates and speeds measured by roadside radar sensors on consecutive freeway segments were used to estimate segment travel-time distributions and correlation coefficients between segments. Accordingly, corridor-level travel-time reliability measures were developed.

### 1.2.2 Research question 2: How to consider stochastic nature of driver behavior into the travel time reliability analysis?

Driver behavior, in terms of following headways and standstill distance, affects the capacity of freeways (Cambridge Systematics and Texas Transportation Institute, 2005). These driver behavior parameters are widely applied in microscopic simulation software. To investigate the impact of the stochastic nature of driver behavior on travel time reliability, microscopic simulation models are used in this study. The core of microsimulation is the car-following model, which describes the interaction of a vehicle and the preceding vehicle traveling in the same lane. Standstill distances (i.e. the distance between stopped vehicles) and following time headways (i.e. the time between successive vehicles) are two of the important parameters in most car-following

models, such as Wiedemann 99 (in VISSIM), Van Aerde model (in INTEGRATION) and Pitt model (in FRESIM). Time headway and standstill distance are also associated with the aggression of the driver population. Some researchers pointed out that the distribution of time headway and standstill distance should be introduced in car-following models (Dijker et al., 1998; Houchin et al., 2015). However, the existing microsimulation models usually only allow time headway and standstill distance to be input as constants.

The car-following behavior calibration concerns with steady-state behavior and non-steady-state behavior (Rakha and Crowther, 2003). The calibration of steady-state behavior concerns with the capacity, speed and jam density. The non-steady-state behavior decides how vehicles move from one steady state to another and is beyond the scope of this study.

The second objective is to investigate macroscopic traffic flow properties of incorporating stochastic standstill distance and time headway parameters in various freeway car following models. In particular, car following models implemented in VISSIM, INTEGRATION and FRESIM under steady-state conditions are considered. Speed-density relationships are generated using four different input modes: deterministic overall headway and standstill distance, deterministic headways and standstill distances by vehicle lead-follow type, stochastic overall headway and standstill distance, and stochastic headway and standstill distance by vehicle lead-follow type. The speed-density relationships are compared with the VISSIM simulation output under various parameter assumptions and with real world observations.

The third objective is to develop a method to estimate corridor-level travel time reliability measures by incorporating stochastic standstill distance and time headway parameters in FRESIM car-following models. The reliability measures are compared with the VISSIM simulation output and field data.

### 1.2.3 Research question 3: How to estimate work zone travel time reliability?

Work zones on freeways usually cause serious disruptions to traffic, significant delays and traffic safety issues. To mitigate the impact and plan proper strategies, forecasting the work zone capacity on an existing freeway is important. Moreover, Edwards and Fontaine (2012) pointed out that travel time reliability in work zone is difficult to quantify and extremely useful to evaluate a work zone's impact. Therefore, it is necessary to develop a method to estimate work zone travel time and its reliability.

Numerous statistical and simulation based methods have been proposed to estimate work zone capacity(Al-Kaisy and Hall, 2003; Heaslip et al., 2008; Kim et al., 2000; Krammes and Lopez, 1994; Racha et al., 2008; Sarasua et al., 2006; Weng and Meng, 2015, 2011). However, although speed, volume and density relationship has been widely used to estimate the capacity of freeways (Modi et al., 2014), only a few work zone capacity estimation methods were derived from speed-volume relationships (Racha et al., 2008; Sarasua et al., 2006; Weng and Meng, 2015).

Moreover, several models, such as Davidson (1978), Akçelik (1991) and Conical (Spiess, 1990) function, have been proposed to estimated travel time. Newman (1986) proposed a travel time estimation method considering the impact factors on freeway capacity, density at capacity and free flow speed. Moses et al. (2013) pointed out the accuracy of these models is heavily dependent on accurately specifying free-flow speed and capacity, which can be derived from speed-density-volume relationship.

In order to estimate work zone travel time and its reliability, developing a speed-density-volume relationship estimation method is the fourth objective. Consequently, work zone travel time and its reliability can be estimated based on the estimated speed-density-volume relationship. Moreover, based on the speed-density model, a framework to predict capacity of work zone is

proposed. The capacity prediction model captures the relationship between capacity and work zone characteristics by considering the impact of work zone on free-flow speed.

## 1.3 Dissertation Structure

This dissertation is organized as follows. Chapter 2 provides a comprehensive literature review on travel time and its reliability estimation methods, stochastic nature of driver behavior and work zone capacity estimation methods. Chapter 3 discusses the methodology of estimating freeway travel time and it reliability using radar sensor data. Chapter 4 presents a modeling approach to generate travel time reliability measures by incorporating stochastic standstill distance and time headway parameters in car-following model. Chapter 5 proposed a capacity prediction method and a travel time reliability estimation method of work zones. Conclusions are presented in Chapter 6.

# CHAPTER 2. LITERATURE REVEW

This chapter presents literature review of conceptual, theoretical and methodological topics related to each research question. In Section 2.1, travel time and its reliability estimation models are reviewed. Section 2.2 represents a comprehensive review of headway distribution, car following models and microscopic traffic simulation models considering randomly-distributed parameters. The work zone capacity estimation and prediction method are reviewed in section 2.3.

## 2.1 Estimation Methods of Travel Time and Its Reliability

With the advances in sensing technology, a number of travel time estimation methods have been proposed based on data collected from various sources (e.g., Soriguera and Robuste, 2011; Tam and Lam, 2008). Reviews of the research efforts on travel time estimation and prediction methods can be found in Mori et al. (2015) and Vlahogianni et al. (2014). In particular, loop detectors have been widely used to measure traffic conditions at specific locations. Link travel times can be estimated by simply extending the point speed measurements to the entire link (Soriguera and Robusté, 2011; van Lint and van der Zijpp, 2003). Moreover, to capture the traffic dynamics along the link, several methods have been proposed to estimate travel time based on traffic flow theories (Aksoy and Celikoglu, 2012; Coifman, 2002; Deniz et al., 2013; Van Arem et al., 1997; Zhang, 2006). Dailey (1991) presented a simple continuous traffic flow model to estimate delay time between two loop detectors. Moreover, the model allow to estimate the travel time between two loop detectors. Coifman (2002) proposed a link travel time estimation method, which exploits basic traffic flow theory to extrapolate local conditions to an extend link. Recently, Yang et al. (2016) developed a travel time estimation method based on General Motors car-following model. Some travel time estimation methods are based on flow conservation and

propagation principles (e.g., Celikoglu, 2013a, 2013b, 2007). Moreover, a number of queuing-based travel time models have been developed in the literature (e.g., Daganzo, 1995; Lei et al., 2015; Nie and Zhang, 2005). These queuing-based models used a vertical queue or point-queue to describe traffic dynamics at bottlenecks. The point-queue models assume that the length of the queue is zero and the link has unlimited storage capacity. As a result, point-queue–based models usually ignore the spillback from a downstream bottleneck.

In addition, various approaches have been developed to estimate travel time reliability (e.g., Kwon et al., 2011; Oh and Chung, 2006; Richardson, 2003). One way to examine travel time variation is to look at the distribution of travel times. Different functional forms have been used to describe link travel time distributions. Van Lint and Van Zuylen (2005) and Susilawati et al. (2010) pointed out that travel time distributions were skewed and had a long right tail. Based on travel time data collected using the automatic vehicle identification system, Li et al. (2006) suggested that a lognormal distribution best characterized the distribution of travel time when a large time window (e.g., in excess of 1 hour) was under consideration and in the presence of congestion, and a normal distribution was more appropriate for departure time windows on the order of minutes. After using Weibull, exponential, lognormal, and normal distributions to fit the travel time data collected from dual-loop detectors, Emam and AI-Deek (2006) suggested that lognormal distribution was the best fit. Furthermore, Isukapati et al. (2013) pointed out that corridor-level travel time distribution can be constructed on the basis of segment-level travel times. Corridor-level travel time can be easily calculated by integrating segment-level travel times across time and space. However, it is hard to synthesize corridor-level travel time distribution from segment-level travel time distributions by considering spatial-temporal correlation.(Caceres et al., 2016; Rahmani et al., 2013). Considering the correlation among multiple bottlenecks along a freeway

corridor, the travel time along a stretch of freeway can be computed as the sum of a set of correlated link travel times (Lei et al., 2015). Accordingly, the corridor-level travel time distributions, as well as various travel time reliability measures, can be estimated.

In order to quantify the travel time reliability, several performance measures are proposed (Van Lint et al., 2008). Among these reliability measures, buffer time, 95th percentile travel times, buffer index and planning time index are easily understand and have technical merit. Therefore, these travel time reliability measures are recommended by Federal Highway Administration (FHWA) (Texas Transportation Institute and Cambridge System Inc., 2006). These measures are widely applied in research for travel time reliability analysis of freeway. Higatani et al. (2009) investigated the impact of traffic incidents on freeway travel time reliability measures, such as buffer time, 95th percentile travel times, buffer index and planning time index. Moreover, these reliability measures to investigate the impact of work zone and ramp metering on freeway travel time reliability (Bhouri et al., 2013; Edwards and Fontaine, 2012).

In summary, existing travel time estimation methods generally ignored the spatial correlation between links with the exception of the study conduct by Chan et al. (2009). To address this methodology gap, a travel time estimation model, which considers the spatially correlated traffic conditions, is proposed.

## 2.2 Effects of Stochastic Driver Behavior Parameter on Travel Time Reliability

The stochastic nature of operational capacity resulted from the variation of microscopic driving behaviors (Wu et al., 2010). Brilon et al. (2005) pointed out that the distribution of capacity directly indicates the traffic flow reliability of the freeway. Meanwhile, traffic flow reliability and travel time reliability are highly correlated (Dong and Mahmassani, 2009). Consequently, microscopic driving behavior impacts travel time reliability.

The following time headways and standstill distances vary from vehicle to vehicle and by vehicle types (Hoogendoorn and Bovy, 1998; Houchin et al., 2015; Ye and Zhang, 2009; Durrani et al., 2016). Various probability distributions, such as gamma, normal, lognormal and Weibull, have been used to describe heterogeneity in time headway data (Zang, 2009; Zhang et al., 2007). In particular, Ye and Zhang (2009) analyzed the headways by four different lead-following vehicle types—car–truck, truck–car, truck–truck, and car–car, and found that vehicle type–specific and mixed vehicle–type distributions are statistically different. Standstill distance distributions, on the other hand, have not been well studied, probably due to the difficulty in data collection. In this research, both time headway and standstill distance data are collected and used to fit corresponding probability distributions.

Various car-following models have been developed over the past decades, including Gazis-Herman-Rothery (GHR) models, safety distance models, linear models, psycho-physical models, and fuzzy logic based models (Brackstone and McDonald, 1999). Among these models, some have been implemented in commercial microscopic traffic simulation software, such as VISSIM and CORSIM. To the best of the authors' knowledge, none of the existing microscopic traffic simulation software allows to input headway and standstill distance parameters as distributions. Nevertheless, randomly-distributed drivers' behavioral parameters have been considered in car-following models. For example, based on the data obtained by video-taping traffic, Ahn et al. (2004) verified that the variation of drivers' behavioral parameters in Newell's car-following, that is, time displacement and space displacement, were well described by a bivariate normal joint distribution. Later, to assure the driver's behavioral parameters are positive. Dong and Mahmassani (2012) used a left-truncated bivariate normal distribution in a modeling approach that

combine Newell's car-following model with a stochastic macroscopic model of flow breakdown to predict travel time reliability.

In summary, existing microscopic simulation software do not allow to input the time headways and standstill distances as distribution. Moreover, the impact of vehicle type–specific time headway and standstill distance distributions on travel time reliability has not been investigated. Consequently, the importance of the stochastic time headway and standstill distance for microscopic simulation is investigated in Chapter 4. Moreover, the stochastic standstill and time headway are incorporated into car-following model to estimate corridor-level travel time reliability on freeway.

## 2.3 Impact of Work Zone on Travel Time Reliability

The travel time reliability of work zones has been estimated using probe vehicle data (Edwards and Fontaine, 2012; Haseman et al., 2010). However, the probe vehicle data may not be available in some place. Therefore, point measurements of traffic conditions obtained from loop detectors or roadside sensors are used to estimate travel time and reliability measures. From point measurements, the capacity, which is one of the main factors influencing travel time reliability, can be easily derived. Generally, capacity significantly decreases with the presence of a work zone. Newman (1986) proposed a segment speed estimation method based on free-flow speed and capacity. By introducing the capacity adjustment factor and free-flow speed adjustment factor, the model is revised to consider the capacity and free-flow speed reduction due to weather condition and incident. Recently, Highway Capacity Manual (2016) proposed a method to estimate work zone free-flow speed. Therefore, how to precisely estimate work zone capacity becomes a very important question for work zone travel time estimation.

Work zone capacity estimation approaches can be categorized into three groups: parametric, non-parametric and simulation based approaches (Weng and Meng, 2013). Non-parametric approaches, such as neural-fuzzy logic, decision tree and ensemble tree model, usually need a large historic traffic dataset to provide reliable prediction (Adeli and Jiang, 2003; Weng and Meng, 2012, 2011). Simulation based approaches have been widely applied to estimate the capacity of freeway work zones with different network and lane closure configurations (Chatterjee et al., 2010; Heaslip et al., 2010). The microscopic simulation models need to be calibrated to local conditions, which is usually a very sophisticated procedure. Parametric approaches use predetermined coefficients of the predictors, calibrated based on the data collected from the work zone site to estimate work zone capacity. For example, Krammes and Lopez (1994) and Kim et al., (2000) developed multi-regression models to estimate short-term work zone capacity. Al-Kaisy and Hall (2003) and Al-kaisy et al. (2000) investigated the variables, such as grade, the day of week and weather condition, and provided a generic multiplicative model to estimate the long-term work zone capacity based on the traffic data collected from Ontario, Canada. These approaches measured the capacity of work zone as the queue discharge flow rate or maximum flow rate. However, Benekohal et al. (2004) pointed out that neither queue discharge rate nor the maximum flow rate provided accurate measurement of work zone capacity.

Consequently, speed-volume-density relationship is an alternative way to derive work zone capacity. Numerous models have been developed to describe the speed-volume-density relationship, including single-regime and multi-regime models. Two parameter single-regime models, such as Greenshields model and Newell's model, usually cannot fit traffic data under congested and non-congested conditions at the same time (Greenshields, 1934; Newell, 1961). Multi-regime models, such as Edie model, modified Greenberg model and the cluster analysis

based model, use two or more curves to model different traffic flow regimes separately (Drake et al., 1967; Edie, 1961; Sun and Zhou, 2005). The major challenge of applying multi-regime model is to determine breakpoints in a scientific way (Wang et al., 2011). In order to overcome these limitations, MacNicholas (2011) proposed a five-parameter logistic speed-density model, which can fit traffic data under the congested and uncongested regimes well.

By applying the speed-volume-density relationship, several work zone capacity estimation methods were developed. Sarasua et al. (2006) derived the speed-flow curve for different lane closure types and included the base capacity as a variable in the model, which depends on lane closure configuration. Racha et al. (2008) used parabolic flow function and hyperbolic speed function to estimate work zone capacity. Most recently, Weng and Meng (2015) proposed a speed-flow and capacity model that incorporated work zone configuration factors. Their model is based on a two-regime speed-flow model. The threshold separating the two regimes is pre-determined.

Moreover, factors other than work zone, such as rainfall intensity and driver behavior, have been shown to have significant effect on the speed-volume-density relationship as well (Kockelman, 1998). Lam et al. (2013) modeled the effects of rainfall intensity on traffic speed-volume-density relationship using the Drake Model, which is a signal-regime speed-density model with four parameters. Their model explained the relationship between volume and rainfall intensity by incorporating the free-flow speed in a function of rainfall intensity, in Drake Model. The results shows that capacity on urban roads decrease as rainfall intensity increases. Similar to rainfall intensity, work zones tend to cause reduced free-flow speed and capacity. In order to model the effects of work zone on traffic speed-volume-density relationship, the free-flow speed in a function of work zone characteristics is incorporated in a five-parameter logistic speed-density model. Accordingly, a work zone capacity estimation method is developed in this study.

In practice, spreadsheet-based traffic analysis is widely used to analyze the impact of work zones. Based on a survey on state department of transportations (DOTs), HCS, QuickZone and QUEWZ are the commonly used software packages to estimate work zone capacity (Benekohal et al., 2003).

In summary, the impact of work zone on capacity has not been investigated based on speed-density model. Consequently, a capacity estimation and prediction method is proposed based on the relationship between free-flow speed and work zone characteristics and the speed-density model. Moreover, the existing work zone travel time estimation method are based on probe vehicle data. Since the probe vehicle data may not always available, a travel time estimation method based on radar sensor data is proposed by considering the impact of work zone on speed-density-volume relationship.

# CHAPTER 3. ESTIMATE FREEWAY CORRIDOR-LEVEL TRAVEL TIME AND ITS RELIABILITY

This chapter presents a method to estimate travel times based on data collected from roadside sensors, considering spatially correlated traffic conditions. This chapter is organized as follows. Section 3.1 introduces the background of the study. Section 3.2 describes the probe vehicle data and radar sensor data. The travel time and its reliability estimation method is described in section 3.3. The discussion of the model results and summary of the findings are presented in Section 3.4 and Section 3.5, respectively.

## 3.1 Introduction

Travel time and its reliability are intuitive system performance measures for freeway traffic operations. Thus, providing travelers with accurate travel time and reliability information has gained paramount importance. In particular, travelers are interested in origin-destination travel time reliability for better planning of their trips.

Travel times can be measured directly from probe vehicles and Automatic Vehicle Identification (AVI). However, these techniques are usually either very expensive or require high rate of public participation (Turner, 1996). Alternatively, travel time can be estimated from roadside sensors or loop detectors. Most metropolitan areas in the United States have such sensors installed on their freeway systems, providing a reliable source of traffic data over a wide region. Therefore, estimating travel time based on roadside or in-pavement sensor is cost effective and can be widely applied. Since the roadside radar sensor and loop detector provide point measurements, it is hard to accurately estimate the link-level travel time, which depends on the space mean speed.

As mentioned in the literature review, some researchers used vertical-queuing-based travel time models to circumvent this issue (e.g., Lei et al., 2015; Nie and Zhang, 2005). However, point-queue–based models ignore the spillback from a downstream bottleneck. In this study, link- and corridor-level travel times are estimated based on data collected from roadside radar sensors, considering spatially correlated traffic conditions to deal with the spillback from a downstream bottleneck.

Travel time variability comes from various sources, which can be categorized into three categorized: regular condition-dependent variations (e.g. day-to-day variation), irregular condition-dependent variations (e.g. incidents), and random variations (Wong and Sussman, 1973). For irregular variations, such as incidents, it is hard to predict their occurrence location and time. Therefore, it is hard to predict traveler from it by adjust their departure time. Alternatively, with known regular condition-dependent variations, travelers may be able to adjust their departure time or route to arrive on time at their destinations.

## 3.2 Data Description

Two independent data sources are used in this study to examine travel time and its reliability at the link and corridor levels—probe vehicle data and radar sensor data. The speed and volume data collected by radar sensors at fixed locations are used to estimate travel time and its distribution. The probe vehicle travel time data are used as the ground truth to verify the accuracy of travel times estimated from roadside sensor data.

### 3.2.1 Probe Vehicle Data

The probe vehicle travel time data used in this study is provided by INRIX, a commercial company that collects real-time traffic data from in-vehicle transponders on commercial vehicles

and cell phones in passenger cars. In the Des Moines metropolitan area INRIX probe vehicle network covers all of the highway and arterial networks. In this study, the probe vehicle travel time data are queried from Regional Integrated Transportation Information System (RITIS), which archives INRIX probe vehicle data at 1-minute aggregation intervals. This dataset provides time-stamped segment-based speeds, travel times, historical average speed, free flow speed, and confidence scores. As stated in the INRIX Interface Guide (2014), the record represents real-time data only when the confidence score equals 30; otherwise the value is estimated from historical data. Consequently, the travel times used in this study are those with the confidence score of 30.

As the INRIX travel times are provided segment by segment, a temporally stitched algorithm (Chase et al., 2012) is adopted to generate probe vehicles at 1-minute time intervals. The temporally stitched algorithm is intended to simulate the experienced travel time of a probe vehicle traveling along the corridor. In this study, the probe vehicle travel times are used as the ground truth.

### 3.2.2 Radar Sensor Data

The Iowa Department of Transportation (DOT) has been placing Wavetronix radar sensors along interstates and major highways in the state. The majority of sensors are in the metropolitan areas and provide valuable information for the DOT in terms of incident management, traffic operations, and planning. The existing Iowa DOT Wavetronix sensors cover the highway network in the Des Moines metropolitan area. These sensors count vehicles, by lane and classification, and register vehicle speeds. The aggregated data were obtained through an online data portal maintained by TransSuite. The data can be aggregated at different time intervals—20 seconds; 5, 15, 30, 60 minutes; and 24 hours. In order to be consistent with the travel time data generated from

INRIX, the 20-second data are aggregated into 1-minute data and used to estimate travel times. The aggregated data obtained from TransSuite include volume, speed, and occupancy, by lane. The volume is broken down by vehicle class.

On-ramps and off-ramps are potential bottlenecks on freeways (Bertini and Malik, 2004; Liu and Danczyk, 2009; Newell, 1999). As a result, roadway sensors are usually placed close to ramps, as illustrated in Figure 3.1. In such cases, both the ramp flow and the mainline flow can be monitored using one side-fired radar sensor, as well as the point speeds.

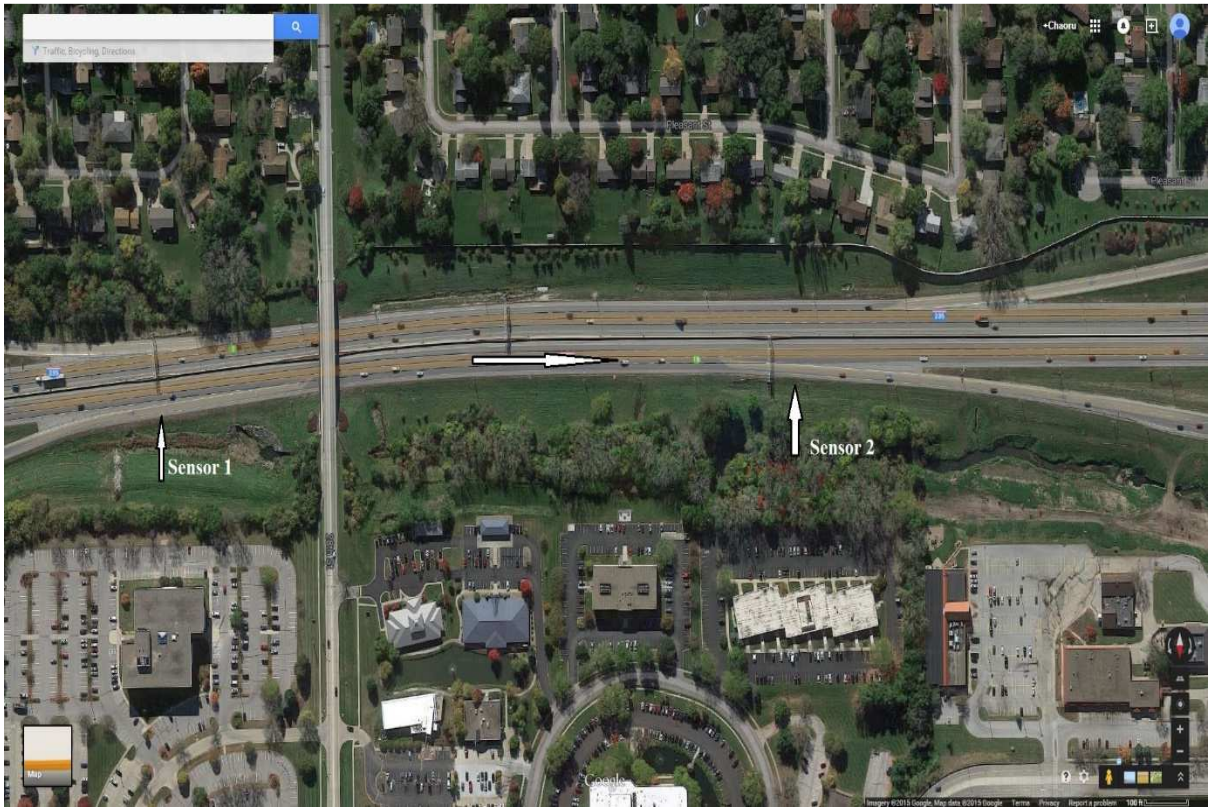


**Figure 3.1 Sensor Locations (source: ©2015 Google)**

The radar sensors sometimes report extreme values due to malfunction. Such abnormal data are identified and removed using the rules proposed by Vanajakshi (2005), as detailed in Table 3.1.

**Table 3.1 Outlier Identification Rules for Radar Sensor Data** (Vanajakshi, 2005)

| Individual Rules | |
|---|---|
| 1) q > 50 | Error |
| 2) v > 100 | Error |
| 3) o > 90 | Error |
| **Combination Rules** | |
| 4) v = 0, q = 0, o > 0 | Error |
| 5) v = 0, q > 0, o > 0 | Error |
| 6) v = 0, q > 0, o = 0 | Error |
| 7) v > 0, q = 0, o = 0 | Error |
| 8) v > 0, q = 0, o > 0 | Error |
| 9) v > 0, q > 0, o = 0 | Error |
| 10) v = 0 - 100, q = 0 - 50, o = 0 - 90 | Accept |

q = volume in vehicles per minute per lane; v = speed in mph; and o = occupancy in percent.

Since the proposed travel time estimation method uses volume and speed data during each time interval, the missing data are handled by the procedure shown in Figure 3.2. Basically, if a significant amount of data is missing on a certain day, that day is removed from the analysis. If data are missing only for a short time period, the data are imputed based on the data collected during the same time period on other day, which has the most similar pattern of the density time series as the target day.

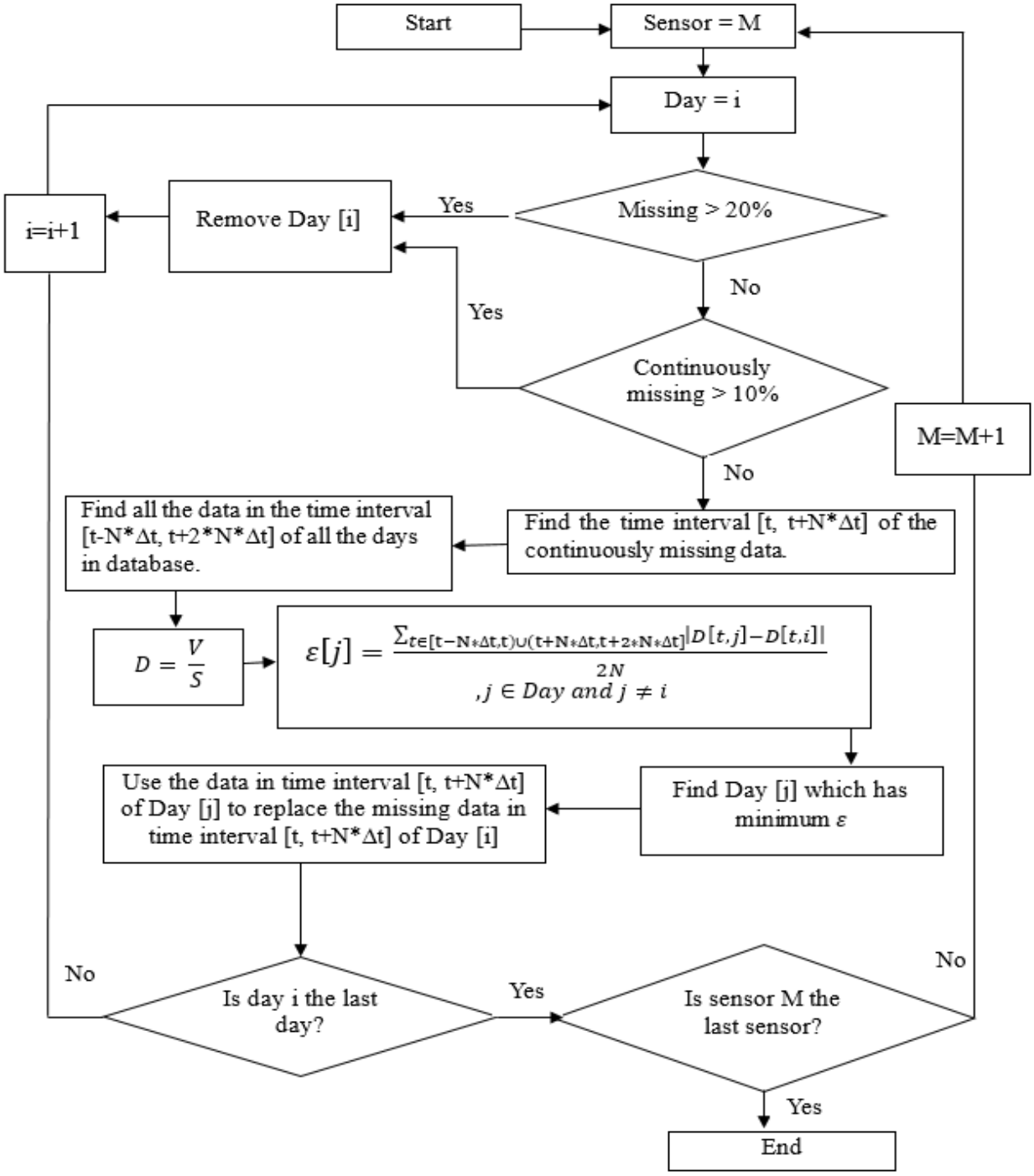


Notation: N is the number of missing values in this interval;
Δt is the data aggregation level;
D is density;
V is volume; and S is speed.

**Figure 3.2 Flow Chart for Handling Missing Data**

The 1-minute interval data from 7:00 a.m. to 9:30 a.m. on weekdays from December 1, 2013, to December 1, 2014, are used in this study. After the outliers are removed and the selected missing data are replaced, the availability of radar sensor data and real-time INRIX data is shown in Figure 3.3. To validate the proposed model against INRIX travel times, data need to be available from both sources. The plot between the black lines indicates the data in April 2014, when both the INRIX and sensor data are available on most days for all links. The inconsistency in missing data of INRIX and sensor data can cause the difference between model-based travel time and INRIX travel time reliability indices.

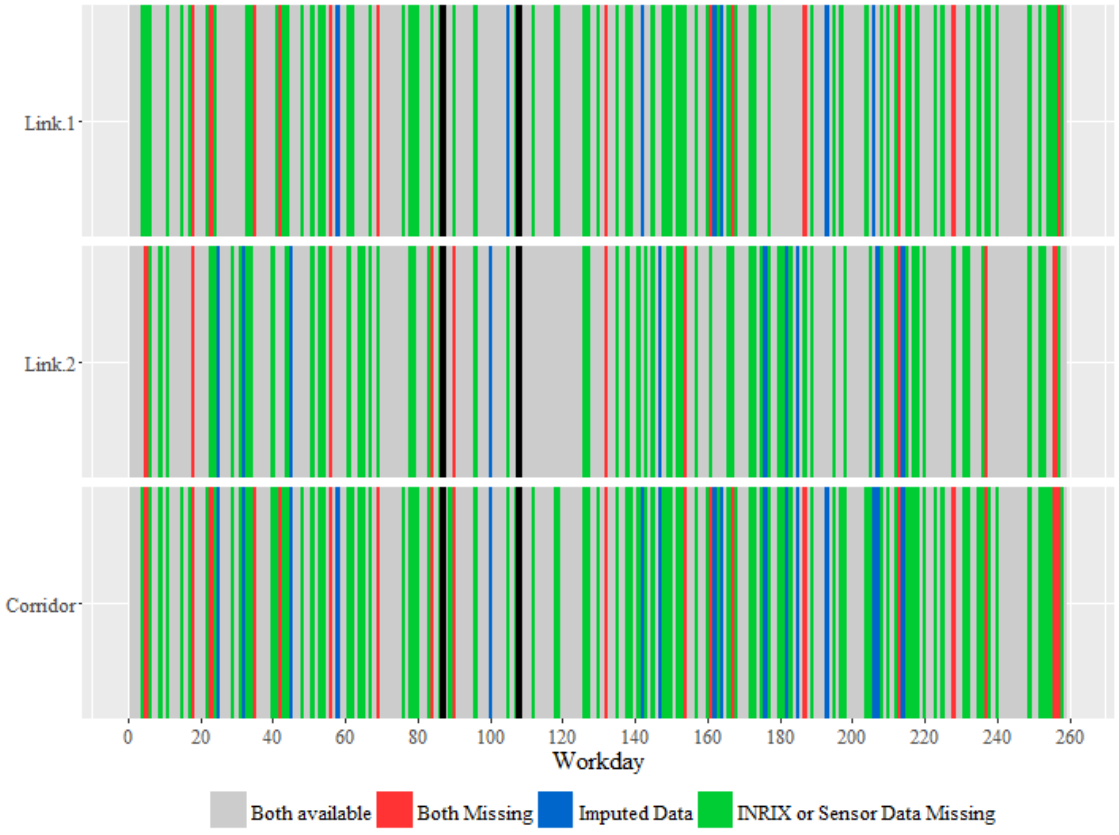


**Figure 3.3 Availability of INRIX and Sensor Data**

## 3.3 Methodology

### 3.3.1 Spatial Correlation of Link Travel Times

In order to examine the spatial correlation of travel times, the correlation coefficient is computed to represent the relation between link travel times. Eq. 3.1 describes the cross-correlation between travel times of different links:

$$\rho_{x,y} = \frac{\sum_{i=1}^{n}(x_i-\mu_x)(y_i-\mu_y)}{\sigma_x\sigma_y} \quad (3.1)$$

where,

$x_i$ and $y_i$ are the travel times of two different links;

$\mu_x$ and $\mu_y$ are the mean of $x_i$ and $y_i$, respectively;

$\sigma_x$ and $\sigma_y$ are the standard deviation of $x_i$ and $y_i$, respectively; and

n is number of observations.

Historic travel time data collected during work days in 2014 on I-235 in Des Moines are used to establish correlation between links. A heat map of correlations between the links of the I-235 corridor (consisting of 19 segments) is shown in Figure 3.4.

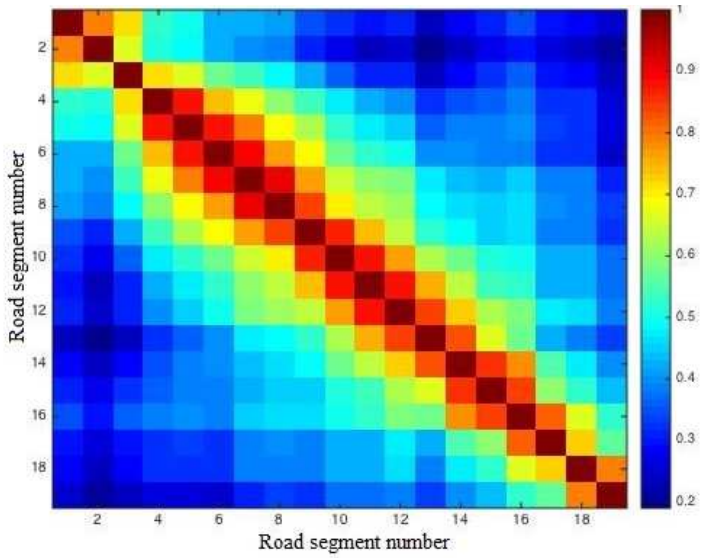


**Figure 3.4 Heat Map of Correlations between Links of the I-235 Corridor**

Significant correlations among link travel times indicate that the links along the corridor should not be considered as independent when examining corridor level travel time reliability. As expected, the correlations between a link and its adjacent upstream or downstream links are generally higher than the correlations between two links that are far apart. This finding is consistent with previous studies (e.g. Park and Rilett 1999, Zou et al. 2014). For example, Zou et al. (2014) also pointed out that a decreasing trend of cross-correlation value between two links can be observed as the distance between two links increases.

### 3.3.2 Travel Time Estimation

Consider a corridor with N potential bottlenecks. Assume that each bottleneck (i.e., sensor location) is a node and the road segment between these nodes is represented by a link with homogeneous capacity. Denote node 1 as the start point and node N as the last node. The segment between node M and node M+1 is denoted as link M. Figure 3.5 illustrates the node-link representation for part of the corridor, from node M to node M+3. An on-ramp or off-ramp might be connected to a node. The on-ramp or off-ramp is denoted as "ramp of M". For example, in Figure 3.5 the on-ramp that is connected to node M+1 is denoted as "ramp of M+1."

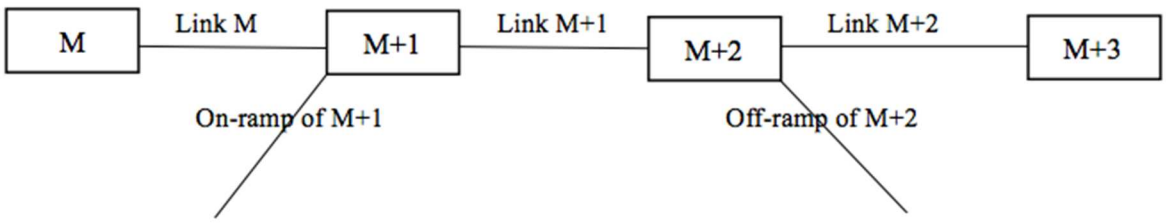


**Figure 3.5 Node-link Representation**

In order to construct a numerically tractable model for computing corridor-level travel time, the first-in, first-out property is assumed to ensure that any vehicles that enter the link first would leave the link first (Lei et al., 2015). In addition, traffic breakdowns can be detected when speed drops significantly (say, 10 mph) and the low speed sustains for a long period (e.g., 15 minutes) (Dong and Mahmassani, 2009). Considering the spatial correlation between links, three possible conditions might occur when estimating travel time of link M. Under each condition, a travel time calculation method is proposed.

The first condition is when no breakdown occurs on link M and link M+1.The travel time of link M at time t can be estimated based on the length of link and the average of speeds measured at two ends of the link, as follows.

$$T_{c1}[M,t] = \frac{2*D[M]}{S[M,t]+S[M+1,t]} \tag{3.2}$$

where,

D[M] is length of link M; and

S[M] and S[M+1] are speeds measured at node M and M+1 at time t, respectively.

The second condition is when the breakdown occurs at bottleneck M+1, causing congestion on link M. The travel time of link M at time t is calculated as follows. Assuming vehicles in the platoon are traveling at the same speed, the spacing between two vehicles in the platoon on link M can be calculated as

$$Space[M,t] = d_0 + S[M+1,t] * \tau \tag{3.3}$$

where,

$d_0$ is the initial space between vehicles;

τ is the reaction time; and

S[M+1] is the speed measured at node M+1 at time t.

The number of vehicles on link M at time t can be computed as

$$x[M,t] = x[M,t-1] + (F[M,t-1] - F[M+1,t-1] + R[M,t-1] + R[M+1,t-1]) * t_{interval} \quad (3.4)$$

where,

$t_{interval}$ is the length of the time intervals;

$x[M,t-1]$ is the number of vehicle on link M at time t-1;

F[M, t-1] and F[M+1, t-1] are the flow rates measured at node M and M+1 at time t-1, respectively; and

R[M, t-1] and R[M+1, t-1] are the ramp flow rates measured at node M and node M+1 at time t-1, respectively. The on-ramp flow rates are positive. The off-ramp flow rates are negative.

Assuming that the increment of vehicles during the period adds to the queue, the number of vehicles in the queue (or queue size) can be computed as

$$Q[M,t] = (F[M,t] - F[M+1,t] + R[M,t] + R[M+1,t]) * t_1 + x[M,t] \quad (3.5)$$

where,

$t_1$ is the free flow travel time on link M.

The queue length is

$$L_Q = Q[M,t] * (L_V + Space[M,t]) \tag{3.6}$$

where,

$L_V$ is the average vehicle length.

The deceleration distance can be calculated, for vehicles entering link M at the speed of S[M] and needing to decelerate before joining the slow moving traffic traveling at the speed of S[M+1].

$$D_s = \frac{S^2[M,t] - S^2[M+1,t]}{2a} \tag{3.7}$$

where,

*a* is the deceleration rate.

The sum of free flow travel distance, deceleration distance, and queue length equals the length of link M; that is,

$$D[M] = D_S + S[M,t] * t_1 + L_Q \tag{3.8}$$

The free flow travel time $t_1$ can be solved for as follows:

$$t_1 = \frac{D[M] - D_S - x[M,t] * (L_V + Space[M,t])}{(F[M,t] - F[M+1,t] + R[M,t] + R[M+1,t]) * (L_V + Space[M,t]) + S[M,t]} \tag{3.9}$$

As a result, the travel time of link M at time t can be calculated:

$$T_{c2}[M,t] = t_1 + \frac{L_Q}{S[M+1,t]} + \frac{S[M,t] - S[M+1,t]}{a} \tag{3.10}$$

The third condition is when the breakdown occurs at bottleneck M+2 at time t. Under this condition, if the queue spills back onto link M, the travel time of link M would be impacted by the

breakdown; otherwise, the travel time of link M can be estimated in the same fashion as when no breakdown occurs.

Similar to the second condition, the average spacing between two vehicles in the platoon, number of vehicles, queue size, and deceleration distance on link M+1 can be derived by changing M and M+1 in Eq. 3.3 to Eq. 3.7 to M+1 and M+2, respectively. Therefore, the following situations are taken into consideration.

When the queue length is longer than the length of link M+1, the travel time is calculated as follows:

$$T_{c3}[M,t] = \frac{D[M]+D[M+1]-L_Q-D_S}{S[M,t]} + \frac{L_Q-D[M+1]}{S[M+2,t]} + \frac{S[M,t]-S[M+2,t]}{a} \quad (3.11)$$

When the queue length is shorter than the distance of link M+1, but the queue length plus deceleration distance is longer than the distance of link M+1, the travel time can be calculated as follows:

$$T_{c3}[M,t] = \frac{D[M]+D[M+1]-L_Q-D_S}{S[M,t]} + \frac{S[M,t]-S[M+2,t]}{a} * \frac{D_S+L_Q-D[M+1]}{D_S} \quad (3.12)$$

If the sum of the queue length and deceleration distance are shorter than the length of link M+1 (i.e., the breakdown at bottleneck M+2 has no impact on travel time on link M), the travel time estimation method for link M is the same as the method described under the first condition.

Furthermore, empirical studies have documented that flow breakdown does not necessarily occur at the same prevailing flow level, and thus pre-breakdown flow rate (i.e., the flow rate observed immediately before traffic breaks down) has been treated as a random variable in order to model the probabilistic nature of traffic breakdown (Brilon et al., 2005; Dong and Mahmassani, 2009). This results in a probability of breakdown occurring at a given flow (demand) level. The probability distribution function of the pre-breakdown flow rates has been calibrated to follow the

Weibull distribution based on data samples from freeway sections in California, USA (Dong and Mahmassani, 2009; Kim et al., 2010) and Germany (Brilon et al., 2005). The pre-breakdown flow distribution function expresses the probability that traffic breaks down in the next time interval (for a given time discretization).

$$P[M,t] = 1 - e^{-(\frac{F[M,t]}{\sigma})^s} \tag{3.13}$$

where,

P[M,t] is the pre-breakdown probability at node M at time t;

s is the shape parameter, σ is the scale parameter; and

F[M,t] is the flow rate measured at node M at time t.

Thus, the expected travel time of link M is

$$T_E[M,t] = \big[(1-P[M,t])(1-P[M+1,t]) + (1-P[M,t])P[M+1,t]\big] * T_{c1}[M,t] + P[M,t]\big(1-P(M+1,t)\big) * T_{c2}[M,t] + P[M,t]P[M+1,t] * T_{c3}[M,t] \tag{3.14}$$

where,

P[M,t] and P[M+1,t] are the pre-breakdown probabilities at nodes M and M+1 at time t, respectively.

Consequently, the vehicle that departs from node M at time t would arrive at node M+1 at time $t+T_E[M]$. The travel time estimation procedure presented above is repeated to estimate travel time on link M+1 using measurements collected at time $t+T_E[M]$. The corridor-level travel time from bottleneck 1 to bottleneck N can be calculated as the sum of the time-dependent link travel times:

$$T_{corridor} = \sum_{i=1}^{N} T_E[i] \tag{3.15}$$

The proposed model detects different spillback conditions and uses the queue length and deceleration distance to calculate the delay at the bottleneck with queue spillback. However, there is a limitation of the proposed model. If the breakdown occurs between two sensors and the queue does not propagate to a sensor located upstream of the bottleneck, the model would not be able to detect the breakdown.

In order to evaluate the performance of the proposed model, the link travel time estimation method proposed by Vanajakshi et al. (2009) is compared with the proposed method. In Vanajakshi et al. (2009) the travel time is calculated as follows:

$$T_E[M,t] = \begin{cases} \frac{D[M]}{2}\frac{[K[M,t-1]+K[M,t]]}{F[M+1,t]} & F[M+1,t] > 500\ veh/hr/ln \\ \frac{2*D[M]}{S[M,t]+S[M+1,t]} & otherwise \end{cases} \tag{3.16}$$

where,

K[M,t-1] and K[M,t] are the density measured at node M at time t-1 and t, respectively.

In addition, a naïve approach is also tested to estimate link travel time solely based on the point measurement of speeds, that is, using Eq. 3.2 to calculate link travel time. The corridor travel time is simply the summation of the link travel times.

### 3.3.3 Travel Time Distribution

To better understand travel time variability, travel times are fitted to specific distribution functions (Caceres et al., 2016). Four statistical distributions are considered to fit the data, as

shown in Table 3.2. The goodness-of-fit is used to validate the assumptions of these statistical distribution.

Table 3.2 Plausible Function Forms of Travel Time Distribution

| | Probability density function | Parameters | Mean | Mode |
|---|---|---|---|---|
| Gamma | $p(x)=\frac{1}{\theta^k\cdot\Gamma(k)}x^{k-1}\cdot e^{-x/\theta}$ | $k>0$ – shape<br>$\theta>0$ – scale | $k\theta$ | $(k-1)\theta$, for $k\geq 1$ |
| Weibull | $p(x)=\frac{k}{\theta}\cdot(\frac{x}{\theta})^{k-1}\cdot e^{-(x/\theta)^k}$ | $k>0$ – shape<br>$\theta>0$ – scale | $\theta\cdot\Gamma(1+\frac{1}{k})$ | $\theta(\frac{k-1}{k})^{1/k}$, for $k>1$ |
| Lognormal | $p(x)=\frac{1}{x\cdot\sqrt{2\pi\sigma^2}}\cdot e^{-\frac{(\ln x-\mu)^2}{2\sigma^2}}$ | $\sigma^2>0$ – shape<br>$\mu\in R$ – log scale | $e^{\mu+\sigma^2/2}$ | $e^{\mu-\sigma^2}$ |
| Normal | $p(x)=\frac{1}{\sqrt{2\pi\sigma^2}}\cdot e^{\frac{(x-\mu)^2}{2\sigma^2}}$ | $\sigma^2>0$ – variance<br>$\mu\in R$ –mean | $\mu$ | $\mu$ |

$\Gamma(\cdot)-$ Gamma function

Based on the travel time distribution, various reliability measures can be derived, including the standard deviation of travel times, 95th percentile travel times, buffer time index, and planning time index. The planning time index is defined as the ratio of the 95th percentile travel time to the free flow travel time. The buffer time index is the ratio of buffer time (i.e., the difference between 95th percentile travel time and the average travel time) to average travel time.

## 3.4 Results

In this section, the proposed methodology is applied to estimate the travel time of part of I-235, as shown in Figure 3.6. This six-lane freeway section (three lanes in each direction) located in West Des Moines is one of the busiest freeways in Iowa, USA. The locations of roadway sensors

are shown in Figure 3.6. All the sensors are located in the merging/diverging areas, where the sensors can collect data from the ramps and the mainline.


**Figure 3.6 Study Corridor and Sensor Locations (source: ©2015 Google)**

### 3.4.1 Travel Time Calculation

Travel times are estimated using the spatial-correlated travel time estimation (SCTTE) model , Vanajakshi et al. (2009) model, naïve-approach, and INRIX travel time (INRIX-TT). Since congestion generally occurred during the morning peak on weekdays at the study site, the travel times are estimated for each 1-minute interval from 7:00 a.m. to 9:30 a.m. with one month of data from April 2014. Figure 3.7 compares the time-dependent travel times estimated by different methods on example days. The SCTTE model-based travel time index estimation followed the pattern of the INRIX travel time index well, at both the link and corridor levels. The naïve-approach and Vanajakshi et al. (2009) model, however, underestimate the delay in terms of congestion duration and severity. Similar patterns are observed for other days as well.

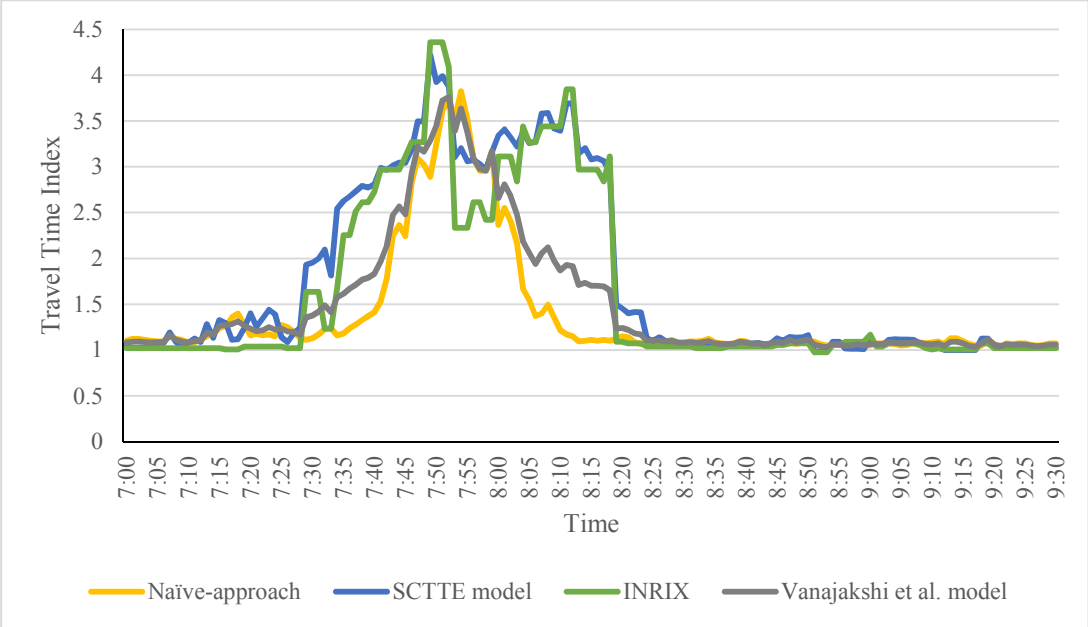


a) Link 1 (April 4th , 2014 [Dry])

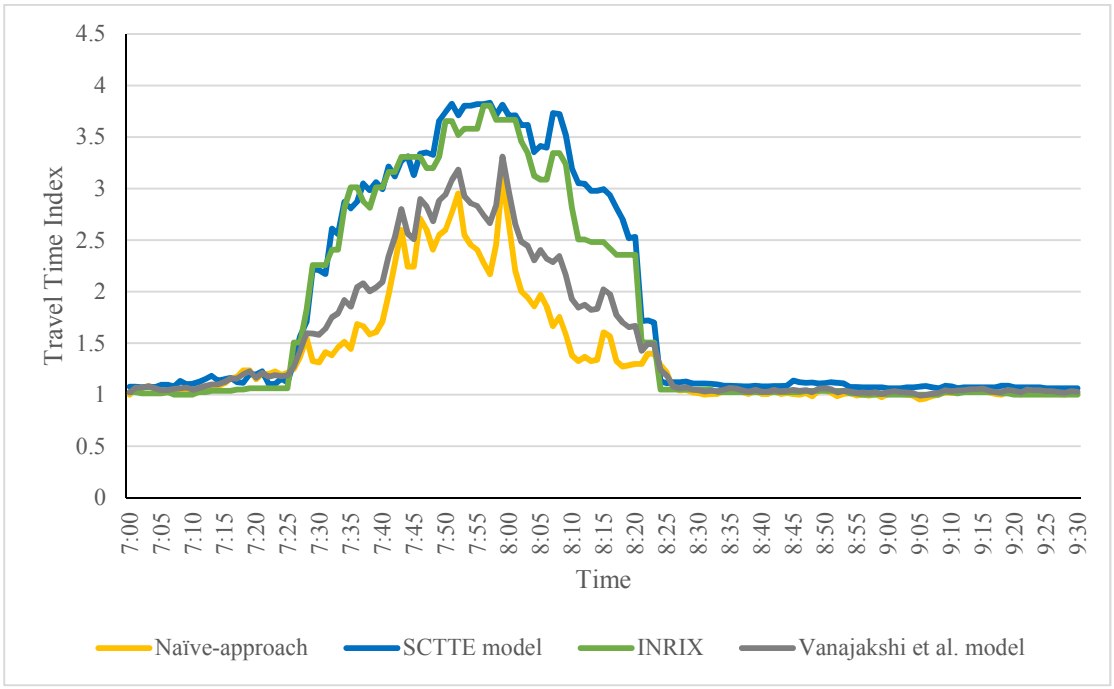


b) Link 2 (April 4th , 2014 [Dry])

**Figure 3.7 Comparison of Model-based Travel Time Index, Vanajakshi et al. (2009) Travel Time Index, Naïve-approach Based Travel Time Index and INRIX Travel Time Index**

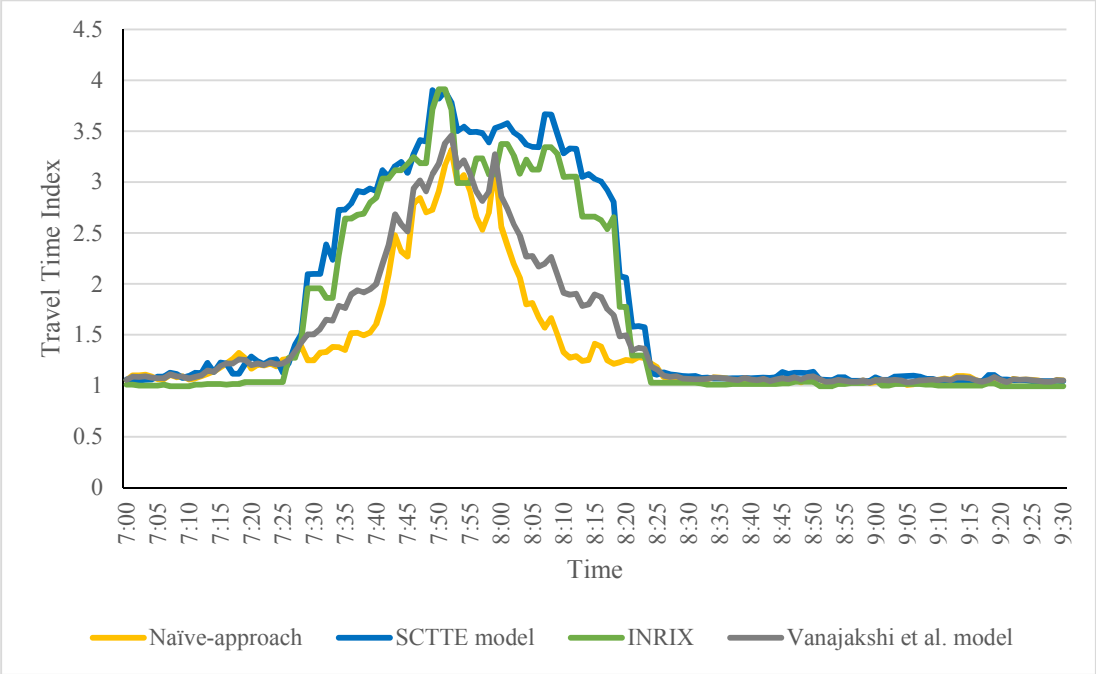


c) Corridor (April 4th , 2014 [Dry])

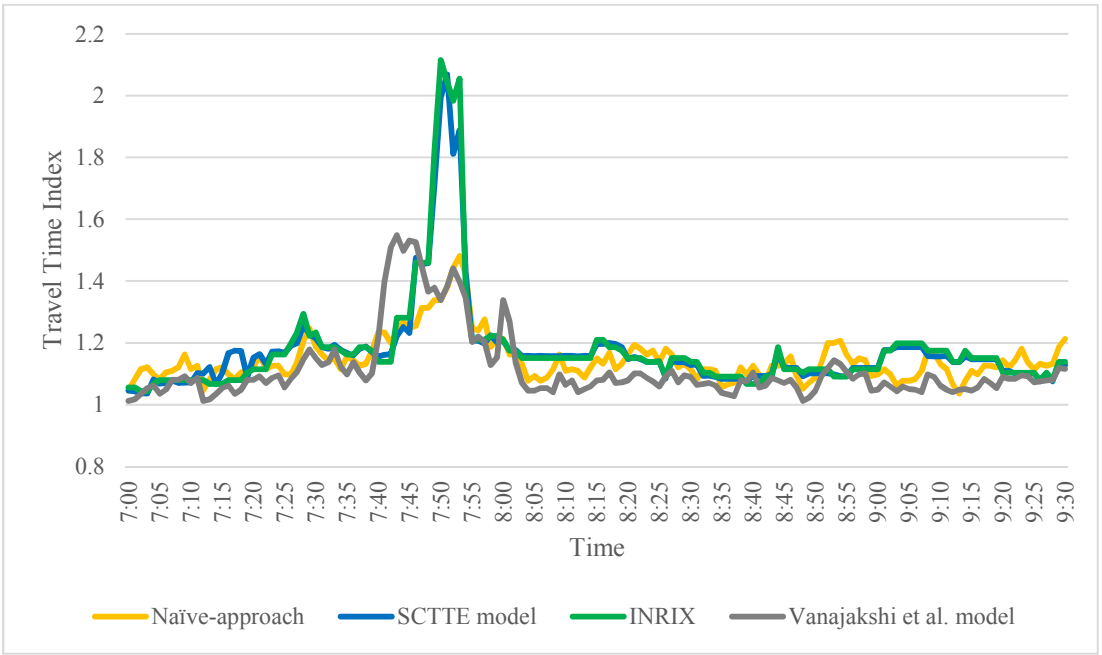


d) Link 1 (April 27th, 2014 [Rain])

**Figure 3.8 Comparison of Model-based Travel Time Index, Vanajakshi et al. (2009) Travel Time Index, Naïve-approach Based Travel Time Index and INRIX Travel Time Index (Continued)**

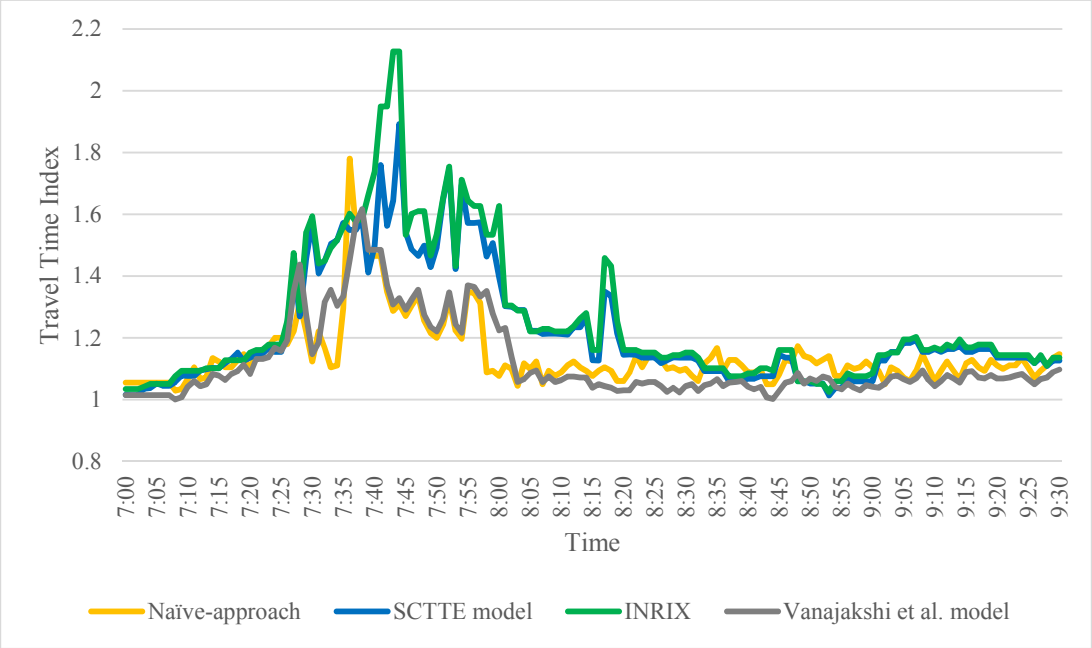


e) Link 2 (April 27th, 2014 [Rain])

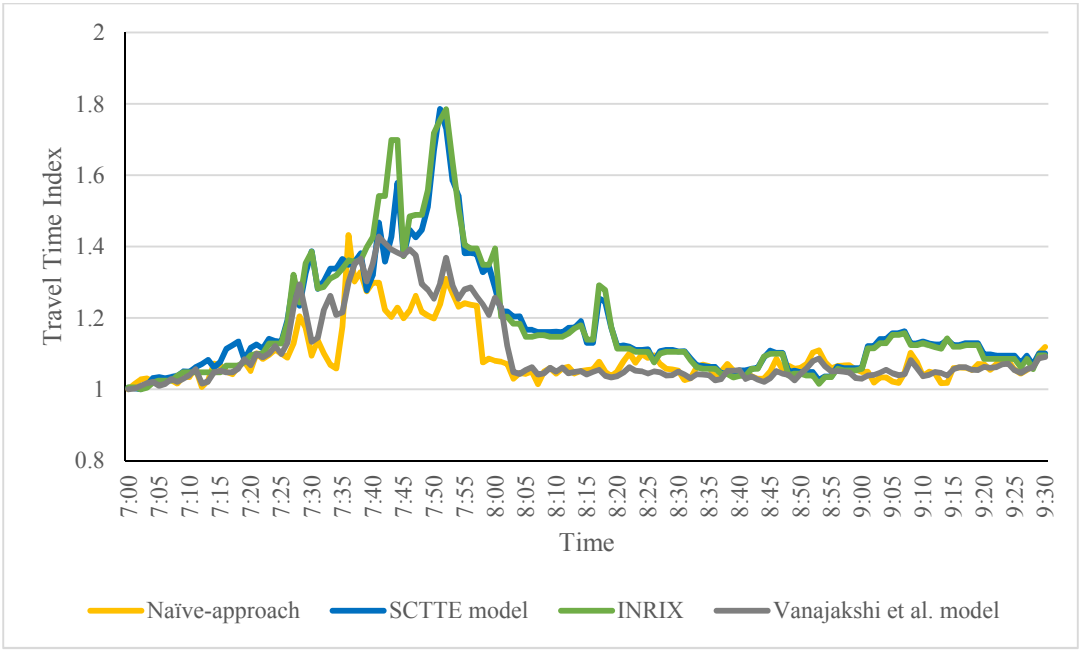


f) Corridor (April 27th, 2014 [Rain])

**Figure 3.9 Comparison of Model-based Travel Time Index, Vanajakshi et al. (2009) Travel Time Index, Naïve-approach Based Travel Time Index and INRIX Travel Time Index (Continued)**

To show shockwave, the speed contour during the congested period of an example day, from 7:20 a.m. to 8:30 a.m., is plotted in Figure 3.8. It can be seen that the speed drops started at sensor 3 and propagated to sensor 1. At sensor 4 the traffic is free flowing.

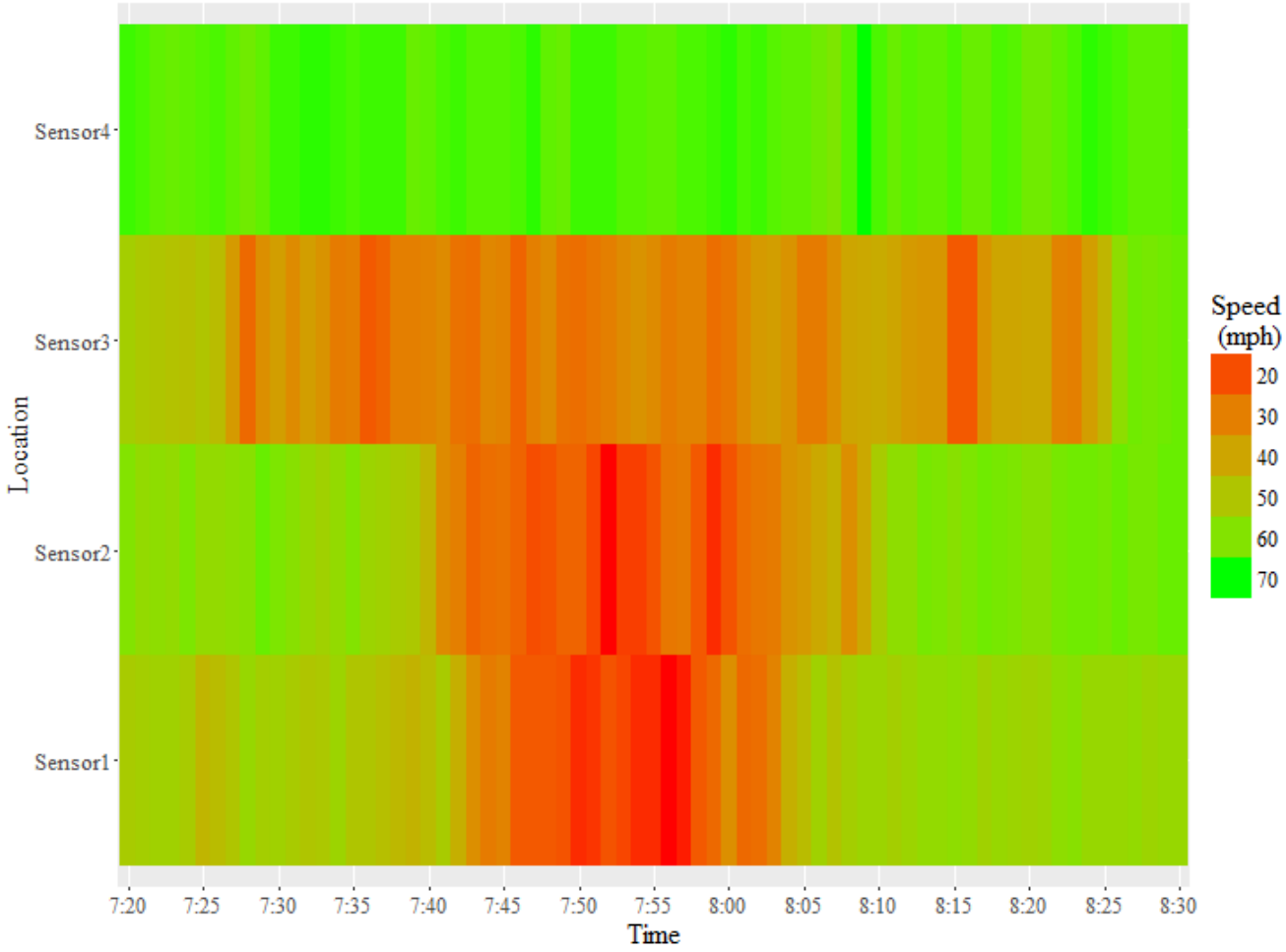


**Figure 3.10 Speed Contour of Sensors**

Performance measures, including mean square error (MSE) and mean absolute percentage error (MAPE), are calculated based on data of April 2014, as follows.

$$MSE = \frac{\sum(estimated - actual)^2}{number\ of\ observations} \tag{3.17}$$

$$MAPE = \frac{\sum^{\frac{|estimated-actual|}{actual}}}{number\ of\ observations} * 100\% \quad (3.18)$$

Table 3.3 compares the values of the performance measures of all the methods at both the link and corridor levels. As it can be seen, the proposed method outperforms other methods.

**Table 3.3 Performance Measures of Different Methods**

| | Corridor | | Link 1 | | Link 2 | |
|---|---|---|---|---|---|---|
| | MSE | MAPE | MSE | MAPE | MSE | MAPE |
| SCTTE model | 0.029 | 0.661 | 0.017 | 0.541 | 0.087 | 1.557 |
| Vanajakshi et al. (2009) model | 0.188 | 7.698 | 0.243 | 12.742 | 0.233 | 9.191 |
| Naïve approach | 0.234 | 12.155 | 0.365 | 13.451 | 0.273 | 13.150 |

Table 3.4 shows the impact of data aggregation on the performance of the proposed model. When the aggregation level increases, the error of the proposed model increases. One of major reason is that the impact of spacing function (Eq. 3.3) on travel time estimation is decreasing with aggregation level increases. Moreover, the differences in errors of three methods become less noticeable at larger aggregation levels. For example, with 1-minute aggregation level data, the proposed model is significantly better than the other two; with 5-minute aggregation level data, the proposed model performs similarly to the Vanajakshi et al. (2009) model.

### 3.4.2 Travel Time Distribution

The maximum likelihood estimation is used to fit the distributions. To evaluate the goodness of fit, the log-likelihood value of each distribution is summarized in Table 3.5. Since the lognormal distribution has the largest log-likelihood value, it was selected as the best distribution to fit the travel time data.

**Table 3.4 Performance Measure of Different Data Aggregation Level**

| | | Corridor | | | Link 1 | | | Link 2 | | |
|---|---|---|---|---|---|---|---|---|---|---|
| | | SCTTE model | Naïve | Vanajakshi et al. model | SCTTE model | Naïve | Vanajakshi et al. model | SCTTE model | Naïve | Vanajakshi et al. model |
| MSE | 1 min | 0.03 | 0.19 | 0.21 | 0.02 | 0.36 | 0.26 | 0.09 | 0.32 | 0.23 |
| | 5 min | 0.18 | 0.22 | 0.20 | 0.14 | 0.24 | 0.12 | 0.23 | 0.26 | 0.23 |
| | 10 min | 0.23 | 0.14 | 0.21 | 0.33 | 0.40 | 0.31 | 0.30 | 0.34 | 0.30 |
| | 15 min | 0.24 | 0.25 | 0.25 | 0.23 | 0.24 | 0.22 | 0.30 | 0.31 | 0.35 |
| MAPE | 1 min | 0.66 | 7.70 | 7.15 | 0.54 | 13.45 | 8.58 | 1.56 | 9.45 | 9.39 |
| | 5 min | 9.32 | 11.01 | 9.45 | 7.73 | 12.71 | 6.71 | 11.13 | 13.96 | 9.24 |
| | 10 min | 10.74 | 4.81 | 8.24 | 12.65 | 16.08 | 12.49 | 11.40 | 14.03 | 12.07 |
| | 15 min | 17.42 | 18.39 | 18.39 | 11.30 | 12.78 | 11.44 | 14.27 | 15.14 | 15.47 |

**Table 3.5 Model Selection Based on Log-likelihood**

| | | Weibull | Gamma | Lognormal | Normal |
|---|---|---|---|---|---|
| INRIX-TT | Link 1 | -8992.79 | -8329.30 | *-7744.00* | -10314.31 |
| | Link 2 | -7331.44 | -6568.86 | *-5617.30* | -9385.41 |
| | Corridor | -13409.20 | -12715.01 | *-12028.62* | -14849.25 |
| SCTTE -TT | Link 1 | -1576.00 | -1465.62 | *-1313.62* | -1968.53 |
| | Link 2 | -1309.03 | -1163.50 | *-1093.47* | -1393.16 |
| | Corridor | -2460.34 | -2320.34 | *-2206.80* | -2684.20 |
| Naïve-TT | Link 1 | -1790.85 | -1240.25 | *-1103.03* | -1853.86 |
| | Link 2 | -1461.62 | -1432.31 | *-1340.04* | -1472.71 |
| | Corridor | -2414.40 | -2346.73 | *-2299.48* | -2488.56 |
| Vanajakshi et al. model | Link 1 | -1611.58 | -1462.37 | *-1300.58* | -1885.87 |
| | Link 2 | -1378.53 | -1154.90 | *-1080.50* | -1487.47 |
| | Corridor | -2085.23 | -2026.78 | *-1985.98* | -2149.27 |

The weekday data for the peak 15-minute travel times (7:45 a.m. to 8:00 a.m.) from December 1, 2013, to December 1, 2014, were used to estimate the travel time distribution. After removing the outliers, the correlation between link 1 and link 2 of the INRIX data and model-based travel time is 0.83 and 0.97, respectively. The proposed SCTTE-TT method slightly overestimated the correlation and the travel time variability. Meanwhile, naïve-approach and Vanajakshi et al. model underestimated the travel time variability. The travel time distributions are shown in Figure 3.9. The SCTTE-TT distribution captured the tendency of the INRIX travel time distribution well.

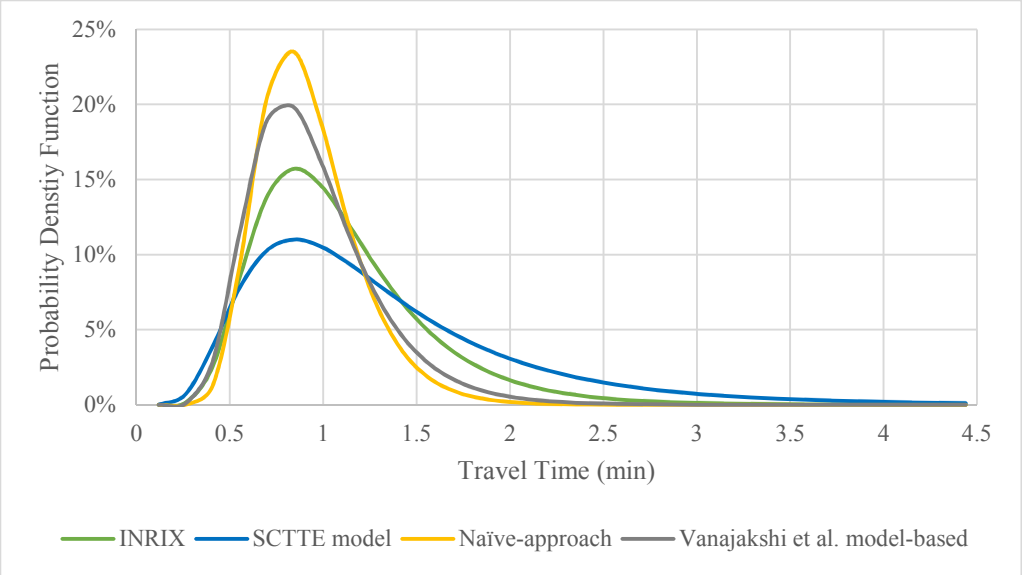


a) Lognormal Distribution of Link 1 Travel Times

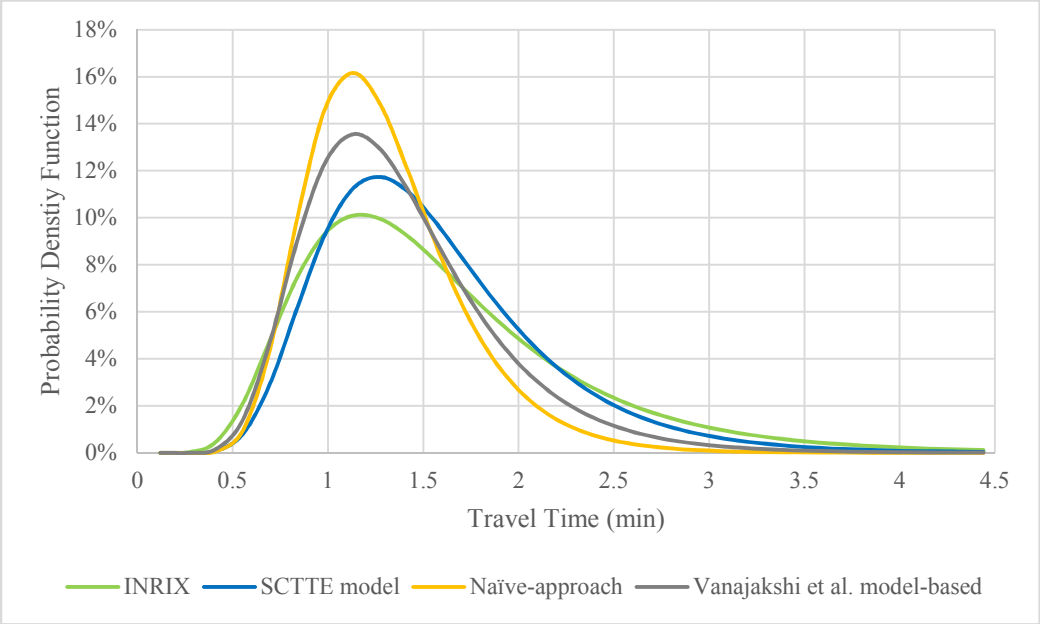


b) Lognormal Distribution of Link 2 Travel Times

**Figure 3.11 Probability Density Distributions of Peak 15-minute Travel Times**

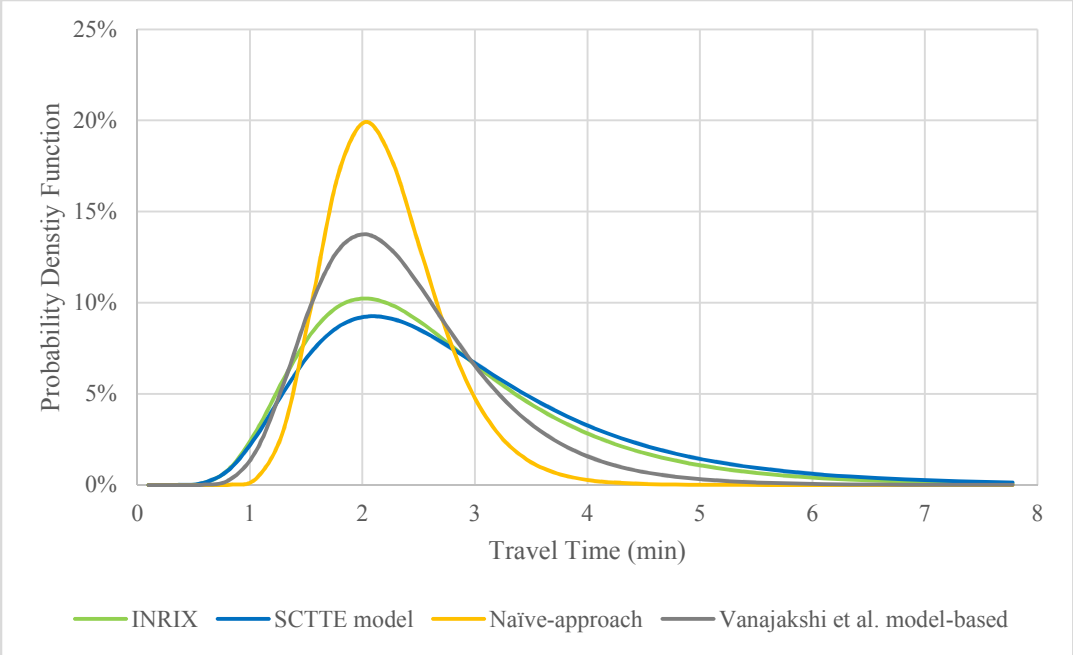


c) Lognormal Distribution of Corridor Travel Times

**Figure 3.12 Probability Density Distributions of Peak 15-minute Travel Times (Continued)**

Figure 3.10 plots the cumulative distribution functions of the lognormal travel time distributions estimated based on the INRIX data, naïve-approach, Vanajakshi et al. model and proposed model.

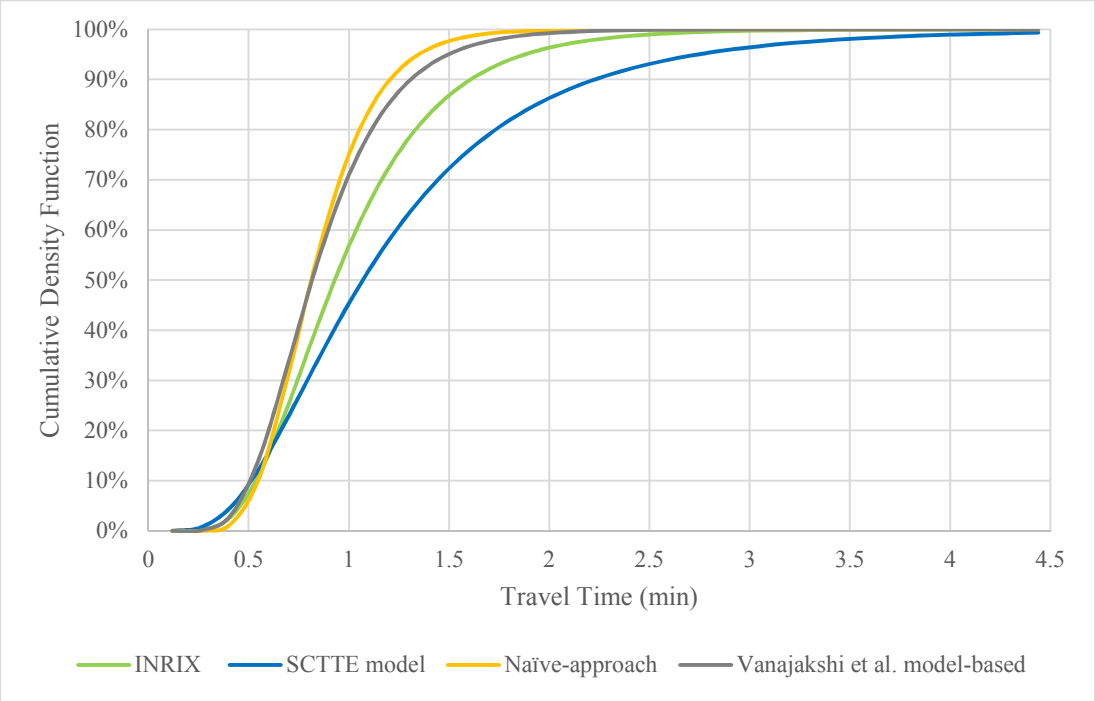


a) Cumulative Distribution of Link 1 Travel Times

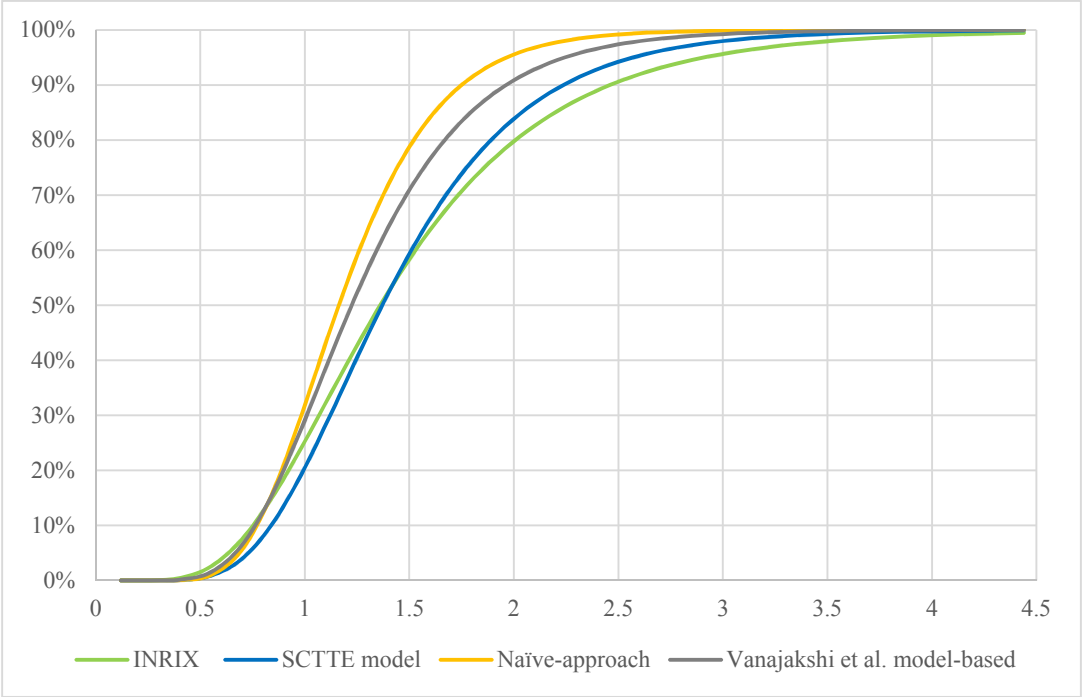


b) Cumulative Distribution of Link 2 Travel Times

**Figure 3.13 Cumulative Density Distributions of Peak 15-minute Travel Times**

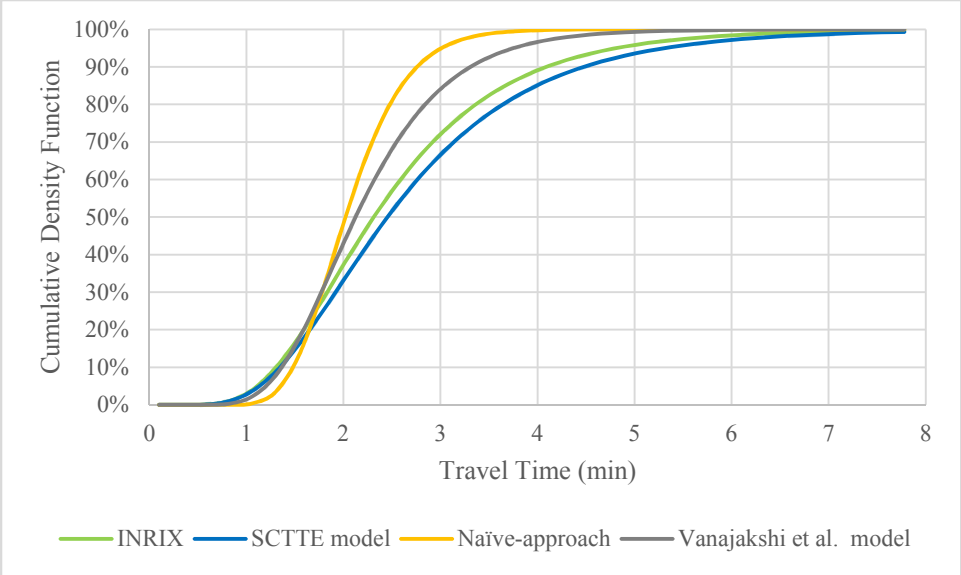


c) Cumulative Distribution of Corridor Travel Times

**Figure 3.14 Cumulative Density Distributions of Peak 15-minute Travel Times (Continued)**

Table 3.6 compares the travel time reliability indices of model-based travel time estimates and INRIX travel times. At corridor level, all SCTTE-TT reliability indices are within 10% error range, compared to the ones calculated based on INRIX travel times. However, all reliability indices of naïve-TT and Vanajakshi et al. model-TT have error larger than 10%. At the link level, although the means and standard deviations of SCTTE-TT s are close to those of the INRIX travel times, the 95th percentile travel time, planning time index, buffer time, and buffer time index show fairly significant discrepancies, up to 70%.

**Table 3.6 The Variance of Reliability Indices of INRIX Travel Time and SCTTE Model-based Travel Time**

| | | Mean (min) | Standard Deviation | 95th Percentile (min) | Planning Time Index | Buffer Time (min) | Buffer Time Index |
|---|---|---|---|---|---|---|---|
| INRIX-TT | Link 1 | 1.14 | 0.51 | 1.88 | 2.04 | 0.74 | 0.65 |
| | Link 2 | 1.51 | 0.74 | 2.56 | 1.95 | 1.05 | 0.69 |
| | Corridor | 2.55 | 1.20 | 4.90 | 2.21 | 2.35 | 0.92 |
| SCTTE-TT | Link 1 | 1.26 | 0.78 | 2.52 | 2.74 | 1.26 | 1.00 |
| | Link 2 | 1.47 | 0.59 | 3.00 | 2.29 | 1.53 | 1.03 |
| | Corridor | 2.74 | 1.36 | 5.32 | 2.40 | 2.58 | 0.94 |
| Naïve-TT | Link 1 | 0.86 | 0.28 | 1.37 | 1.49 | 0.51 | 0.59 |
| | Link 2 | 1.21 | 0.41 | 1.92 | 1.47 | 0.71 | 0.59 |
| | Corridor | 2.13 | 0.74 | 3.55 | 1.60 | 1.42 | 0.67 |
| Vanajakshi et al. model-TT | Link 1 | 0.88 | 0.34 | 1.48 | 1.61 | 0.60 | 0.68 |
| | Link 2 | 1.32 | 0.51 | 2.24 | 1.71 | 0.92 | 0.69 |
| | Corridor | 2.31 | 0.81 | 3.78 | 1.70 | 1.47 | 0.64 |

The errors in the proposed travel time estimation model could be attributed to several factors. First, the first-in, first-out assumption does not take lane change behavior into consideration in the calculation. As a result, the number of vehicles approaching the bottleneck might be underestimated or overestimated by the model. Second, missing values from the radar sensor data might also cause errors in estimating travel times, thus causing errors in computing travel time reliability indices.

The proposed travel time estimation model performs better than the other two methods. One of the main reason is that the proposed method considers the impact of queue length under different traffic conditions on travel time. However, there are some limitations of the proposed method. First, the congestion occurred between two sensors could only be detected when the queue built up to the upstream sensor. Thus, the accuracy of the proposed method may vary

with the distance between sensors. Second, the proposed method requires the traffic data from downstream links to estimate the travel time of the target link. Because of sensor errors, the traffic data for these links may not always available for the same time point. By considering correlations among multiple links, the accuracy of the proposed model will increase.

## 3.5 Summary

This chapter proposed a travel time estimation model that considers the spatially correlated traffic conditions. Link- and corridor-level travel time distributions were estimated using probe vehicle data and roadside radar sensor data. Corridor-level travel time reliability measures were extracted from the travel time distributions. Compared to the probe vehicle data from INRIX, the proposed travel time estimation model captured the patterns of travel time and its distribution well. Moreover, the inconsistency of the missing data of INRIX and sensor data can randomly cause the travel time reliability be overestimated/underestimated by the SCTTE-TT method.

The proposed model provides a method to assess corridor-level travel time and its distribution using the point measurements collected from the side-fired radar sensors. In order to estimate travel times accurately under congested condition, Yang et al. (2016) proposed a travel time estimation model which is integrated with car-following model. Consequently, it is desirable to consider the distinct car-following behavior of passenger cars and heavy vehicles in the travel time reliability analysis. In the next chapter, the impact of car-following behavior of passenger cars and heavy vehicle on travel time reliability is investigated.

# CHAPTER 4. ESTIMATE TRAVEL TIME RELIABILITY MEASURES BY CONSIDERING THE STOCHASTIC NATURE OF DRIVER BEHAVIOR PARAMETERS

This chapter presents a method to estimate corridor travel time reliability measures by incorporating stochastic standstill distance and time headway parameters in car-following model. The chapter is organized as follows. Section 4.1 introduces the background of the study. The corridor travel time reliability measure estimation model, which incorporated stochastic standstill distance and time headway parameters in FRESIM car following model, is described in section 4.2. The discussion of the results and summary of the findings are presented in Section 4.3 and Section 4.4, respectively.

## 4.1 Introduction

Car following behavior, which describes the relationship between a following vehicle and a leading vehicle, plays an important role in determining the freeway capacity (Cambridge Systematics and Texas Transportation Institute, 2005). Meanwhile, capacity of freeways has been widely considered as an important parameter in delay-volume function to estimate travel time. Stochastic nature of capacity is influenced by weather, traffic composition and stochastic travel behavior (Neuhold and Fellendorf, 2014). As a result, it is important to investigate the impact of the stochastic driver behavior on travel time reliability.

Generally, standstill distance and following time headway are the key parameters of car-following models. Historical data shows that the time headway and standstill distance follow probabilistic distributions. However, existing microsimulation software usually

considers the driving behavior parameters as deterministic values. In order to better reflect the dynamic nature of the transportation system, the stochastic driving behavior parameters are incorporated into car-following model to estimate travel time reliability measures.

In this chapter, the INRIX travel time data and Wavetronix data (e.g. speed, flow and occupancy) are collected during 2015, which are collected during 2014 in Chapter 3, is used to estimate travel time reliability.

## 4.2 Methodology

This section presents a modeling approach to generate travel time reliability measures using car-following models with stochastic headway and standstill parameters. The modeling approach consists of three parts. First, a two-component travel time distribution is proposed to derive reliability measures. Second, the mathematical formulation of travel time under congested state is derived from Pipes Car-following model. Third, Monte Carlo simulation method is used to generate travel times under congested state considering stochastic time headways and standstill distances.

### 4.2.1 Two-component travel time distribution

Multi-state models have been proposed to fit travel time distributions (Guo et al., 2010; Park et al., 2011), which contains multiple component distributions. Normal, gamma, and lognormal distributions have been considered as component distributions of the multi-state models. Guo et al. (2010) proposed a two-component travel time distribution model containing free-flow state and congested state. Mixture normal, mixture lognormal, or mixture Weibull distributions can be used to describe the two-component travel time distribution. However,

deriving travel time reliability measures from existing two-component travel time distribution is more sophisticated than single-component travel time distribution. Since the variations of free-flow travel times are generally small, the reliability measures are mostly determined by the congested travel times. Therefore, to simplify the calculation of reliability measures, the two component model is simplified by ignoring the free-flow travel time variation and treating the travel time in free-flow state as a Dirac delta distribution.

Based on the travel time data collected on I-235 in Des Moines, IA, two-component travel time distribution is shown in Figure 4.1. In Figure 4.1(a), the probability density function (PDF) of travel times can be viewed as a mixture Gaussian distribution consisting of a free flow travel time distribution and a congested travel time distribution. As the travel time variation is small under free flow conditions, the PDF of free-flow state can be simplified as a Dirac delta distribution, as show in Figure 4.1(b).

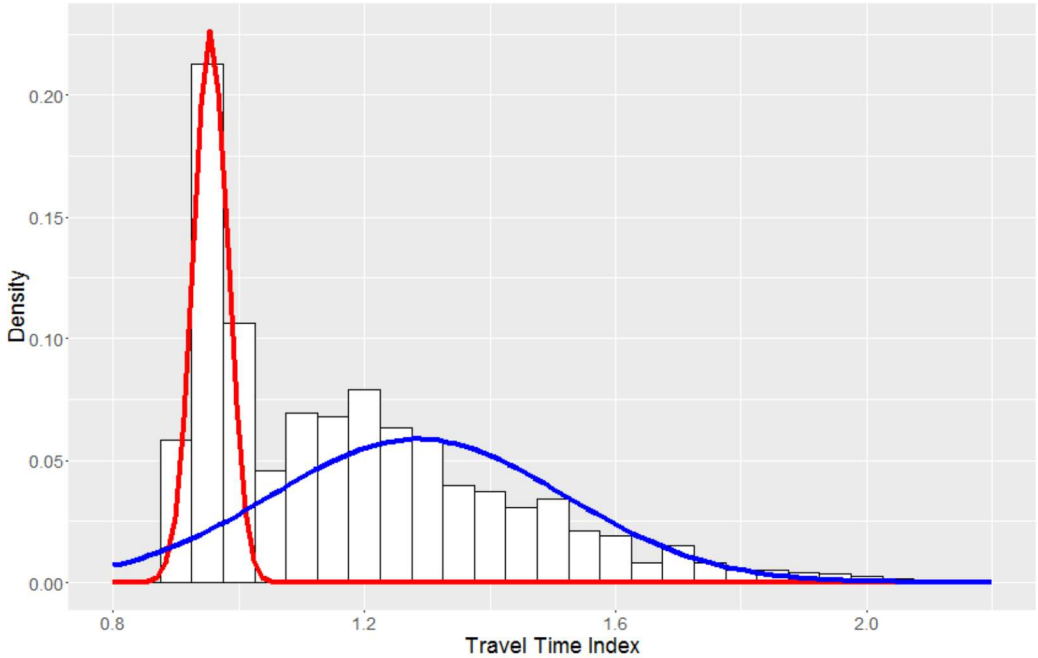


a) Mixture Gaussian Distribution

**Figure 4.1 Two-component Travel Time Model**

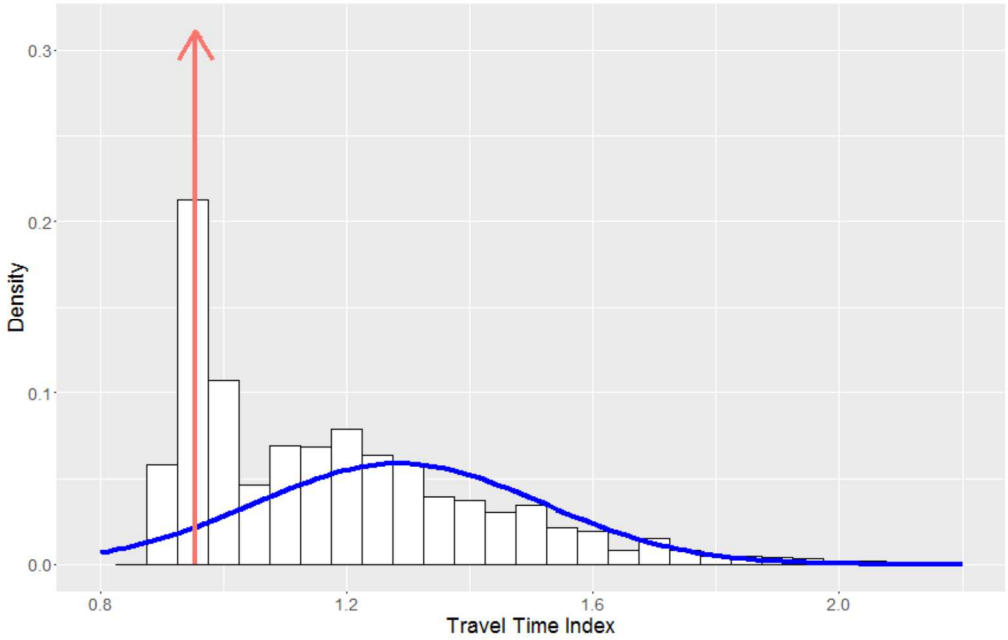


b) Simplified Distribution

**Figure 4.2 Two-component Travel Time Model (Continued)**

To calculate travel time reliability measures, such as planning index and buffer time, the 95$^{th}$ percentile and mean travel times are needed. The cumulative density function (CDF) of the simplified two component travel time distribution can be written as

$$\boldsymbol{F(x) = \alpha F_F(x) + (1 - \alpha) F_C(x)} \tag{4.1}$$

where,

$F_F(x)$ is cumulative density functions of Dirac delta distribution;

$F_C(x)$ is cumulative density functions of congested state.

$\alpha$ is the mixture proportion.

For Dirac delta distribution, the cumulative distribution function is Heaviside step function as follows:

$$F_F(x) = \begin{cases} 1 & , x \geq t_0 \\ 0 & , x < t_0 \end{cases} \tag{4.2}$$

where,

$t_0$ is the mean free flow travel time.

As a result, the 95th percentile travel time can be calculated as follows:

$$TT_{95} = \begin{cases} F_C^{-1}\left(\frac{0.95-\alpha}{1-\alpha}\right), 0 \leq \alpha < 0.95 \\ t_0, \quad \alpha \geq 0.95 \end{cases} \tag{4.3}$$

Where,

$TT_{95}$ is the 95th percentile travel time

$F_C^{-1}(\cdot)$ is the inverse CDF of congested travel times

The mean travel time of the two-component model can be calculated as follows:

$$\mu = \alpha * t_0 + (1-\alpha)\mu_C \tag{4.4}$$

Where,

$\mu$ is the mean travel time

$\mu_C$ is the mean travel time of the congested state.

Based on the 95th percentile travel time, free-flow travel time and mean travel time, travel time reliability measures can be derived, including:

- Planning time – The 95th percentile travel time.
- Planning time index – The ratio of 95th percentile travel time to ideal or free-flow travel time.

$$Planning\ time\ index = \frac{TT_{95}}{t_0} \tag{4.5}$$

- Buffer time – The difference between the 95th percentile travel time and the mean travel time.

$$Buffer\ time = TT_{95} - \mu \tag{4.6}$$

- Buffer index – The size of the buffer as a percentage of the average, calculated as the 95th percentile travel time minus the average, divided by the average.

$$Buffer\ index = \frac{TT_{95} - \mu}{\mu} \tag{4.7}$$

The travel time reliability estimation framework is shown in Figure 4.2. First, the real world density data is clustered into free-flow state and congested state based on the upper value of level of service D in Highway Capacity Manual 2016 (HCM 2016), that is, the congested state is defined as when density is larger than 26 pc/mi/ln. Accordingly, $\alpha$ and free flow travel time can be calculated as the ratio of free-flow state occurrence during the data collection period. Second, the stochastic car-following model is used to generate travel time distribution under congested state. Finally, based on the simplified two-component travel time distribution, the reliability measure can be calculated.

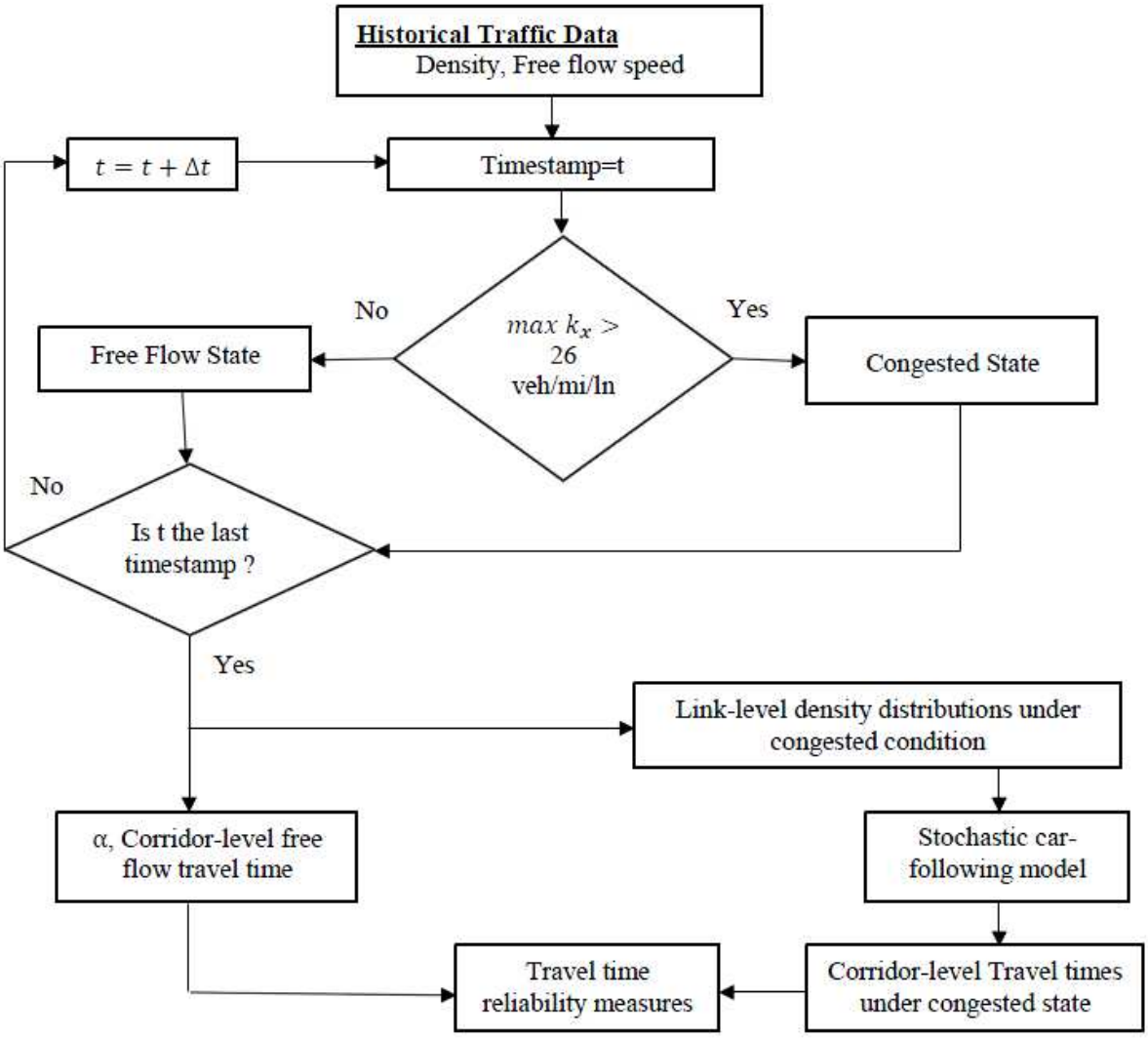


**Figure 4.3 Corridor-level Travel Time Reliability Measure Estimation Framework**

### 4.2.2 Stochastic Headways and Standstill Distances

The time headways and standstill distances were collected from various freeway segments throughout Iowa. In order to collect the time headway data, side-fired radar sensors were installed temporarily with video cameras at several locations. The radar sensors collect the vehicle length, speed, lane detected, and time detected for each vehicle. Vehicle

classification is determined based on the vehicle length. Vehicles longer than 40 feet is classified as truck. Other vehicles are considered as cars. The time headway is calculated as the time difference between two vehicle arrivals at the same location. According to the research of Houchin et al. (2015), the standstill distances are measured from the videos when the vehicles stopped in queue on freeway. In particular, videos from Iowa Department of Transportation closed-circuit cameras (CCTV) when stop-and-go traffic occurred were downloaded after the fact. Screen captures of the video were taken when vehicles were stopped within the frame. Those stopped vehicles were identified and the distances between them are measured using a Photoshop tool that is capable of measuring distances on plane distorted by perspective. Painted lane lines (10 feet long) were used as a control measurement on which the software based the rest of its measurements on. The length of the lane lines was confirmed using Google Earth. Thus, the standstill distances were measured between every pair of stopped vehicles.

Four statistical distributions are considered to fit the time headway and standstill distance data, as shown in Table 4.1. In order to determine how well the distributions fit the observations, log-likelihood values are compared.

The likelihood ratio test was used to compare the vehicle type-specific models (i.e. car following car, car following truck, truck following car, and truck following truck) with the overall model. The test statistic, which is chi-square distributed, is shown below in Eq. 4.8.

$$\chi^2 = -2(LL_R - LL_U) \tag{4.8}$$

where:

$LL_R$ is the log likelihood value for the overall model; and

$LL_U$ is the sum of the log likelihood values for vehicle type-specific models.

**Table 4.1 Plausible Function Forms of Time Headway and Standstill Distance Distributions**

| | Probability density function | Parameters | Mean | Mode |
|---|---|---|---|---|
| Gamma | $p(x) = \frac{\beta^{\alpha}}{\Gamma(\alpha)} x^{\alpha-1} e^{-\beta x}$ | $\alpha > 0$ – shape<br>$\beta > 0$ – rate | $\frac{\alpha}{\beta}$ | $\frac{\alpha-1}{\beta}$, for $\alpha \geq 1$ |
| Weibull | $p(x) = \frac{k}{\theta} \cdot (\frac{x}{\theta})^{k-1} \cdot e^{-(x/\theta)^k}$ | $k > 0$ – shape<br>$\theta > 0$ – scale | $\theta \cdot \Gamma(1+\frac{1}{k})$ | $\theta(\frac{k-1}{k})^{1/k}$, for $k > 1$ |
| Lognormal | $p(x) = \frac{1}{x \cdot \sqrt{2\pi\sigma^2}} \cdot e^{\frac{(\ln x - \mu)^2}{2\sigma^2}}$ | $\sigma^2 > 0$ – shape<br>$\mu \in$ R – log scale | $e^{\mu + \sigma^2/2}$ | $e^{\mu - \sigma^2}$ |
| Normal | $p(x) = \frac{1}{\sqrt{2\pi\sigma^2}} \cdot e^{\frac{(x-\mu)^2}{2\sigma^2}}$ | $\sigma^2 > 0$ – variance<br>$\mu \in$ R – mean | $\mu$ | $\mu$ |

$\Gamma(\cdot)$ – Gamma function

### 4.2.3 Steady-State Car-Following Behavior

The steady-state car-following models describe the relationship between the desired speed of following vehicles, the speed of leading vehicles and the spacing between the lead and the following vehicles. The macroscopic speed-density relationship can be derived from the steady-state car-following behavior, as described in this section.

4.2.3.1 *FRESIM car-following behavior*

Pitt car-following model, developed by the University of Pittsburgh, is implemented in FRESIM (Halati et al., 1997). The basic model is described as follows

$$S[m] = S_j[m] + c_3[m]u[m] + bc_3\Delta u[m]^2 \quad (4.9)$$

where,

$S[m]$ is the spacing between the lead vehicle m-1 and the following vehicle m (mile);

$S_j[m]$ is the spacing when vehicles are completely stop in a queue (mile);

$c_3[m]$ is the car-following sensitivity factor of vehicle m;

$u[m]$ is the speed of the following vehicle m (mph);

b is the calibration constant that equals to 0.1 if the speed of the following vehicle exceeds the speed of lead vehicle; otherwise b is 0; and

$\Delta u[m]$ is the difference in speeds of the lead vehicle m-1 and the following vehicle m (mph).

The spacing when vehicles are completely stopped is the summation of standstill distance and vehicle length, as show in Eq. 4.10.

$$S_j[m] = d_j[m] + l_v[m-1] \quad (4.10)$$

where,

$d_j[m]$ is the standstill distance between the lead vehicle m-1 and the following vehicle m (mile); and

$l_v[m-1]$ is the length of vehicle m-1 (mile).

Since the steady-state assumes equal and constant speeds, the car-following model in FRESIM is simplified as follows:

$$S[m] = S_j[m] + c_3[m]u[m] \tag{4.11}$$

$$u[m] = min(\frac{S[m]-S_j[m]}{c_3[m]}, u_f) \tag{4.12}$$

In fact, the FRESIM stead-state car-following behavior can be characterized by Pipes model (1953) (Rakha and Crowther 2003). The speed-density relationship developed from the Pipes car-following model is as follows.

$$U = \frac{n(1-k\times\overline{S_j})}{k\times\sum_{m=1}^{n} c_3[m]}, U \in [0, u_f] \tag{4.13}$$

where,

$k$ is the density (veh/mile/ln);

$U$ is the speed (mph); and

$\overline{S_j}$ is the average spacing, that is, $\overline{S_j} = \frac{\sum_{m=1}^{n} S_j[m]}{n}$.

Moreover, Rakha and Crowther (2003) showed that the driver sensitivity factor can be written as

$$\overline{c_3} = \frac{1}{q_c} - \frac{1}{k_j u_f} \tag{4.14}$$

where,

$q_c$ is the roadway capacity (veh/hr/ln);

$k_j$ is the jam density (veh/mile); and

$u_f$ is the free-flow speed (mph).

The relationship between flow rate and headway and the relationship between jam density and congested spacing are represented by Eq. 4.15 and Eq. 4.16, respectively.

$$q[m] = \frac{1}{h_a[m]} \tag{4.15}$$

$$k_j[m] = \frac{1}{S_j[m]} \tag{4.16}$$

where,

$h_a[m]$ is the time headway between the lead vehicle m-1 and the following vehicle m (hour).

By substituting Eq. 4.15 and Eq. 4.16 into Eq. 4.14, we have

$$c_3[m] = h_a[m] - \frac{S_j[m]}{u_f} \tag{4.17}$$

4.2.3.2 *INTEGRATION car-following behavior*

By combining the Pipes model and Greenshields model, Van Aerde and Rakha (1995) proposed a car-following model, which is implemented in INTEGRATION (M. Van Aerde & Assoc., 2005a, 2005b). The Van Aerde model is as follows (Rakha & Crowther, 2003).

$$S[m] = a_1[m] + \frac{a_2[m]}{u_f - u} + a_3[m]u \tag{4.18}$$

where,

$a_1[m]$ is the fixed distance headway between the lead vehicle m-1 and the following vehicle m (mile);

$a_2[m]$ is the first variable distance headway between the lead vehicle m-1 and the following vehicle m (mile$^2$/h); and

$a_3[m]$ is the second variable distance headway between the lead vehicle m-1 and the following vehicle m (h).

The speed-density relationship can be derived

$$k = \frac{1}{a_1 + \frac{a_2}{u_f - u} + a_3 u} \tag{4.19}$$

The model parameters– $a_1$, $a_2$ and $a_3$–can be computed as follows (Demarchi, 2002)

$$a_1 = \frac{u_f}{k_j u_c^2}(2u_c - u_f) \tag{4.20}$$

$$a_2 = \frac{u_f}{k_j u_c^2}(u_f - u_c)^2 \tag{4.21}$$

$$a_3 = \frac{1}{q_c} - \frac{u_f}{k_j u_c^2} \tag{4.22}$$

where,

$u_c$ is the speed at capacity (mph).

By substituting Eq. 4.15 and Eq. 4.16 into Eq. 4.20, Eq. 4.21 and Eq. 4.22, the model parameters for each vehicle pair can be derived as follows

$$a_1[m] = \frac{S_j[m]u_f}{u_c^2}(2u_c - u_f) \tag{4.23}$$

$$a_2[m] = \frac{S_j[m]u_f}{u_c^2}(u_f - u_c)^2 \tag{4.24}$$

$$a_3[m] = h_a[m] - \frac{S_j[M]u_f}{u_c^2} \tag{4.25}$$

Based on Eq. 19, Eq.23, Eq.24 and Eq.25, speed is calculated as follows:

$$U = \frac{\left(\bar{a}_3 u_f + \frac{1}{k} - \bar{a}_1\right) \pm \sqrt{\left(\bar{a}_3 u_f - \frac{1}{k} + \bar{a}_1\right)^2 + 4\bar{a}_3\bar{a}_2}}{2\bar{a}_3}, U \in [0, u_f] \tag{4.26}$$

Where,

$\bar{a}_i$ is the average of $a_i[m]$, that is, $\bar{a}_i = \frac{\sum_{m=1}^{n} a_i[m]}{n}$.

4.2.3.3 *VISSIM* car-*following behavior*

Weidemann 74 and Weidemann 99 car-following models are implemented in VISSIM, which belong to psychophysical or action-point models (Gao, 2008). The model was developed from Pipes car-following logic and considers other factors, such as the spacing at which the vehicle reacts to a speed difference and driver's perception of the speed difference. Under steady-state conditions the car-following model in VISSIM reverted to the Pipes model (as shown in Eq. 4.12) (Rakha and Crowther 2002).

### 4.2.4 Travel time reliability based on steady-state car-following models

By incorporating standstill distance and time headway distributions in the above mentioned car-following models, travel time reliability measures can be estimated using Monte Carlo simulation. In each simulation run, a realization of the stochastic parameters leads to a

realization of the speed-density point. Collectively, the speed-density region can be estimated. A sufficient number of simulations can provide a good representation of the speed-density regions under uncertainty. Given the standstill distance and time headway distributions, the following procedure is implemented to estimate speed-density region through Monte Carlo simulation. Accordingly, the travel times in congest regime can be generated. The 95th percentile and mean travel time are calculate based on Eq. 5.3~5.4. The reliability measures are derived from Eq. 5.5~5.7. The detailed procedure is described as follows.

**Input**:

Free Flow Speed, $u_f$;
Truck percentage, P;
Number of links = $X$;
Link length, $L_x, x \in [1, X]$;
Density distribution under congested condition for link x, $k_x, x \in [1, X]$;
Truncated vehicle type-specific standstill distance distributions (see Section 4.3.1.2), $S_j \in (0, Upper\ Bound]$;
Truncated vehicle type-specific headway distributions (see Section 4.3.1.1), $H \in [Lower\ Bound, Upper\ Bound]$ ;
Number of simulations = $Z$.

**For z=1 to Z**,
**For x= 1 to X**,
**1:** Generate a set of random samples for vehicles, say M vehicles, with P percent of trucks.
**2:** Randomly generate density values for link x from the density distribution.
**For m=2 to M**
**3**: Determine the vehicle following type between the leading vehicle (m-1) and the following vehicle (m) in the vehicle set.
**4**: According to the truncated vehicle type-specific standstill distance and headway distributions, generate the standstill distances and time headways for the vehicle pair based on the corresponding probability distributions.
**5**: Calculate $S_j$ for each vehicle pair using Eq.10
**6**: ***FRESIM***: Calculate $c_3$ for following vehicle (m) using Eq. 17.
***INTEGRATION***: Calculate $a_1$, $a_2$ and $a_3$ for the following vehicle (m) using Eq. 23~25.
**End For**
**7**: Select first n observations, where

$\boldsymbol{max}\ \sum_{m=2}^{n} headway\ [m] \leq time\ interval$

**8**: ***FRESIM***: Use Eq. 13 to calculate the speed on target link for the density point.

***INTEGRATION***: Use Eq. 27 to calculate the speed on target link for the density point.

**9**: Calculate travel time on target link by using link length divided by speed from step 8.

**End For**

**10**: Calculate corridor-level travel time by adding the travel times on all the links

**End For**

**Output:** Speed-Density Range/ Travel Times under Congested State

In order to evaluate the accuracy and efficiency of the proposed framework, the FRESIM car-following model is used to compare with VISSIM simulation results. Note that logic of FRESIM and VISSIM under steady-state condition reverts to Pipes model (Rakha and Crowther 2002).

### 4.2.5 Travel time reliability based on VISSIM

The corridor-level travel time can be obtained through PTV VISSIM 7. VISSIM is microscopic traffic simulation software that adopts the psycho-physical car-following model developed by Wiedemann (PTV AG 2014). Because VISSIM can simulate the behavior of individual vehicles and produce diverse evaluation parameters, it has been widely used in transportation engineering for modeling various traffic scenarios. There are two car following models available in VISSIM, Wiedemann 74 and Wiedemann 99, which are used to model urban traffic and freeway traffic, respectively. In this study, the Wiedemann 99 car following model was used to estimate travel time reliability measures of freeways.

The driver behavior parameters were calibrated by Dong et al. (2015) using locally collected data. Three car-following model parameters, including standstill distance (CC0),

headway time (CC1), and "following" variation (CC2), have been found to have a significant influence on traffic capacity. The traffic volume on the study corridor was balanced based on the method proposed by Shaw and Noyce (2014). The congested and uncongested conditions were simulated separately. The travel time reliability measures were calculated by sampling the travel times from the VISSIM output based on the percentage of the congested and uncongested conditions occurred in the real world.

## 4.3 Results

### 4.3.1 Time Headway and Standstill Distance Distribution

4.3.1.1 *Time headway distribution*

Figure 4.3 shows the histograms of time headways by different vehicle lead-follow type and for the pooled data (labeled as "Overall"). The distributions are right skewed which is consistent with the finding in the research of Ye and Zhang (2009). Makishita and Matsunaga (2008) found that the reaction time range of drivers were 61-64 years old is larger than the drivers were 20-54 years old. Considering the safety issue, the headway is related to reaction time (Brackstone and Mcdonald, 2007). Therefore, one of the possible reasons of right skewness of time headway distributions is that drivers in different age group has different reaction time range.

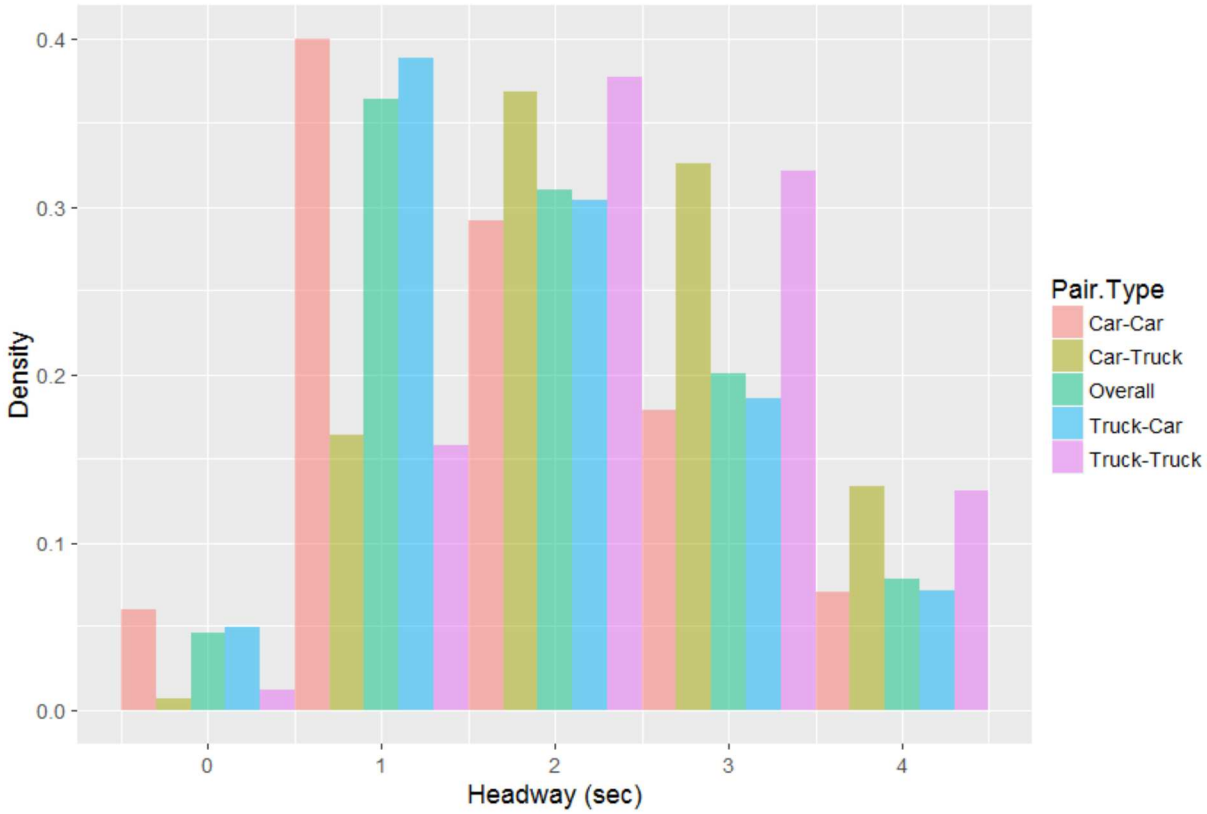


**Figure 4.4 Histograms of Vehicle Type–specific and All Vehicle–type Time Headways**

Table 4.2 summaries the means and standard deviations of time headways. The mean time headways when a car is following (i.e. Car-Car and Truck-Car) are significantly different from the ones when a truck is following (i.e. Car-Truck and Truck-Truck). In addition, large standard deviations are associated with each group of observations, as well as the pooled dataset, indicating fairly disperse distributions.

**Table 4.2 Summary Statistics of Time Headways**

| | Overall | Car-Car | Car-Truck | Truck-Car | Truck-Truck |
|---|---|---|---|---|---|
| Number of observations | 260415 | 200994 | 22324 | 30467 | 6630 |
| Mean | 1.90 | 1.80 | 2.40 | 1.84 | 2.41 |
| Standard deviation | 0.96 | 0.97 | 0.87 | 0.90 | 0.88 |

Log-normal, gamma, normal and Weibull distributions are used to fit vehicle type-specific and overall time headways. Table 4.3 lists the log likelihood values and the log-likelihood ratio test statistics. The test statistics, $\chi 2$, are all greater than the critical value of the chi-square distribution at the 5% significance level, indicating that vehicle type-specific headway models are significantly different from the overall headway model. In addition, based on the log likelihood values, Weibull distribution is the best fit model for Car-Car, Car-Truck, Truck-Car and Overall time headways. For Truck-Truck time headways, the best fit model is Normal distribution, although Weibull distribution provides a similar fit. The best fit models are considered as input in the car-following models in the subsequent sections. Table 4.4 lists the estimated parameters.

**Table 4.3 Log-likelihood Ratio Test Statistic of Headway Models**

| Distribution | Overall | Car-Car | Truck-Car | Car-Truck | Truck-Truck | $\chi^2$ |
|---|---|---|---|---|---|---|
| Log-Normal | -365935 | -273963 | -43161 | -32813 | -10243 | 11511 |
| Gamma | -349881 | -264511 | -40681 | -29884 | -9127 | 11356 |
| Weibull | **-346687** | **-263588** | **-40303** | **-28605** | -8605 | 11172 |
| Normal | -360322 | -276102 | -42211 | -28617 | **-8522** | 9741 |

**Table 4.4 Estimated Parameters of Time Headway Distributions**

| Vehicle-following Type | Model | Parameters | |
|---|---|---|---|
| Overall | Weibull | Shape | 2.082 |
| | | Scale | 2.148 |
| Car-Car | Weibull | Shape | 1.950 |
| | | Scale | 2.033 |
| Car-Truck | Weibull | Shape | 3.042 |
| | | Scale | 2.699 |
| Truck-Car | Weibull | Shape | 2.040 |
| | | Scale | 2.083 |
| Truck-Truck | Normal | Mean | 2.399 |
| | | Standard deviation | 0.875 |

Furthermore, the estimated distributions are truncated to constraint the time headway values within a reasonable range. In particular, the lower bound of the time headway distributions is set as 0. The upper bound of the following time headways is set as 4 seconds (Wasielewski 1979, Dong et al. 2015).

4.3.1.1 *Standstill Distance*

Figure 4.4 shows the histograms of vehicle type–specific and overall standstill distances. The Car-Car and Overall plots follow similar shape and are slightly right skewed. The Car-Truck and Truck-Car plots follow a bimodal shape. The two peaks in the plots correspond to medium size and large trucks, both of which are considered as trucks in the analysis. The sample size of Truck-Truck pairs is too small to draw a firm conclusion, and thus was not included in the plot.

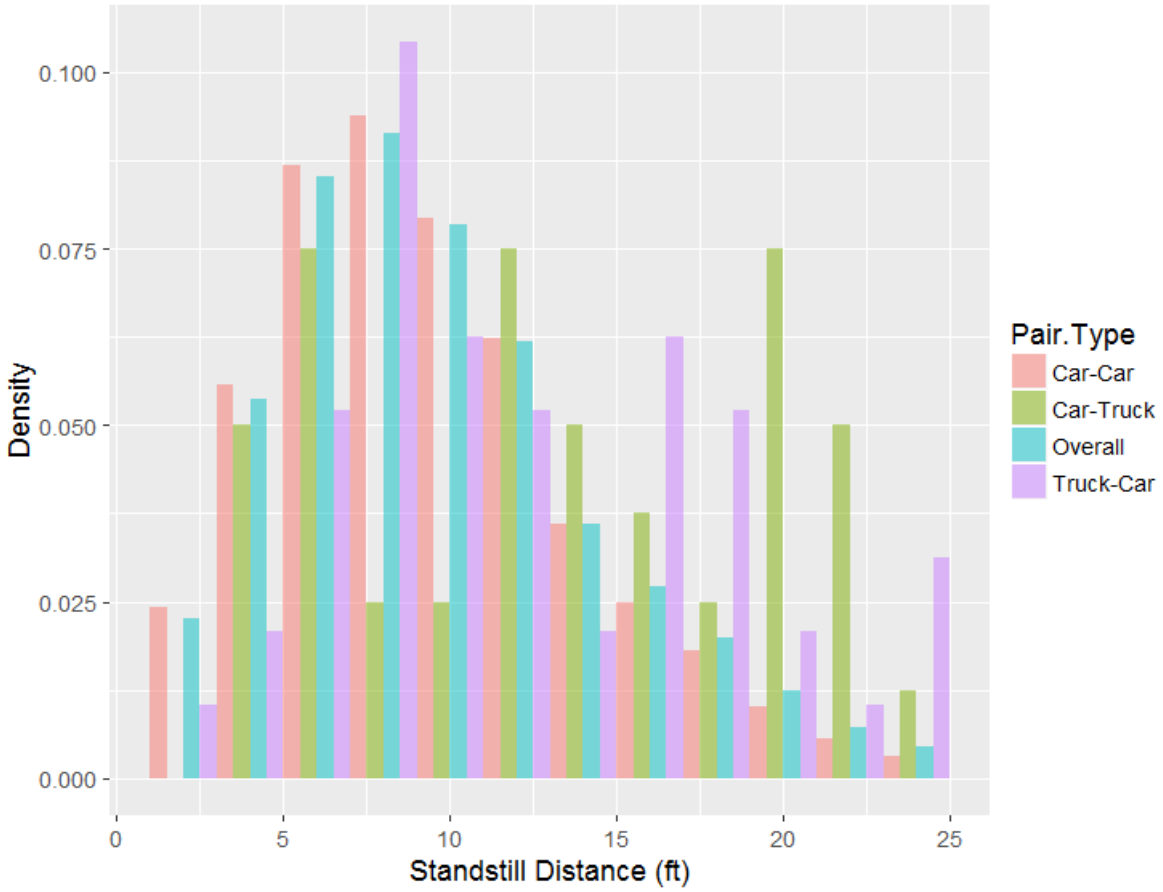


**Figure 4.5 Histograms of Vehicle Type–specific and Overall Standstill Distances**

Table 4.5 lists the means and standard deviations of standstill distances. Note that Car-Car is the most frequent vehicle-following type, which dominates the distribution of overall data. As expected, the mean standstill distances of Car-Truck and Truck-Car are significantly larger than the mean of Car-Car. The means of Car-Truck and Truck-Car standstill distances do not significantly different from each other. Because of the limited sample size of Truck-Truck case, the mean standstill distance of Truck-Truck is not a reliable estimate. In the subsequent analysis, Car-Truck, Truck-Car and Truck-Truck are combined as one group, named Truck.

**Table 4.5 Summary Statistics of Standstill Distances**

| | Overall | Car-Car | Car-Truck | Truck-Car | Truck-Truck |
|---|---|---|---|---|---|
| Number of observations | 1,238 | 1,140 | 40 | 48 | 10 |
| Mean | 9.67 | 9.41 | 13.35 | 12.37 | 11.07 |
| Standard deviation | 4.53 | 6.32 | 4.73 | 5.78 | 3.69 |

Table 4.6 lists the log likelihood values of using log-normal, gamma, normal and Weibull distributions to fit the standstill distances of Overall, Car-Car and Truck data. The test statistics, $\chi^2$, are all greater than the critical value of the chi-square distribution at the 5% significance level (i.e. 5.99). This indicates that Car-Car and Truck standstill distance models are significantly different from the overall standstill distance distribution. Based on the log likelihood values, log-normal distribution is the best fit of Car-Car data. Gamma distribution is the best fit of Overall data. Weibull distribution is the best fit of Truck data. The best fit models are used as input in the subsequent analysis. Note that the differences between alternative distributions for the standstill distances of these groups are small. The estimated parameters of the best fit distributions are listed in Table 4.7.

**Table 4.6 Log-likelihood Ratio Test Statistic of Standstill Distance Models**

| Distribution | Overall | Car-Car | Truck | $\chi^2$ |
|---|---|---|---|---|
| Log-Normal | -3647.64 | **-3320.06** | -313.76 | 27.64 |
| Gamma | **-3604.40** | -3277.99 | -309.36 | 34.1 |
| Weibull | -3611.13 | -3282.28 | **-307.80** | 42.1 |
| Normal | -3680.66 | -3341.68 | -311.36 | 55.24 |

**Table 4.7 Estimated Parameters for Standstill Distance Distributions**

| Vehicle-following Type | Model | Parameters | |
|---|---|---|---|
| Overall | Gamma | Shape | 3.95 |
| | | Rate | 0.41 |
| Car-Car | Log-Normal | Log Scale | 2.11 |
| | | Shape | 0.54 |
| Truck | Gamma | Shape | 4.17 |
| | | Rate | 0.33 |

Furthermore, the estimated distributions are truncated to constraint the standstill distance values within a reasonable range. In particular, the lower and upper bounds of the standstill distance distributions are set as 0 and 25 feet, respectively (Dong et al. 2015).

### 4.3.2 Speed-Density Relationship

Four different input modes are used to derive speed-density relationships for different car-following models:

1) Use overall mean time headway and mean standstill distance as deterministic parameters. This is the typical input method in traffic simulation software.
2) Use the means of vehicle type–specific time headways as deterministic time headway parameter. Use the means of Car-Car and Truck standstill distances as deterministic standstill distance parameters.
3) Use overall distributions of time headways and standstill distances as stochastic parameters.
4) Use distributions of vehicle type–specific time headways as stochastic time headway parameter. Use standstill distance distributions of Car-Car and Truck group as stochastic standstill distance parameters.

Using Pipes car-following model, the speed-density relationships of the congested regime can be generated. Figure 4.5(a) plots the speed-density curves generated using deterministic parameters. Considering the vehicle type-specific time headways and standstill distances, four speed-density curves are plotted, corresponding to different vehicle-following types. The vehicle following type-specific speed-density curves are fairly close to the overall speed-density curve. Figure 4.5(b) plots the speed-density region generated using stochastic parameters. By changing the time headway and standstill distance parameters from constants to distributions, the speed-density relationship change from a curve to a region. The stochastically distributed parameters result in a wide region of speed-density plot. The speed-density region generated by vehicle type-specific distributions is slightly larger than the one generated by the overall distribution.

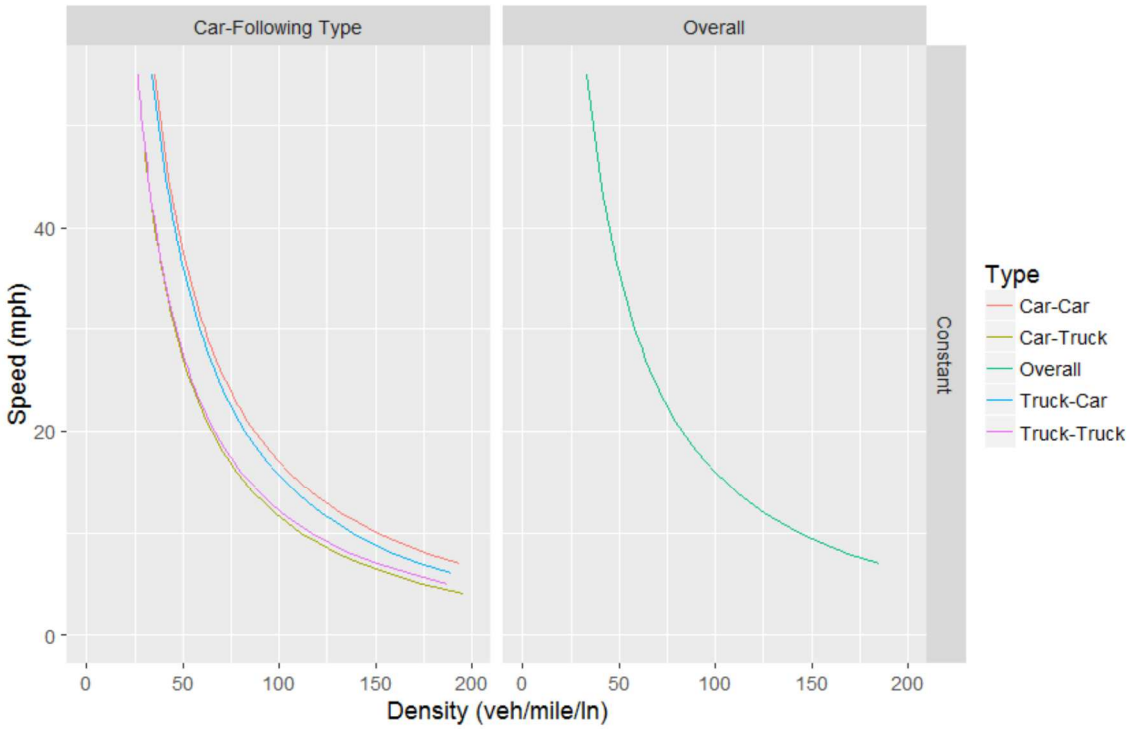


a) Deterministic Parameters

**Figure 4.6 Speed-Density Plots Generated Using Pipes Car-following Model**

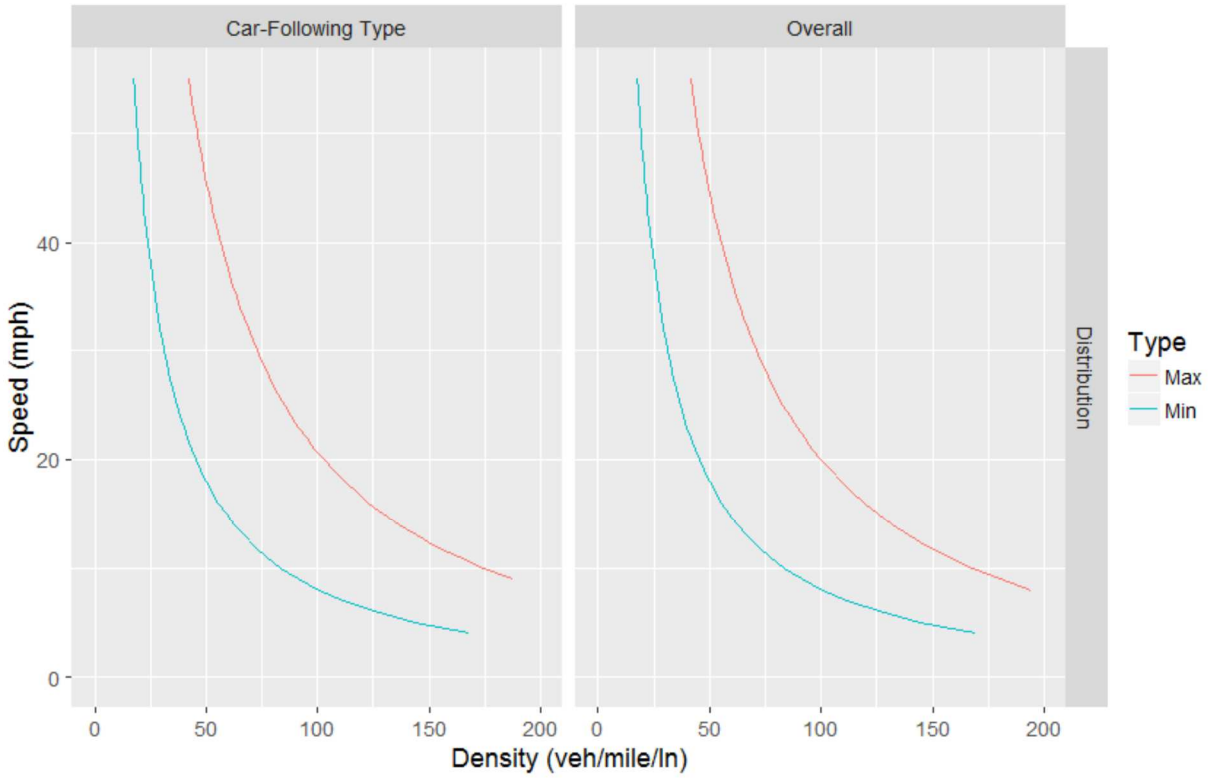


b) Stochastic Parameters

**Figure 4.7 Speed-Density Plots Generated Using Pipes Car-following Model (Continued)**

The speed-density relationships of the congested regime estimated using the stead-state INTEGRATION car-following model are shown in Figure 4.6. Similar to Pipes car-following model results, using vehicle following type-specific distributions results in the largest region of speed-density plot (see Figure 4.6(b)). As shown in Figure 4.6(a), with deterministic time headway and standstill distance parameters, the speed-density curve generated using Car-Car parameters is significantly different from the one associated with from Car-Truck parameters.

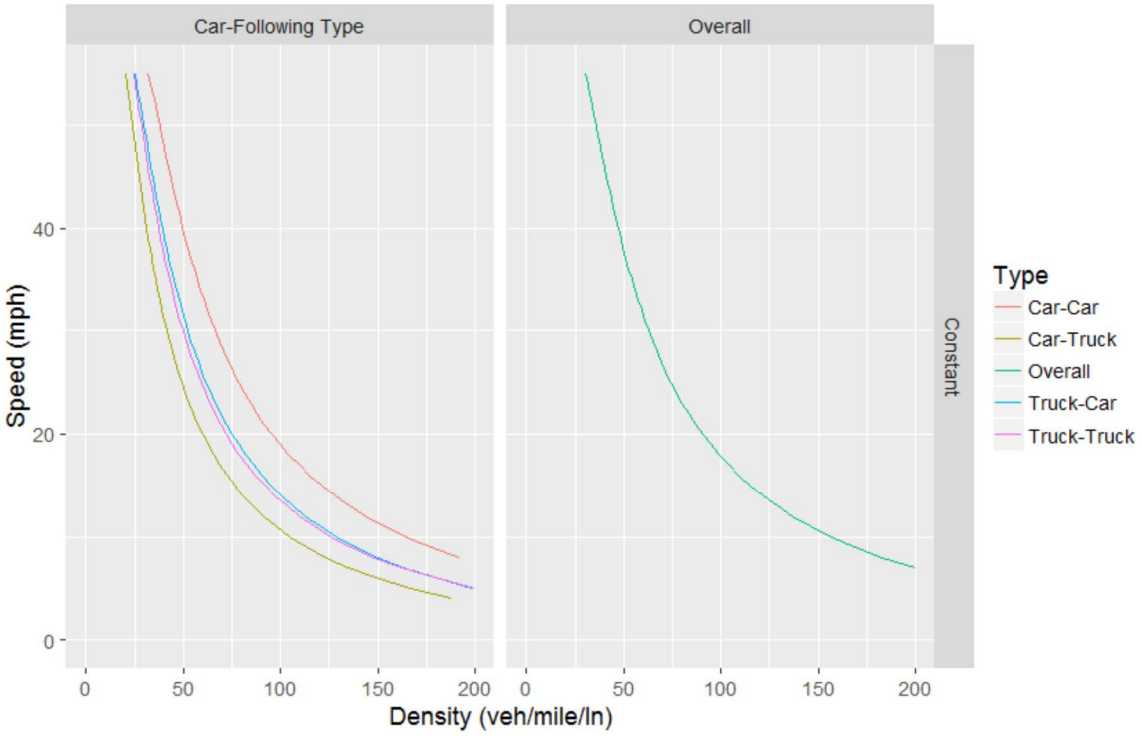


a) Deterministic Parameters

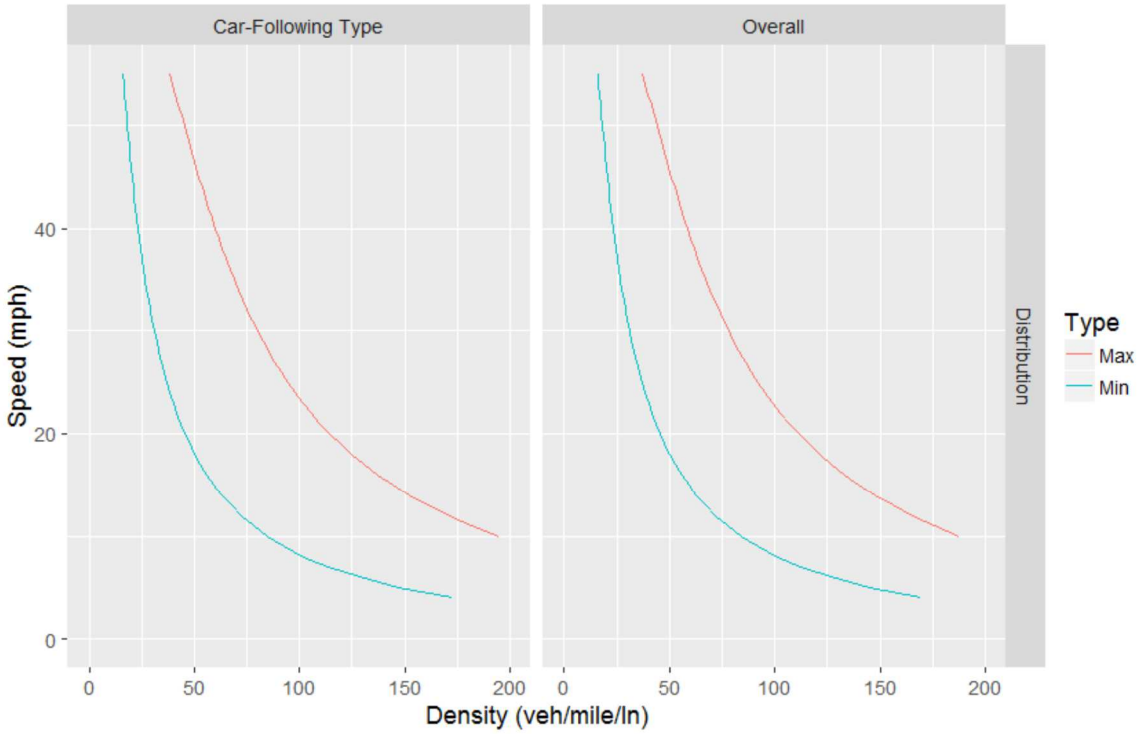


b) Stochastic Parameters

**Figure 4.8 Speed-Density Plots Generated Using INTEGRATION Car-following Model**

By comparing Figure 4.5 and 4.6, INTEGRATION Car-following model generate a larger speed-density region than Pipes model when using the vehicle type-specific distributions of time headways and standstill distances. The vehicle type-specific distribution input mode results in the largest speed-density region, as this input mode considered both systematic and stochastic user heterogeneity in drivers' behavior. The vehicle type-specific distribution input mode of steady state Pipes car-following model is used to compare with VISSIM simulation output and field measurements in the next subsections.

### 4.3.3 Comparison of stochastic Pipes car-following model and VISSIM simulation

The North America default values (PTV Group, 2014), as well as mean, 5$^{th}$ percentile and 95$^{th}$ percentile of the measured time headways and standstill distances were used as input to run VISSIM simulations. The time headway is converted to the CC1 parameter in VISSIM based on the following equation:

$$CC1 = Time\ Headway - \frac{CC0 + Leader\ Vehicle\ Length}{Speed} \tag{4.27}$$

where

$CC1$ is the desired time headway for the following vehicle.

$CC0$ is the standstill distance between two vehicles.

By varying the standstill distance in VISSIM and keeping other parameters as default, the scatter plot of speed-density results are shown in Figure 4.7. There is a difference between

speed-density regions of VISSIM result and the proposed method. The reason could be that the VISSIM has more parameters than proposed model to control the simulation results.

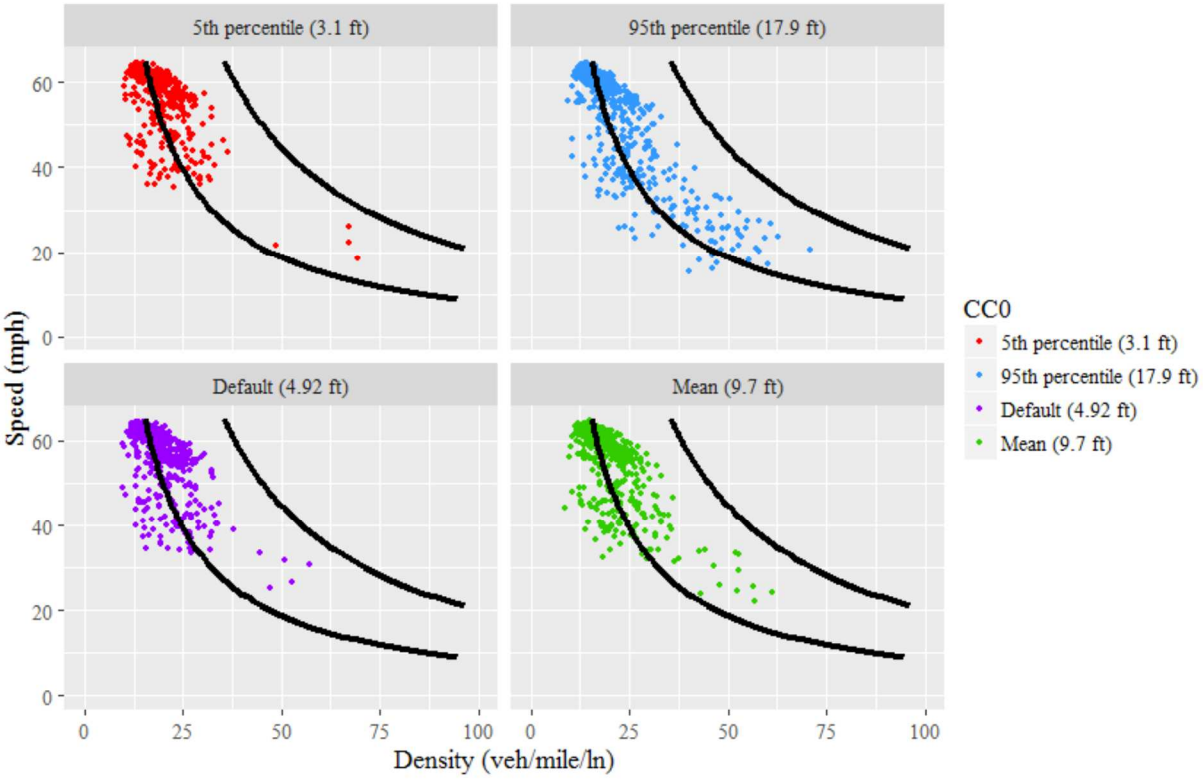


**Figure 4.9 Simulated Speed-Density Plots Using VISSIM with Varying CC0 Parameters, Compared with Speed-Density Region Generated Using Stochastic Pipes Car-following Model**

By changing the CC1 in VISSIM and keeping other parameters as default, the scatter plot of the simulated speeds and densities are shown in Figure 4.8. Similar to Figure 4.7, VISSIM tends to overestimate the congestion effect compared to the proposed method.

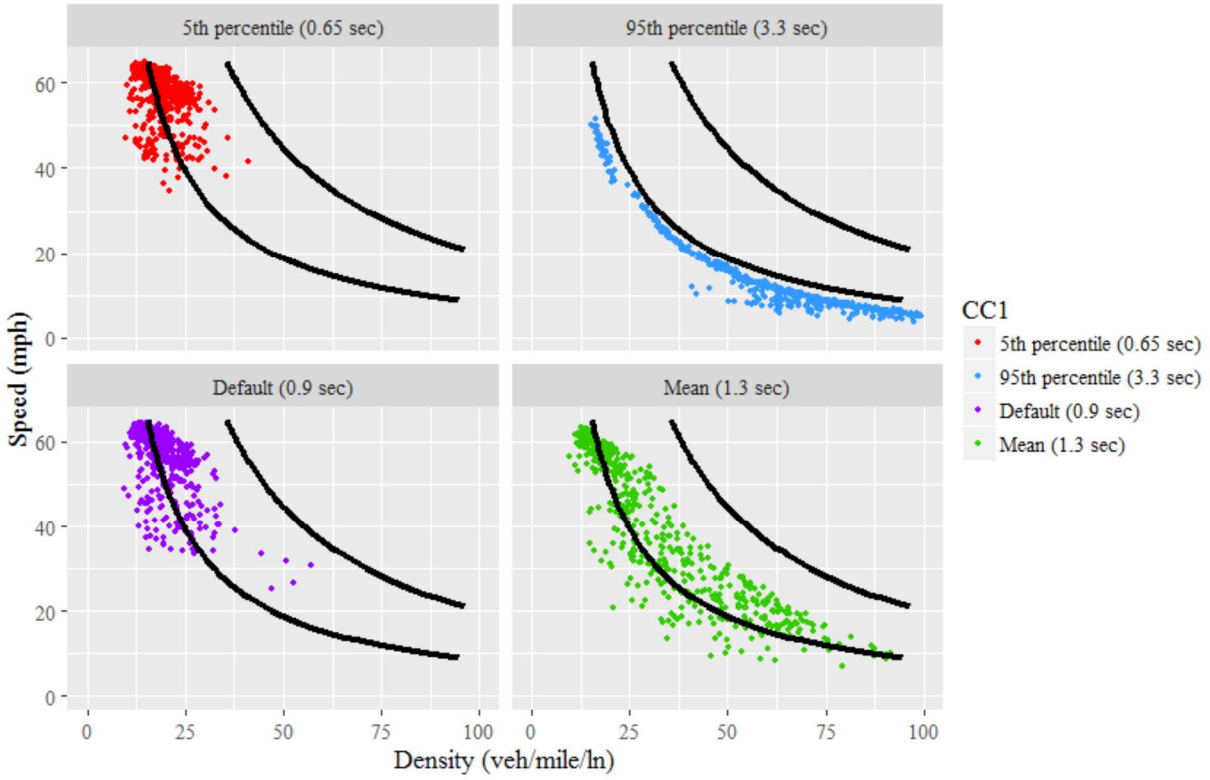


**Figure 4.10 Simulated Speed-Density Plots Using VISSIM with Varying CC1 Parameters, Compared with Speed-Density Region Generated Using Stochastic Pipes Car-following Model**

### 4.3.4 Comparison of vehicle type-specific distribution input mode results and field data

Traffic volume and speed data were collected from I-235, which is one of the busiest freeways in West Des Moines, Iowa, USA. The data from four sensors on I-235 are select to compare with the speed-density region generated using stochastic Pipes car following model. The data used in the analysis are collected during peak hours (7:00-9:00 a.m. and 4:00-7:00 p.m.) on weekdays from January 1st to December 31st 2015.

Figure 4.9 plots the speed density data under congested traffic conditions. Most field data fall in the region generated from the stochastic Pipes car following model that incorporated vehicle type-specific time headway and standstill distance distributions. Some of the outliers may be caused by the conservative drivers who drive slowly and leave large time headway. Moreover, sensor errors can also result these outliers. By comparing Figures 4.7, 4.8 and 4.9, we can see that the speed-density region generated by the proposed method can better represent real world observations than VISSIM simulation outputs.

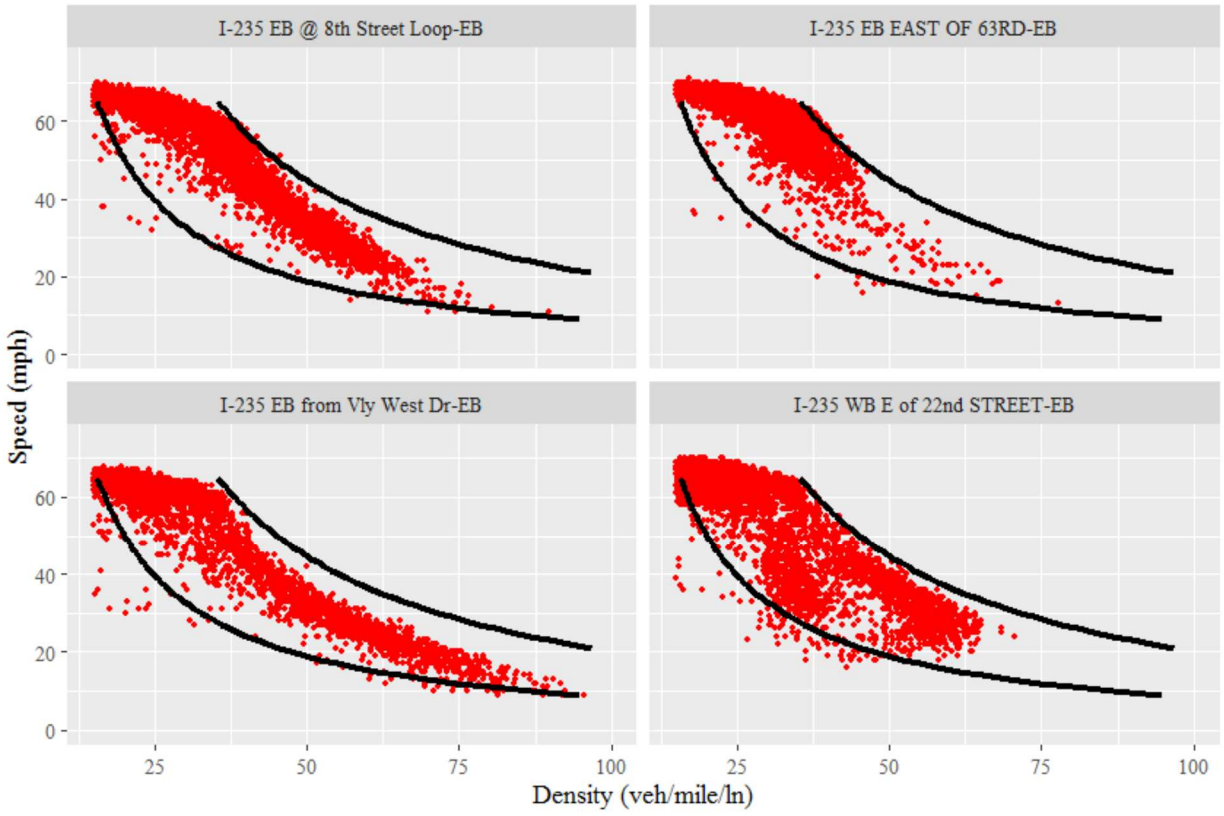


**Figure 4.11 Field Data Compared with Speed-Density Region Generated Using Stochastic Pipes Car-Following Model**

### 4.3.5 Travel time reliability

One potential application of the proposed stochastic car-following model is to estimate travel time reliability. A Monte Carlo simulation is performed to generate the travel times under congested conditions. The weight of free-flow state is calculated according to the framework shown in Figure 4.2. Travel time reliability measures are calculated according to Eq. 4.3~4.7.

The study freeway corridor of I-235, where radar sensor data and INRIX data were collected, is shown in Figure 10. The locations of radar sensor are shown in Figure 4.10. The study freeway segment is 13-mile long.

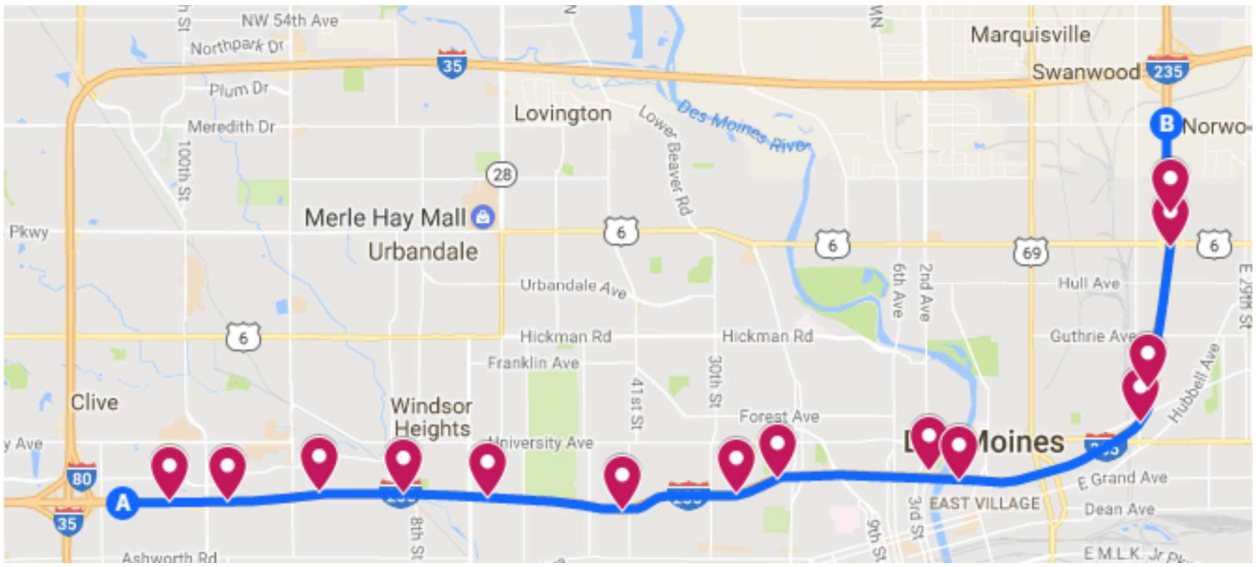


**Figure 4.12 Study Freeway Segment (Google 2017)**

In addition, multiple VISSIM simulation runs were executed to generate congested and uncongested travel times. The traffic volumes of each mainline segment, on-ramp and off-

ramp for both congested and uncongested scenarios are shown in Table 8. CC0 and CC1 are set as 9.7 feet and 1.3 seconds, respectively, based on the measured mean time headway and standstill distance as described in Section 4.3.1. Other parameters are kept as default. Ten replications were performed for each scenario. The planning horizon of the simulation is set as 5,400 seconds, including 1,800-second warm up period. The travel time of each vehicle traveling from the starting point to the ending point was collected, excluding the data during the warm-up period.

**Table 4.8 Traffic Volumes in Congested and Uncongested Conditions**

| Segment Description | | | | Volume (veh/hr) | |
|---|---|---|---|---|---|
| **ID** | **Station** | **Type** | **Lanes** | **Congested** | **Uncongested** |
| 1 | I-235 EB to VALLEY WEST-EB | Mainline | 3 | 5727 | 1733 |
| 2 | I-235 EB to VALLEY WEST-EB-R | Off-ramp | 1 | 340 | 108 |
| 3 | Ramp 1 | On-ramp | 1 | 285 | 438 |
| 4 | I-235 EB from Vly West Dr-EB | Mainline | 3 | 5672 | 2063 |
| 5 | I-235 EB from Vly West Dr-EB-R | On-ramp | 1 | 230 | 580 |
| 6 | Ramp 2 | Off-ramp | 1 | 146 | 114 |
| 8 | I-235 WB E of 22nd STREET-EB | Mainline | 3 | 5756 | 2529 |
| 7 | I-235 WB E of 22nd STREET-EB-R | On-ramp | 1 | 874 | 308 |
| 9 | Ramp 3 | Off-ramp | 1 | 470 | 455 |
| 10 | I-235 EB @ 8th Street Loop-EB | Mainline | 3 | 6160 | 2382 |
| 11 | I-235 EB @ 8th Street Loop-EB-R | On-ramp | 1 | 408 | 307 |
| 12 | Ramp 4 | Off-ramp | 1 | 176 | 52 |
| 13 | I-235 EB EAST OF 63RD-EB | Mainline | 3 | 6392 | 2637 |

**Table 4.9 Traffic Volumes in Congested and Uncongested Conditions (Continued)**

| Segment Description | | | | Volume (veh/hr) | |
|---|---|---|---|---|---|
| **ID** | **Station** | **Type** | **Lanes** | **Congested** | **Uncongested** |
| 14 | I-235 EB EAST OF 63RD-EB-R | On-ramp | 1 | 644 | 360 |
| 15 | Ramp 5 | On-ramp | 1 | 127 | 127 |
| 16 | Ramp 6 | Off-ramp | 1 | 982 | 665 |
| 17 | I-235 at 42nd STREET EB-EB | Mainline | 4 | 6181 | 2459 |
| 18 | Ramp 7 | On-ramp | 1 | 12 | 380 |
| 19 | Ramp 8 | On-ramp | 1 | 39 | 172 |
| 20 | I-235 EB 28th STREET-EB | Mainline | 4 | 6232 | 3011 |
| 21 | Ramp 9 | Off-ramp | 1 | 751 | 385 |
| 22 | Ramp 10 | On-ramp | 1 | 35 | 35 |
| 23 | I-235 EB to MLK-EB | Mainline | 4 | 5516 | 2661 |
| 24 | Ramp 11 | Off-ramp | 1 | 278 | 346 |
| 25 | Ramp 12 | Off-ramp | 1 | 171 | 214 |
| 26 | Ramp 13 | Off-ramp | 1 | 310 | 387 |
| 27 | Ramp 14 | On-ramp | 1 | 120 | 120 |
| 28 | Ramp 15 | On-ramp | 1 | 15 | 15 |
| 29 | I-235 WB WEST END of BRIDGE-EB | Mainline | 4 | 4892 | 1848 |
| 30 | Ramp 16 | On-ramp | 1 | 247 | 462 |
| 31 | I-235 EB at WALKWAY-EB | Mainline | 4 | 5139 | 2310 |
| 32 | I-235 EB at WALKWAY-EB-R | Off-ramp | 1 | 375 | 108 |
| 33 | I-235 EB 9th STREET WALL-EB | Mainline | 3 | 4764 | 1460 |
| 34 | I-235 EB 9th STREET WALL-EB-R | Off-ramp | 1 | 460 | 42 |
| 35 | Ramp 17 | On-ramp | 1 | 46 | 524 |
| 36 | Ramp 18 | Off-ramp | 1 | 373 | 273 |
| 37 | Ramp 19 | On-ramp | 1 | 2 | 46 |
| 38 | Ramp 20 | Off-ramp | 1 | 59 | 59 |
| 39 | I-235 EB at E 21st St-EB | Mainline | 3 | 3920 | 1656 |
| 40 | I-235 WB at Washington-EB | Mainline | 3 | 3920 | 1656 |
| 41 | I-235 WB at Washington-EB-R | On-ramp | 1 | 374 | 192 |

**Table 4.10 Traffic Volumes in Congested and Uncongested Conditions (Continued)**

| Segment Description | | | | Volume (veh/hr) | |
|---|---|---|---|---|---|
| **ID** | **Station** | **Type** | **Lanes** | **Congested** | **Uncongested** |
| 42 | Ramp 21 | Off-ramp | 1 | 20 | 164 |
| 43 | Ramp 22 | On-ramp | 1 | 57 | 107 |
| 44 | Ramp 23 | Off-ramp | 1 | 642 | 317 |
| 45 | I-235 NB EUCLID LOOP-EB | Mainline | 3 | 3689 | 1474 |
| 46 | I-235 NB EUCLID LOOP-EB-R | On-ramp | 1 | 216 | 52 |
| 47 | Ramp 24 | On-ramp | 1 | 201 | 10 |
| 48 | I-235 NB from EUCLID-EB | Mainline | 3 | 4106 | 1536 |
| 49 | I-235 NB from EUCLID-EB-R | On-ramp | 1 | 425 | 144 |

The travel time reliability measures calculated using INRIX travel time data are compared with the reliability measures obtained from the proposed model and VISSIM. As shown in Table 4.9, both the proposed model and VISSIM overestimated the mean travel time and underestimated the travel time reliability of the study freeway corridor. The errors in the proposed travel time estimation model could be attributed to simplified two component travel time distribution. Travel time distribution of free-flow state is simplified to Dirac delta distribution. Consequently, the travel times larger than free-flow travel time are ignored. The proposed model generates more accurate reliability measures than VISSIM with less computational time.

**Table 4.11 Comparison of Travel Time Reliability Measures Calculated using Different Methods**

| | Mean | 95th percentile travel time | Planning time index | Buffer time | Buffer time index | CPU Time (sec) |
|---|---|---|---|---|---|---|
| INRIX | 17.26 | 24.69 | 1.90 | 7.43 | 0.43 | — |
| Model-based | 17.52 | 24.30 | 1.87 | 6.78 | 0.39 | 278 |
| VISSIM | 17.78 | 23.90 | 1.84 | 6.12 | 0.34 | 1198 |

## 4.4 Summary

This chapter presented a method to estimate travel time reliability measures by incorporating standstill distance and time headway distributions in car-following models. First, standstill distance and following time headway distributions were estimated based on data collected at various locations in Iowa, USA. For time headway distributions, five distributions were estimated for different vehicle following type, Car-Car, Truck-Truck, Car-Truck and Truck-Car and Overall. For standstill distance distributions, Car-Car standstill distances are significantly different from Car-Truck and Truck-Car standstill distances. Since Truck-Truck, Car-Truck and Truck-Car standstill distance distributions do not significantly differ from each other, Car-Truck, Truck-Car and Truck-Truck data are combined as one group. Thus, three distributions were estimated for Car-Car, Truck and Overall standstill distances. Second, time headway and standstill distance distributions are incorporated in the steady-state of FRESIM and INTEGRATION car-following models to generate speed-density relationships. The results showed that the vehicle type-specific distribution input could result in a speed-density region

that better replicate real world observations, compared to the speed-density curves generated using mean standstill distance and headway parameters. In addition, since the car-following logic within VISSIM under steady-state conditions reverts to the Pipes model, the results of vehicle type-specific distribution input mode incorporated in steady-state Pipes model is compared with the VISSIM simulation output. The results showed that the speed-density region derived from the steady-state Pipes model enclose most of the field data and outperforms VISSIM simulation output. Third, travel times under congested state are generated using the steady-state of Pipes car-following model with stochastic standstill distance and time headway parameters. The simplified two-component model is applied to estimate travel time reliability measures. The travel time reliability measures generated using the proposed model, VISSIM and INRIX data are compared. Both the proposed method and VISSIM the mean travel time and underestimated the travel time reliability of the study freeway corridor. The proposed method provides better estimates with less computational time, compared to VISSIM simulation.

In this study, I recommended that microsimulation models are modified to include the option for standstill distance and time headways to follow distributions as well as be set separately for different vehicle classes. The proposed model provided an accurate and fast way to estimate corridor-level travel time reliability considering heterogeneity in driver behavior in terms of following time headways and standstill distances. Moreover, the proposed method can estimate real-time travel time reliability. Considering stochastic driver behavior parameter, travel time reliability measures can be derived based on real time density.

# CHAPTER 5. TRAVEL TIME RELIABILITY IN URBAN FREEWAY WORK ZONES

This chapter aims to develop a framework to predict the capacity of work zone. And travel time reliability of work zone is estimated based on the predicted speed-density-volume relationship. This chapter is organized as follows. Section 5.1 introduces the background of the study. Section 5.2 describes the work zone and non-work zone data. The capacity prediction method is describes in section 5.3, as well as the travel time reliability estimation method. The results and summary of the findings are presented in Section 5.4 and Section 5.5, respectively.

## 5.1 Introduction

Due to an aging infrastructure and increasing demand on the transportation network, work zones increase continuously in United States. In particular, work zones on freeways usually cause serious disruptions to traffic, significant delays, and traffic unreliability. To mitigate the impact and plan proper strategies, forecasting the work zone capacity on an existing freeway is important. Moreover, estimating work zone travel time and its reliability helps agencies to evaluate the performance of the freeway segment.

## 5.2 Data Description

Traffic flow, speed, and occupancy data were collected by Iowa Department of Transportation (DOT) by placing Wavetronix radar sensors in the work zone areas. The work zones in Iowa during 2015 and 2016 construction seasons are investigated in this study.

- Work zone data: Traffic volume, speed and occupancy data collected when the work zone is active in 2015 and 2016. The date and time of work zones are determined by combining traveler information from Iowa DOT and the contractor reports and plans. Traffic data collected during an active work zone is categorized as work zone data.
- Non-work zone data: Traffic volume, speed and occupancy data collected from May to August in 2015 at a freeway section in Des Moines where no work zone presented. The freeways in Des Moines have the high annual average daily traffic and the detailed information, such as incident, special events and weather reports. As shown in Table 1, the traffic data from station "I-35/80 EB WEST of 2nd AVENUE-EB" is treated as the baseline data because this location has the same speed limit and similar geometric characteristic as the work zones in Quad Cities and Sioux City.
- Before work zone data: Traffic data collected from May to August in 2014 from the sensors located in the same or nearby locations of the work zone sites in 2015 and 2016.

The configurations of the work zones are summarized in Table 5.1. The layouts of study work zones are shown in Figure 5.1. Traffic data were collected during the daytime. Due to the lack of vehicle classification information in the dataset, the truck percentage is estimated based on annual average daily traffic data published by Iowa DOT.

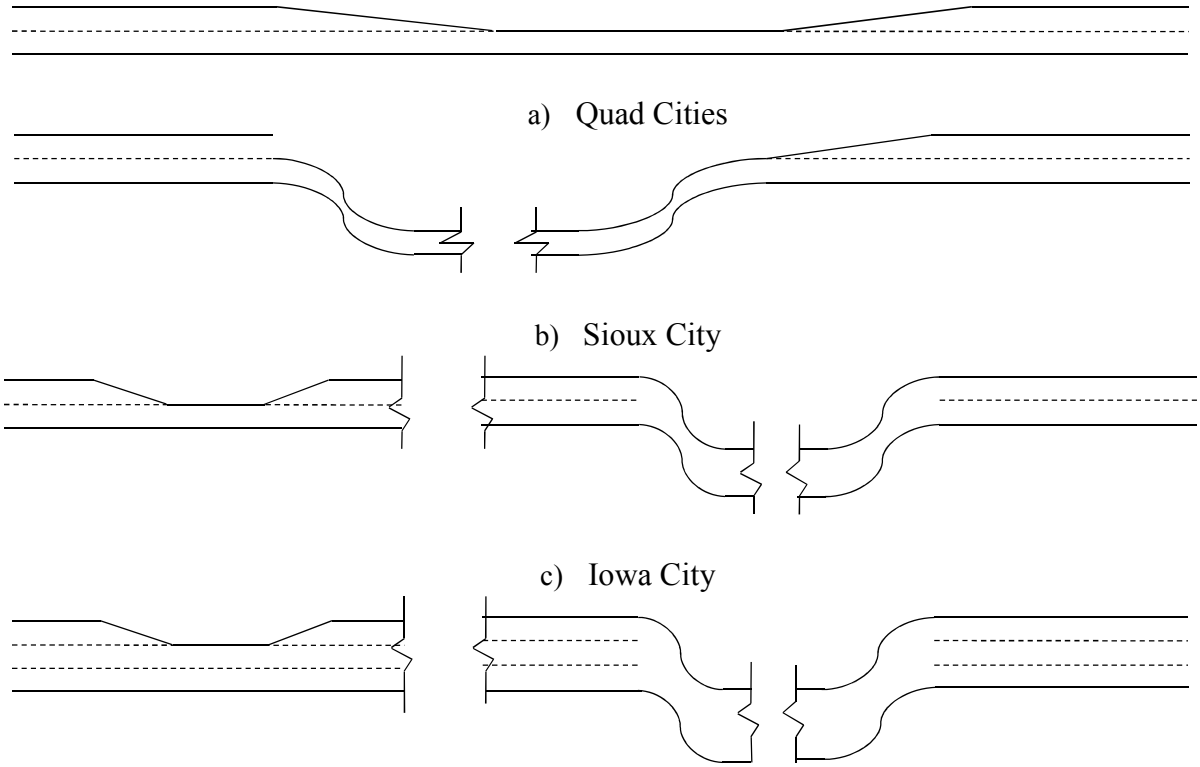


**Figure 5.1 Work Zone Layouts**.

Based on the volume and speed measurements, the density is calculated by Eq. 5.1.

$$\boldsymbol{k = q/V} \tag{5.1}$$

where,

V is speed (mph);

$k$ is density (veh/mile/ln); and

$q$ is volume (veh/hr/ln).

**Table 5.1 Summary of Work Zone Configurations**

| Condition | City | Station ID | Truck Percentage | Speed limit (mph) | | Control Type | Barrier Type | Area Type | Work Time |
|---|---|---|---|---|---|---|---|---|---|
| | | | | Original | Work zone | | | | |
| Work Zone | Quad Cities | IWZ 3077 WB | 29% | 65 | 55 | Lane closure | Concrete | Urban | Daylight |
| | Quad Cities | IWZ 3542 EB | 29% | 65 | 55 | Lane closure | Concrete | Urban | Daylight |
| | Sioux City | IWZ 3074 NB | 13% | 65 | 55 | Lane closure and shift | Concrete | Urban | Daylight |
| | Iowa City | I-380 NB North of Swan Lake to North of River | 15% | 70 | 55 | Lane closure /shift | Plastic Drum | Urban | Daylight |
| | Council Bluffs | CBDS 12 WB | 17% | 65 | 55 | Lane closure /shift | Concrete | Urban | Daylight |
| Before Work Zone | Iowa City | I-380 NB North of Swan Lake to North of River | 15% | 70 | — | — | — | — | — |
| | Council Bluffs | CBDS 10 WB | 17% | 65 | — | — | — | — | — |
| Non-work Zone | Des Moines | I-35/80 EB WEST of 2nd AVENUE-EB | 14% | 65 | — | — | — | — | — |

To focus on the impact of work zones, the data collected on rainy days are removed based on the weather data obtained from Road Weather Information System (RWIS). In addition, raw data was filtered to remove erroneous measurements. First, the faulty sensors or sensor data that violated traffic flow theory were removed. Wells et al. (2008) proposed a method that used the relationship of speed, volume and occupancy to detect loop sensor errors. In this study, this method was applied for radar sensor anomaly detection, as shown in Eq. 5.2. According to the technical reports from FHWA (2004) and Minnesota Department of Transportation (Minge et al., 2012), the possible vehicle length is from 10 to 75 ft. The average effective vehicle lengths (AEVL) are within this range. . For traditional loop sensors the detection range (DTR) is the length of the detector. However, for Wavetronix HD sensors, one virtual line was used to represent the detector (Wavetronix LLC 2013). Thus, only AEVL was used to identify anomalies. After calculating the AEVL of each observation using speed, volume and occupancy collected from Wavetronix sensors, the ones that were out of the normal range were marked as data error and removed from the dataset. The overall reduction rate is 24.50%.

$$AEVL = \frac{5280VO}{q} \tag{5.2}$$

where
AEVL is the average effective vehicle length (feet); and
O is occupancy.

## 5.3 Methodology

Work zones may reduce speed limits and affect capacity (HCM 2016). Thus, it can have significantly impact on travel time variability (Edwards and Fontaine, 2012). This section

presents an approach to predict work zone capacity based on logistic speed-density model. Based on the predicted capacity, a work zone travel time and its reliability estimation method is proposed.

### 5.3.1 Work Zone Capacity

As described in literature review (Chapter 2.3), speed-volume-density relationship has been applied to estimate work zone capacities. To overcome the limitation of multi-regime models, single-regime is used in this study. Many single-regime models have been developed to describe the speed-volume-density relationship, including Greenshields model (Greenshields, 1934), Greenberg model (Greenberg, 1959), Underwood model (Underwood, 1961), Northwestern model (Drake et al., 1967), Del Castillo model (Castillo and Benítez, 1995a, 1995b) and five-parameter logistic speed-density model (MacNicholas' model). Wang et al. (2011) compared these models and found that the five-parameter logistic speed-density model outperformed other models in terms of fitting the field observations. Consequently, five-parameter logistic speed-density model is used in this study.

Based on logistic speed-density model, the relationship between free-flow speed and work zone capacity is derived. The work zone free-flow speed is a function of speed limits and work zone configurations (HCM 2016). The relationship between turning density of the logistic model and the free-flow speed is also derived to predict speed-density and speed-volume relationships.

According to MacNicholas' model, the function of general logistic speed-density relationship is expressed as Eq. 5.3.

$$\boldsymbol{V = V_b + \frac{V_f - V_b}{\left(1+exp\left(\frac{k-k_t}{\theta_1}\right)\right)^{\theta_2}}} \tag{5.3}$$

where,

$V_f$ is the free flow speed (mph);

$V_b$ is the average speed under stop and go conditions (mph);

$k_t$ is the turning point that the speed–density curve transitions from free flow to congested flow (veh/mile/ln);

$\theta_1$ is the scale parameter; and

$\theta_2$ is the parameter that controls the lopsidedness of the curve.

From Eq. 5.3, traffic density can be derived as follows:

$$k = k_t + \theta_1 \log\left[exp\left(\frac{log\left(\frac{V_f - V_b}{V - V_b}\right)}{\theta_2}\right) - 1\right] \tag{5.4}$$

By substituting Eq. 5.4 into Eq. 5.1, the speed-volume function is derived as follows:

$$q = k_t V + \theta_1 \log\left[exp\left(\frac{log\left(\frac{V_f - V_b}{V - V_b}\right)}{\theta_2}\right) - 1\right] V \tag{5.5}$$

The relationship between turning point ($k_t$) and inflection point ($k_{IP}$) in the five-parameter logistic model is written in Eq. 5.6 (Wang et al., 2011).

$$k_t = k_{IP} + \theta_1 \log(\theta_2) \tag{5.6}$$

Where,

$k_{IP}$ is the inflection point, where the logistic speed-density curve switches from being concave to convex.

Moreover, $k_t$ has a linear relationship with $\theta_1$ and $\theta_2$ (Wang et al. 2011). In order to remove the collinearity between $k_t$ and $\theta_1$, $\theta_2$ , $\alpha$ is introduced as turning parameter. In other words, $k_t$ is represented by a formula of $\alpha, \theta_1, \theta_2, V_b$ and $V_f$. When $\theta_2$ equal to 1, $k_t = k_{IP} = k_c$ (Wang et al., 2011). Therefore, we assume

$$k_c = k_{IP} + \alpha\, \theta_1 \log(\theta_2) \tag{5.7}$$

where

$k_c$ is the density at capacity (veh/mile/ln).

As a result,

$$V_c = V_b + \frac{V_f - V_b}{\left(1+\theta_2^{\alpha-1}\right)^{\theta_2}} \tag{5.8}$$

where

$V_c$ is the speed at capacity (mph).

Using the speed-volume relationship, the capacity is reached when the following two conditions are met:

$$\frac{\partial q}{\partial V} = \frac{\partial k}{\partial V} \cdot V + k = 0 \tag{5.9}$$

$$\frac{\partial^2 q}{\partial V^2} = \frac{\partial k}{\partial V} + \frac{\partial^2 k}{\partial V^2} \cdot V + \frac{\partial k}{\partial V} < 0 \tag{5.10}$$

The derivation of the first condition and the second condition are shown in Appendix A.

Based on the first condition (i.e. Eq. 5.9), the inflection density is derived as follows:

$$k_{IP} = \frac{\theta_1[V_b(1+\theta_2^{\alpha-1})^{\theta_2}+V_f-V_b](1+\theta_2^{\alpha-1})}{\theta_2^{\alpha}(V_f-V_b)} - \alpha\,\theta_1\log(\theta_2) \tag{5.11}$$

As a result,

$$k_t = \frac{\theta_1[V_b(1+\theta_2^{\alpha-1})^{\theta_2}+V_f-V_b](1+\theta_2^{\alpha-1})}{\theta_2^{\alpha}(V_f-V_b)} + (1-\alpha)\theta_1\log(\theta_2) \tag{5.12}$$

The derivation of Eq. 5.11 is shown in Appendix B.

Therefore, the modified five-parameter logistic speed-density relationship and the speed-volume relationship are shown as follows:

$$k = \frac{\theta_1[V_b(1+\theta_2^{\alpha-1})^{\theta_2}+V_f-V_b](1+\theta_2^{\alpha-1})}{\theta_2^{\alpha}(V_f-V_b)} + (1-\alpha)\theta_1\log(\theta_2) + \theta_1\log\left[exp\left(\frac{log\left(\frac{V_f-V_b}{V-V_b}\right)}{\theta_2}\right)-1\right] \tag{5.13}$$

$$q = \left[\frac{\theta_1[V_b(1+\theta_2^{\alpha-1})^{\theta_2}+V_f-V_b](1+\theta_2^{\alpha-1})}{\theta_2^{\alpha}(V_f-V_b)} + (1-\alpha)\theta_1\log(\theta_2) + \theta_1\log\left[exp\left(\frac{log\left(\frac{V_f-V_b}{V-V_b}\right)}{\theta_2}\right)-1\right]\right]V \tag{5.14}$$

Based on Eq. 5.12, the turning point changes with free flow speed, average speed at stop-and-go condition, $\theta_1$ , $\theta_2$ and $\alpha$. $\theta_1$ and $\theta_2$ are the shape parameters of the speed-density curves. In addition, two assumptions are made:

- During the work zone $V_b$, $\theta_1$ and $\theta_2$ remain the same as the ones before work zone.
- The same type of work zones have the same value of $\alpha$.

From the second condition derived from Eq. 5.10, the exponential function is always greater than 0. Since $\theta_1$ is positive, when $\left[\exp\left(\frac{\log\left(\frac{V_f-V_b}{V-V_b}\right)}{\theta_2}\right)-1\right]\times\theta_2\times(V-2V_b)+V$ is greater than 0, the condition stated in Eq. 5.10 is satisfied. As a result, we assume that

$$\left[\exp\left(\frac{\log\left(\frac{V_f-V_b}{V_c-V_b}\right)}{\theta_2}\right)-1\right]\times\theta_2\times(V_c-2V_b)+V_c>0 \tag{5.15}$$

When $V_c \geq 2V_b$, the second condition is satisfied.

As a result, the capacity is calculated as follows:

$$q_c = Max\ q,\ \ V\epsilon[2V_b, V_f] \tag{5.16}$$

By adopting the free-flow speed prediction method proposed by HCM (2016), a work zone capacity prediction framework is proposed, as follows:

Step 1: Calibrate the five-parameter logistic model using traffic data collected before work zones. The function "nls" in R statistics package (R Development Core Team, 2011) is utilized to fit the speed-density curve based on traffic data before work zones.

Step 2: Compute the standard deviation of free-flow speed distribution before work zone.

Step 3: Predict the mean work zone free-flow speed based on HCM (2016):

$$V_f = 9.95 + 33.49\times f_{sr} + 0.53\times f_s - 5.6\times f_{LCSI} - 3.94\times f_{Br} - 1.71\times f_{DN} - 1.45\times f_{Nr} \tag{5.17}$$

where

$f_{sr}$ is the ratio of the normal speed limit to the work zone speed limit;

$f_s$ is the speed limit of work zone (mph);

$f_{Br}$ is the barrier type, 0 for concrete, 1 for plastic cone or drum;

$f_{DN}$ indicates the time of the work zone; 1 for daytime, 0 for nighttime;

$f_{Nr}$ is the number of ramps within 3 miles upstream and 3 miles downstream from the midpoint of work zone; and

$f_{LCSI}$ is the lane closure severity index, $f_{LCSI} = \frac{total\ number\ of\ lanes}{number\ of\ open\ lanes^2}$.

Step 4: Determine $\alpha$ based on the work zone type.

Step 5: By assuming the standard deviations of the normally-distributed free-flow speeds during work zone are the same as before work zone, the 95$^{th}$ percentile and 5$^{th}$ percentile free-flow speeds of work zone can be derived, given the mean and the standard deviation of work zone free-flow speeds calculated in Step 3 and Step 2, respectively.

Step 6: Predict the range of work zone capacities using Eq. 5.14 and 5.16. In particular, $V_b$, $\theta_1$ and $\theta_2$ are determined in Step 1. $\alpha$ is determined in Step 4. The 95$^{th}$ percentile and 5$^{th}$ percentile free-flow speeds are determined in Step 5.

### 5.3.2 Work Zone Travel Time and Its Reliability Estimation

In the study of Newman (1986), a method is proposed to estimate segment speed by considering the impact factors, such as weather and lane closure, on freeway capacity and free-flow speed. Based on the modified logistic speed-density model proposed in section 5.3.1, the capacity, density at capacity and free flow speed of work zone can be derived. By using the

derived parameters in the Newman segment speed estimation model, the segment speed of work zone can be estimated. Accordingly, the travel time through the work zone is estimated.

According to the study of Newman (1986), the segment speed of work zone is calculated as follows:

$$S = FFS \times SAF + \left[1 - e^{ln\left(FFS \times SAF + 1 - \frac{C \times CAF}{45}\right) \times \frac{q}{C \times CAF}}\right] \quad (5.18)$$

where

S is the segment speed of the work zone (mph);

FFS is the original free-flow speed (mph);

SAF is the speed adjustment factor;

C is the original capacity (veh/hr/ln);

CAF is the capacity adjustment factor; and

q is segment flow rate (veh/hr/ln).

Free-flow speed, density at capacity and capacity of work zone can be estimated from the framework proposed in section 5.3.1. Consequently, Eq. 5.18 is modified as follows:

$$S = V_f + \left[1 - e^{ln\left(V_f + 1 - \frac{q_c}{k_c}\right) \times \frac{q}{q_c}}\right] \quad (5.19)$$

As a result, the travel time of work zone is calculated as follows:

$$T = \frac{L}{V_f + \left[1 - e^{ln\left(V_f + 1 - \frac{q_c}{k_c}\right) \times \frac{q}{q_c}}\right]} \times 60 \quad (5.20)$$

where,

T is the travel time (min); and

L is the length of work zone (mile).

For each measured work zone flow rate, the travel time is estimated by using Eq. 5.20. Moreover, the travel time reliability measures are derived based on the estimated travel times.

## 5.4 Result

### 5.4.1 Speed-Volume-Density Relationship

The observed and calibrated traffic speed-volume-density relationships for different work zones are compared with the non-work zone site. The calibrated parameters are shown in Table 5.2.

**Table 5.2 Parameters of Logistic Speed-Density Models**

| Data collection site | | $V_f$ (mph) | $V_b$ (mph) | $k_t$ (veh/mile/ln) | $\theta_1$ | $\theta_2$ | α |
|---|---|---|---|---|---|---|---|
| Typical Non-work Zone | | 69.39 | 5.14 | 34.95 | 7.61 | 0.35 | 0.489 |
| Work Zone | IWZ 3077 WB | 63.74 | 5.32 | 21.02 | 7.53 | 0.37 | -0.263 |
| | IWZ 3542 EB | 64.46 | 5.06 | 24.54 | 7.82 | 0.37 | -0.274 |
| | IWZ 3074 NB | 51.67 | 5.17 | 20.54 | 7.51 | 0.38 | -0.289 |

As shown in Figure 5.2 and Figure 5.3, free flow speeds and turning density are smaller at the work zone sites compared to the ones at the non-work zone site. The free flow speeds are decreased because of the reduction of speed limits. Moreover, the lane reduction and roadside objects could affect capacity which is related to free flow speed and turning density

in logistic speed-density relationship. Table 5.2 shows that the work zone speed-density curves have similar stop-and-go speed ($V_b$) and shape parameters ($\theta_1$ and $\theta_2$) as the typical non-work zone curve. $\theta_2$ controls the lopsidedness of the curve. And $\theta_1$ describes how fast the speed will drop with density increases. Based on the sensitivity analysis by Wang et al. (2011), jam density increases when shape parameters increases. Since jam density is driven by standstill distance, the shape parameters are related to standstill distance which may not be effected by work zone. Moreover, the stop-and-go speed ($V_b$) increases when the shape parameters ($\theta_1$ and $\theta_2$) increase. Since the work zone have similar shape parameters as non-work zone, the stop-and-go speeds are similar. Moreover, the values of turning parameter (α) at work zone sites are significantly smaller than the one at the non-work zone site. However, the values of turning parameter (α) at different work zones are similar. Besides free flow speed, turning parameter is another factor that impacts turning density. Moreover, turning density is highly related to capacity which depends on time headway. Therefore, the difference of turning parameters between work zone and non-work zone could be attributed to the time headway in work zone is larger than non-work zone, as described by Weng et al. (2014). Since the work zones have similar characteristics, such as original speed limit, speed limit during work zone and control type, the turning parameters are similar. In the subsequent analysis, α of work zones is set as -0.27.

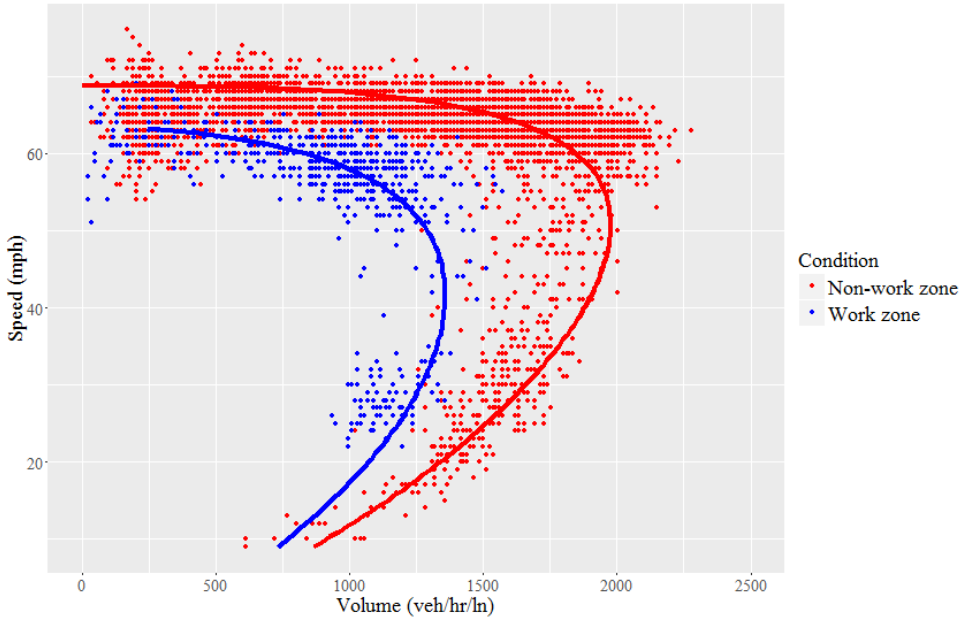


a) IWZ 3077

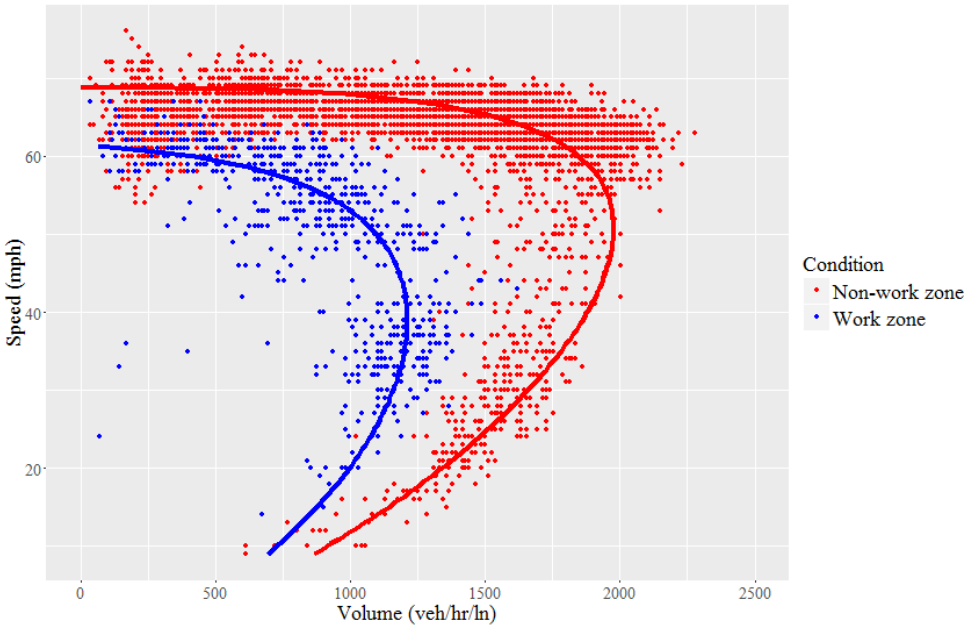


b) IWZ 3542

**Figure 5.2 Comparison of Typical Speed-volume Relationship of Non-work Zone and Work Zone.**

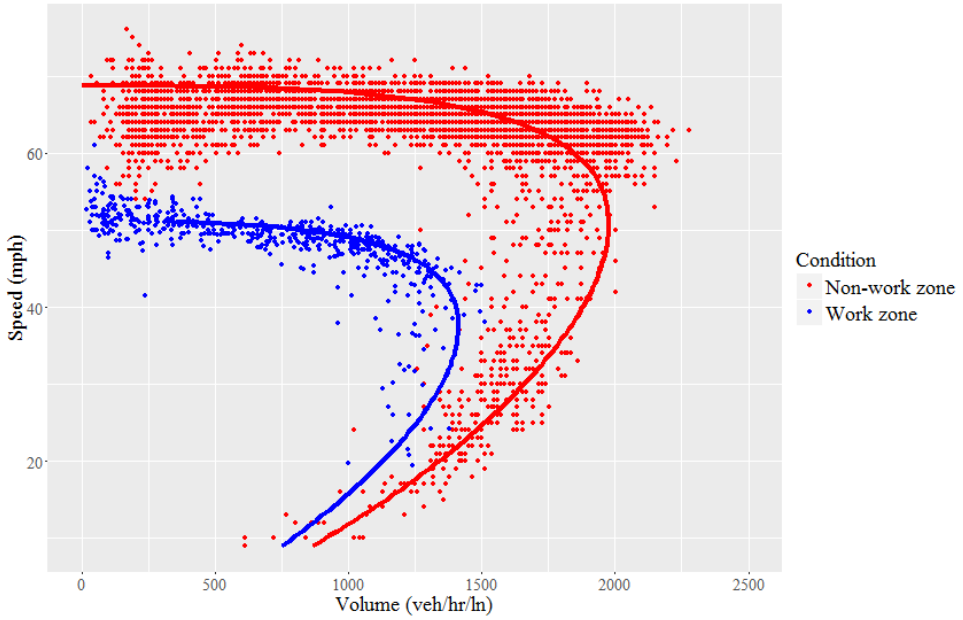


c) IWZ 3074

**Figure 5.3 Comparison of Typical Speed-volume Relationship of Non-work Zone and Work Zone. (Continued)**

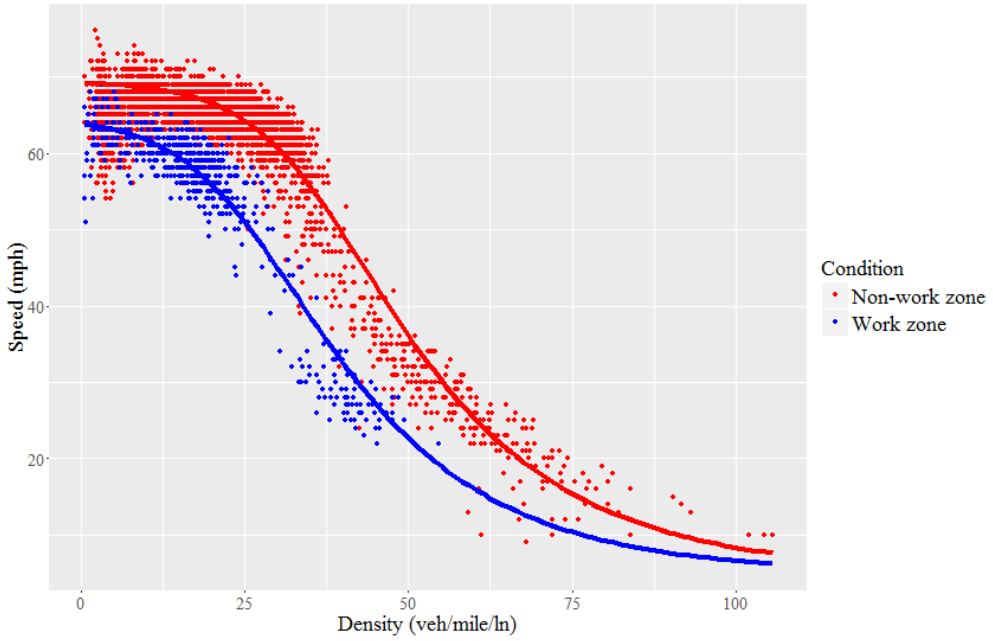


a) IWZ 3077

**Figure 5.4 Comparison of Typical Speed-density Relationship of Non-work Zone and Work Zone.**

b)

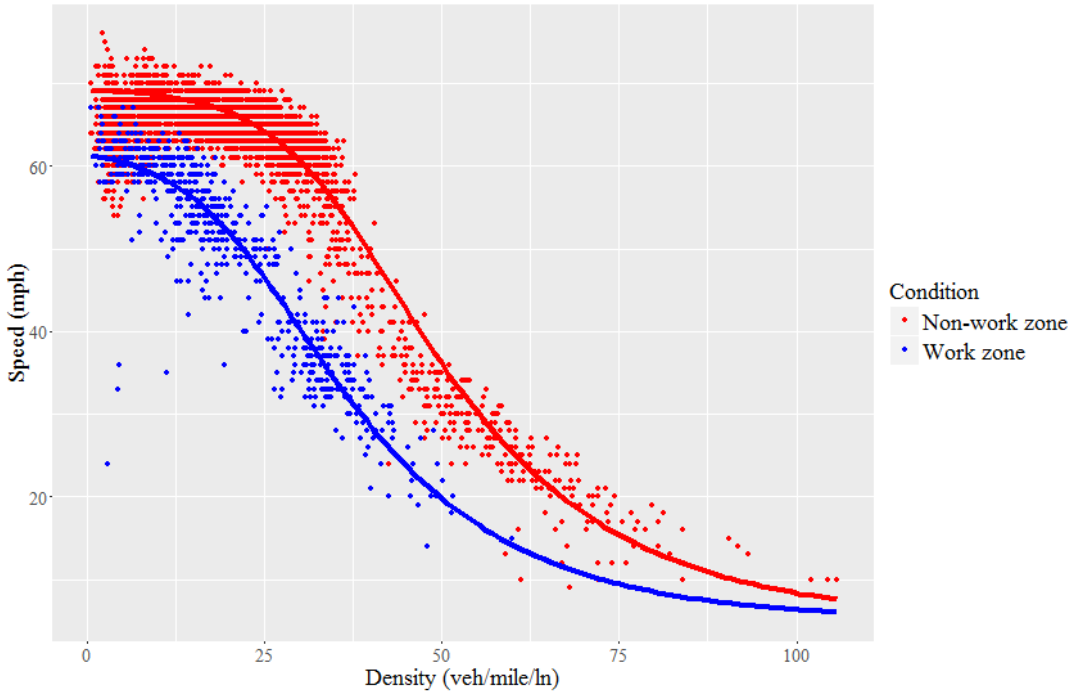


c) IWZ 3542

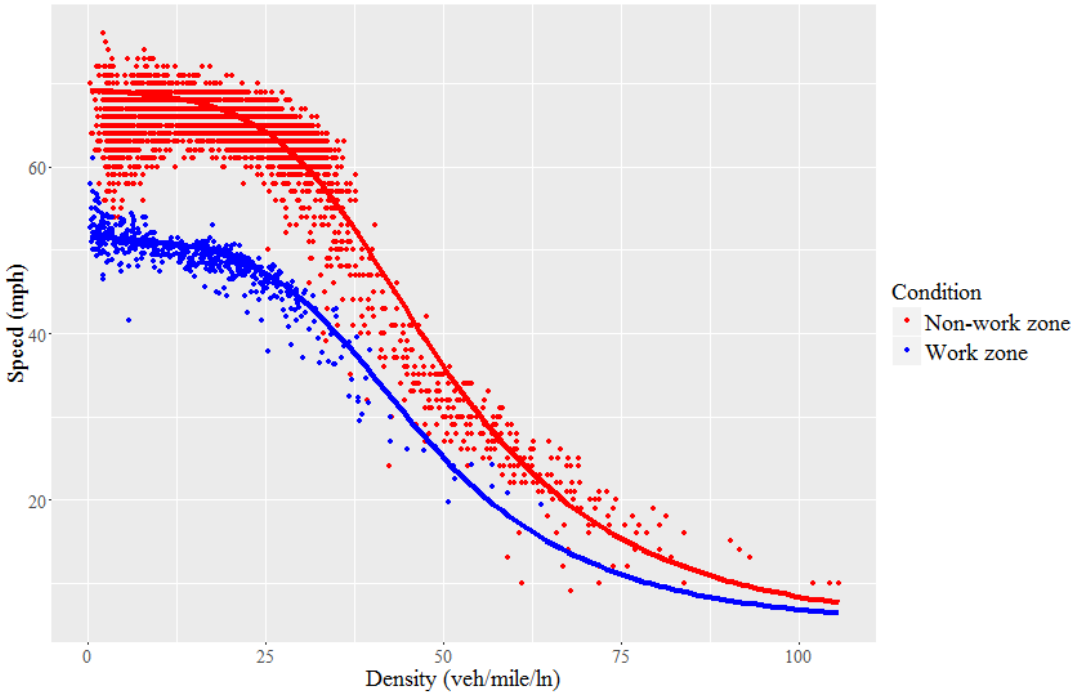


d) IWZ 3074

**Figure 5.5 Comparison of Typical Speed-density Relationship of Non-work Zone and Work Zone. (Continued)**

The diagnostic plots are shown in Figure 5.4. Figure 5.4(a) shows the residuals against the predicted speeds. The residuals randomly scattered around 0. Figure 5.4(b) shows the normal probability plot of the residuals. It shows that the residual distributions have the bell-shape and are slightly skewed. The skewness might be because that the least squares estimation does not require the residuals to be normally distributed as long as the mean squared error is minimized. The skewness may be eliminated by increasing the sample size. Generally, the modified five-parameter logistic model fits the field data well.

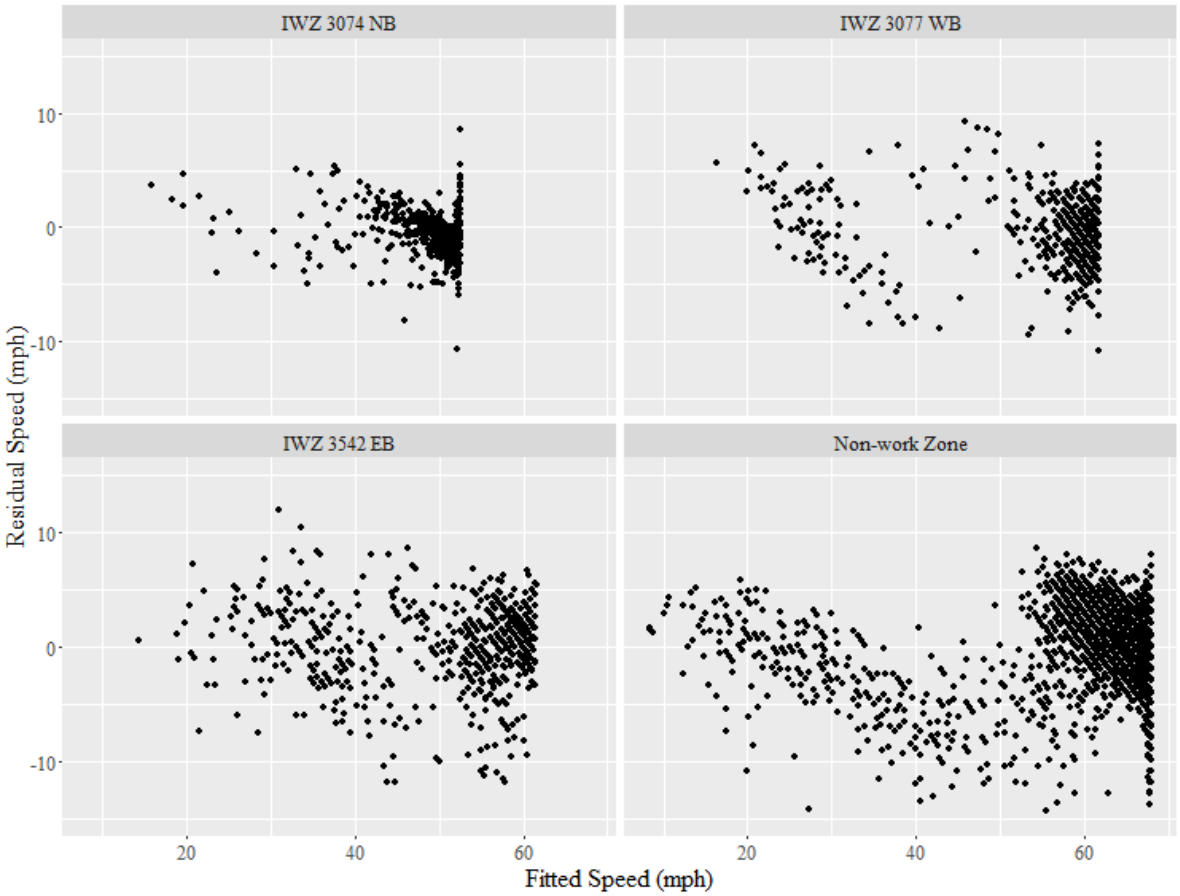


a) Residual plots

**Figure 5.6 Diagnostic Plots of Speed-density Relationships of Typical Non-work Zone and Work Zone.**

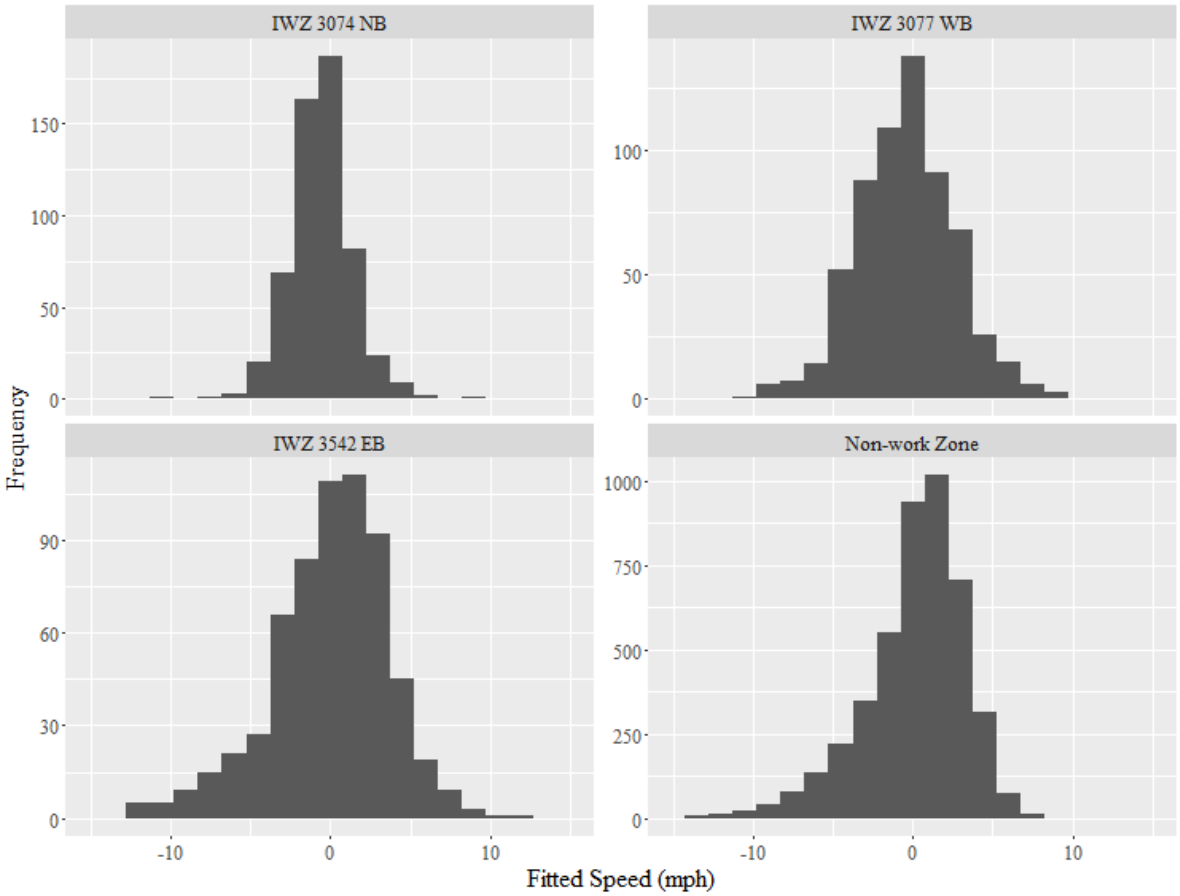


b) Residual distributions

**Figure 5.7 Diagnostic Plots of Speed-density Relationships of Typical Non-work Zone and Work Zone. (Continued)**

### 5.4.2 Performance Evaluation of Capacity Prediction Framework

The speed-volume-density relationships before and after work zone started are compared, as shown in Figure 5.5 and Figure 5.6, respectively. In order to investigate the relationship between work zone capacity and the free-flow speed, $V_b, \theta_1$ and $\theta_2$ are calibrated by using the before work zone data and are assumed to remain the same during the work zone. Based on the predicted free-flow speed range, the range of capacity can be predicted, which

covers the capacity estimated from the work zone data. The estimated work zone speed-volume-density relationship fall into the predicted speed-volume-density range. For the work zone in Iowa City, the predicted capacity range is slightly smaller than the observed capacity range. One reason is that the predicted free-flow speed range is smaller than the observed free-flow speed range at the work zone, while we assumed the same standard deviation of free-flow speeds before and during work zone.

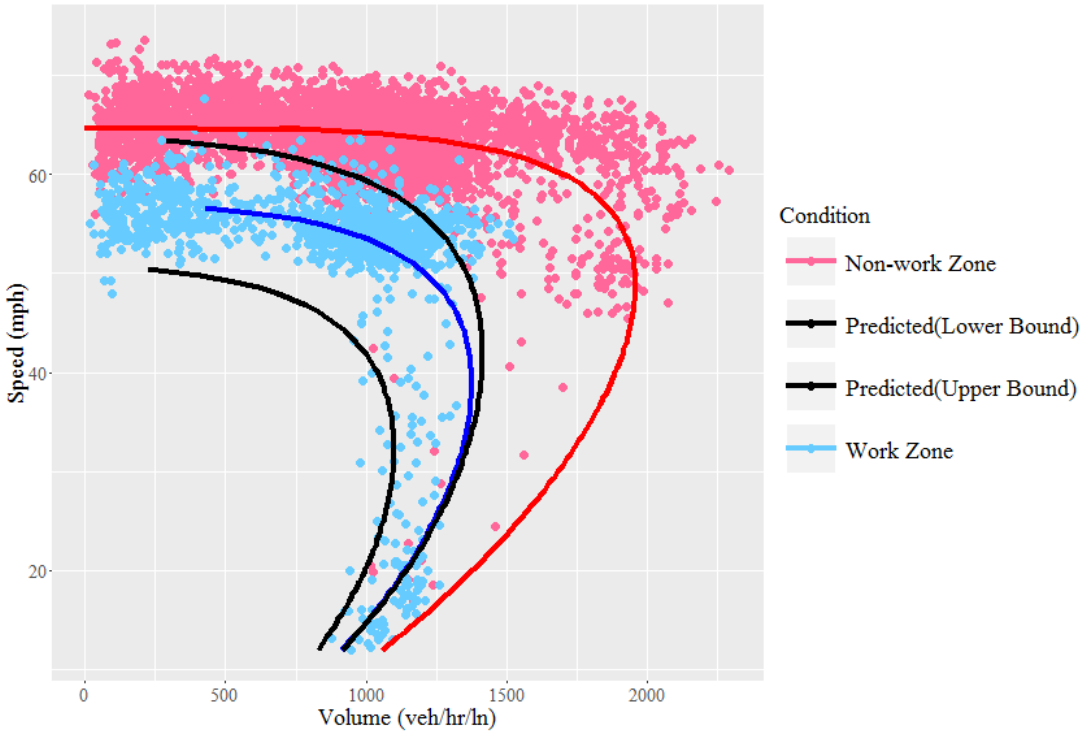


a) Council Bluffs

**Figure 5.8 Speed-volume Relationships Before and During Work Zone**

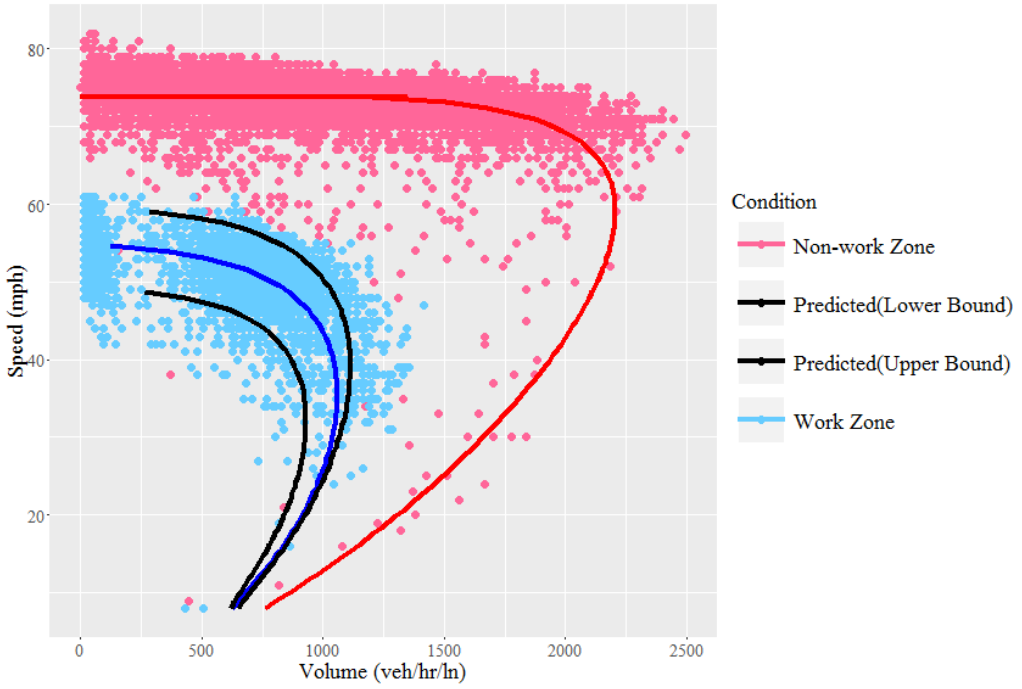


b) Iowa City

**Figure 5.9 Speed-volume Relationships Before and During Work Zone (Continued)**

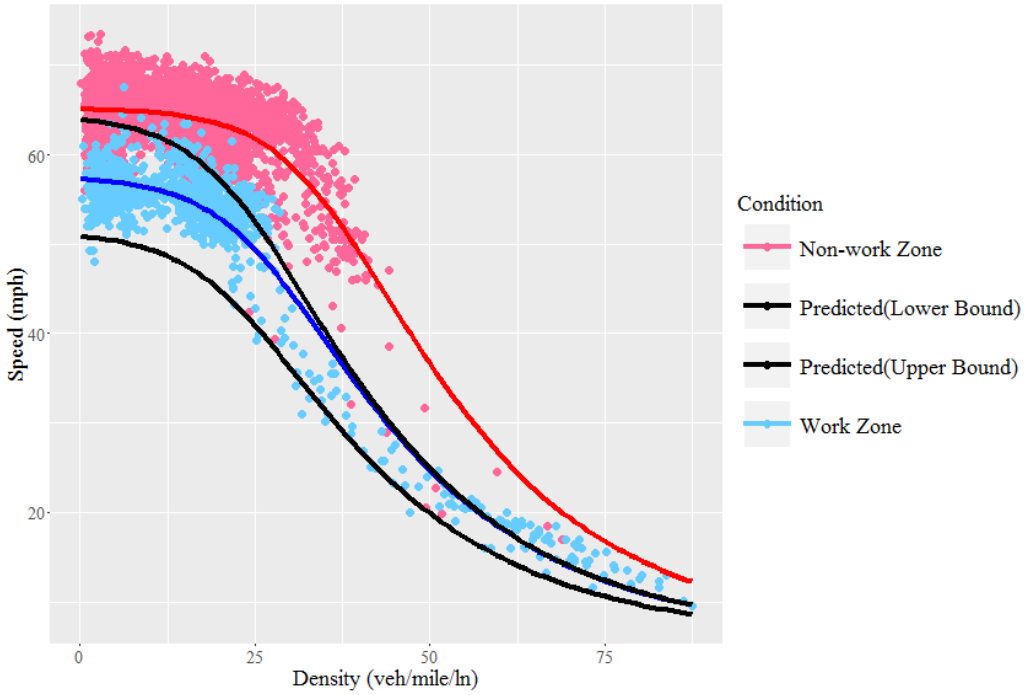


a) Council Bluffs

**Figure 5.10 Speed-density Relationships Before and During Work Zone**

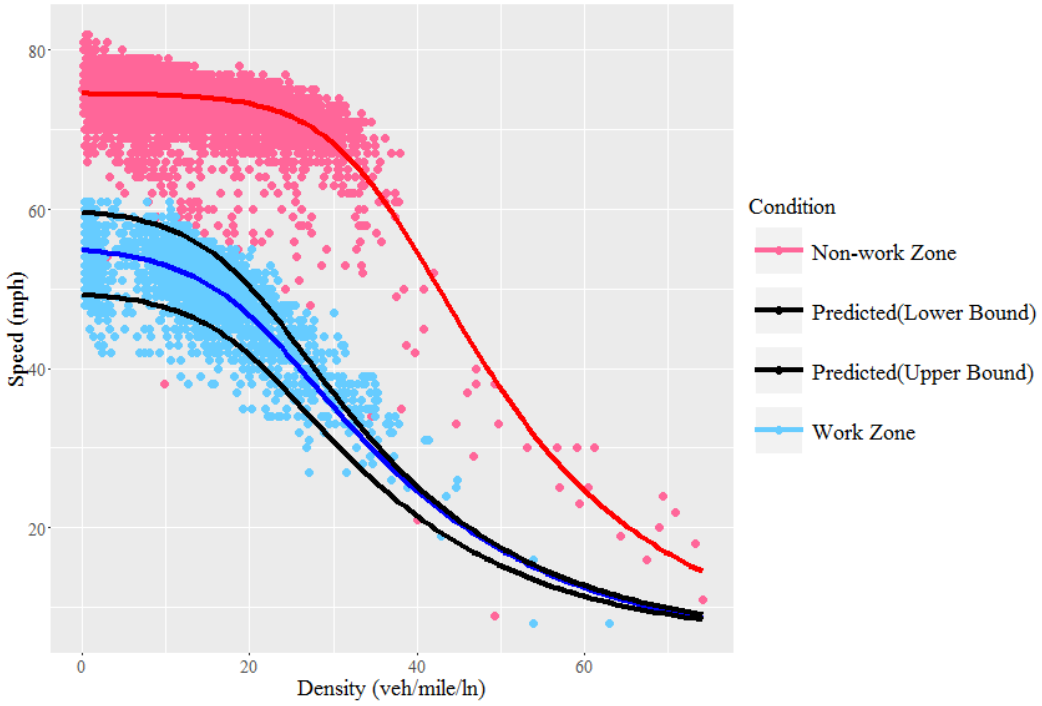


b) Iowa City

**Figure 5.11 Speed-density Relationships Before and During Work Zone (Continued)**

The diagnostic plots are shown in Figure 5.7. Figure 5.7(a) shows the residuals against the predicted speeds. The residuals randomly scattered about 0, with some outliers. Figure 5.7(b) shows the normal probability plot of the residuals. It shows that the residual distributions have the bell-shape and are slightly skewed.

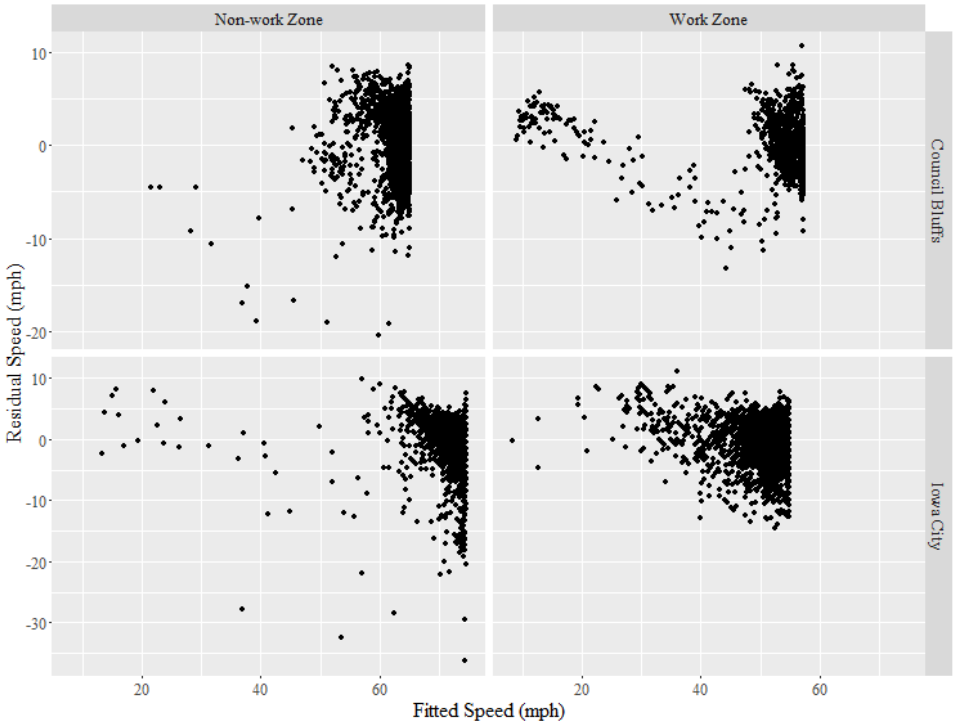


a) Residual plots

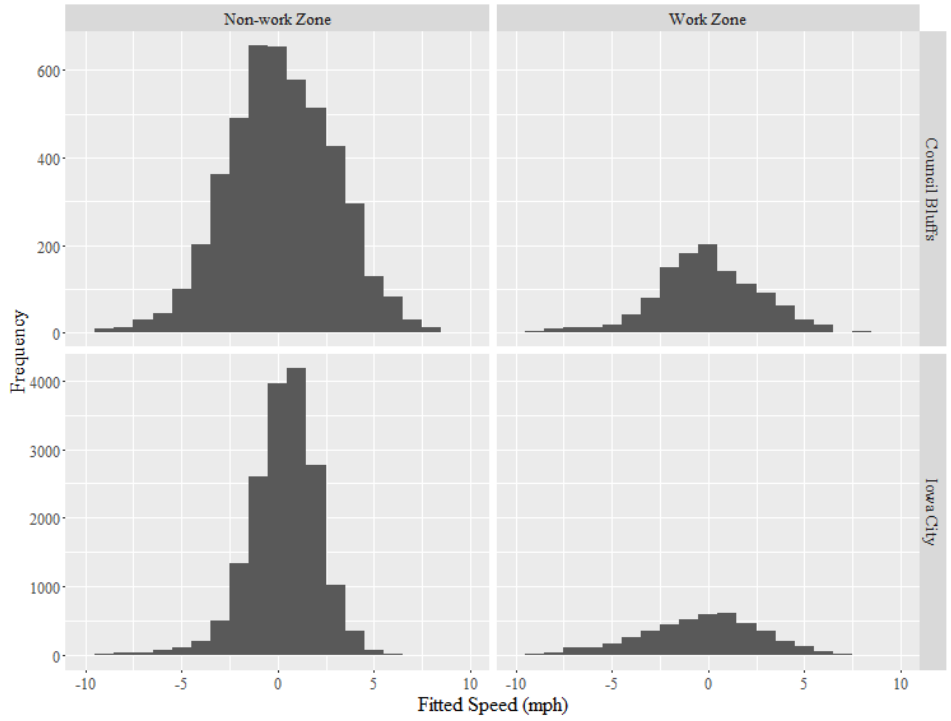


b) Residual Distributions

**Figure 5.12 Diagnostic Plots of Speed-density Relationships Before-and During Work Zone**

Additionally, the predicted capacity is compared with the capacity estimated using WorkZoneQ software, HCM and the maximum 15-minute flow rate. As shown in Table 5.3, the modified five-parameter logistic model generates similar results as WorkZoneQ and HCM. The maximum 15-minute volume tends to overestimate capacity, compared to logistic model and WorkZoneQ. Moreover, most of the estimated capacities using logistic model, HCM, and WorkZoneQ are within the predicted capacity range. The upper bound of the predicted capacity, which is based on 95th percentile of free-flow speeds, is close to the maximum 15-min flow rate. The lower bound of the predicted capacity is based on 5th percentile of free-flow speeds. As expected, the work zone in Iowa City, which has a larger free-flow speed reduction, has a lower capacity. The work zones that have similar free-flow speed reduction demonstrate similar capacities.

**Table 5.3 Capacities from Proposed Method, HCM, WorkZoneQ and Maximum 15-min Flow Rate**

| City | Work Zone | Maximum 15-min Flow Rate(veh/hr/ln) | Estimated Capacity (veh/hr/ln) | | | Predicted Capacity (veh/hr/ln) | |
|---|---|---|---|---|---|---|---|
| | | | HCM | Logistic Model | WorkZone Q | Upper bound | Lower bound |
| Quad Cities | IWZ 3077 WB | 1572 | 1239 | 1267 | 1296 | 1392 | 1128 |
| Quad Cities | IWZ 3542 EB | 1488 | 1245 | 1206 | 1296 | 1318 | 1129 |
| Sioux City | IWZ 3074 NB | 1512 | 1394 | 1413 | 1313 | 1455 | 1156 |
| Iowa City | I-380 NB North of Swan Lake to North of River | 1296 | 1199 | 1058 | 1424 | 1114 | 933 |
| Council Bluffs | CBDS 12 WB | 1524 | 1517 | 1376 | 1313 | 1414 | 1100 |

In Figure 5.8, the lower and upper bounds of the capacity predicted by the proposed method (i.e. the shaded area) is compared with the results reported in the literature. The predicted capacities are located in the capacity range of the literature. However, the prediction tend to be lower than the work zone capacities in the literature. One of main reasons is that maximum observed volume is used as capacities in the most of the literatures.

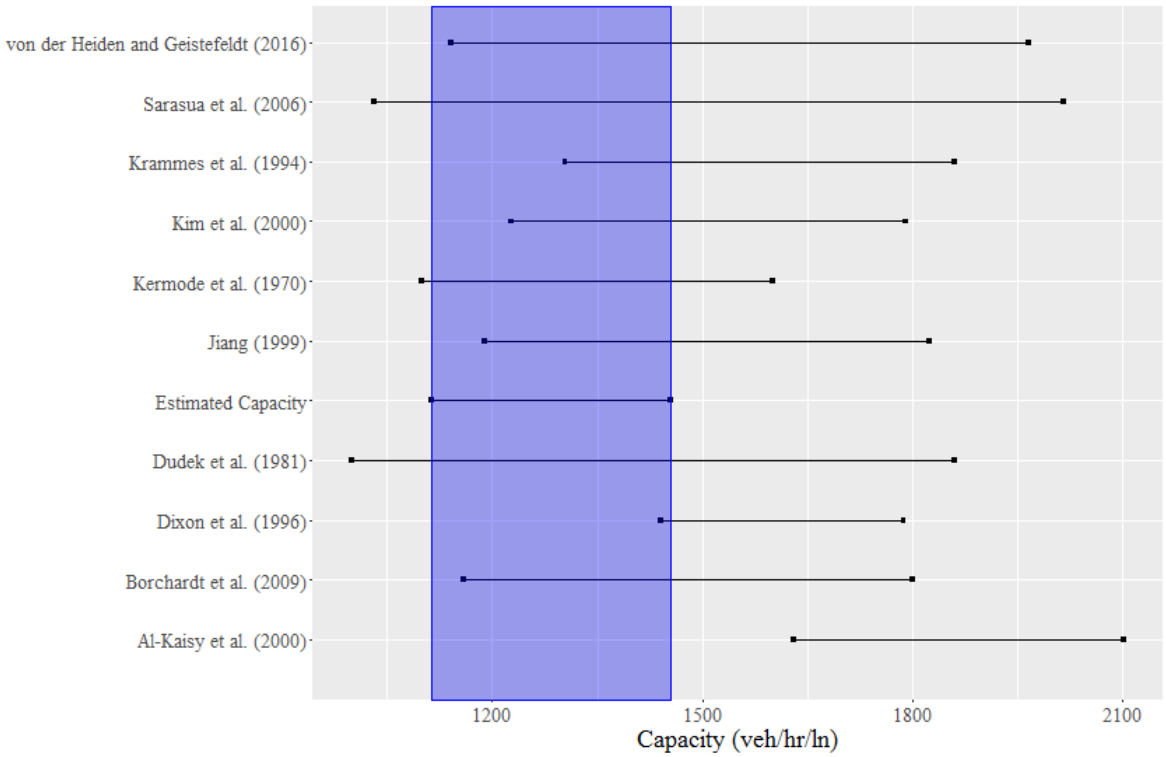


**Figure 5.13 Comparison of Estimated Capacity and Existing Literatures**

### 5.4.3 Work Zone Travel Time and Its Reliability Estimation

The proposed methodology in section 5.3.2 is applied to estimate the travel time of work zone in Iowa City. The Newman model-based travel time (Newman-TT) and INRIX

travel time (INRIX-TT), represented as travel time index, are plotted in Figure 5.7. Travel times are estimated for the morning peak and afternoon peak during the construction season. Figure 5.7 compares the time-dependent travel times estimated by the proposed Newman - based model and INRIX data on example days. It shows that the Newman model-based travel time index estimation roughly followed the pattern of the INRIX travel time index. Similar patterns are observed for other days as well.

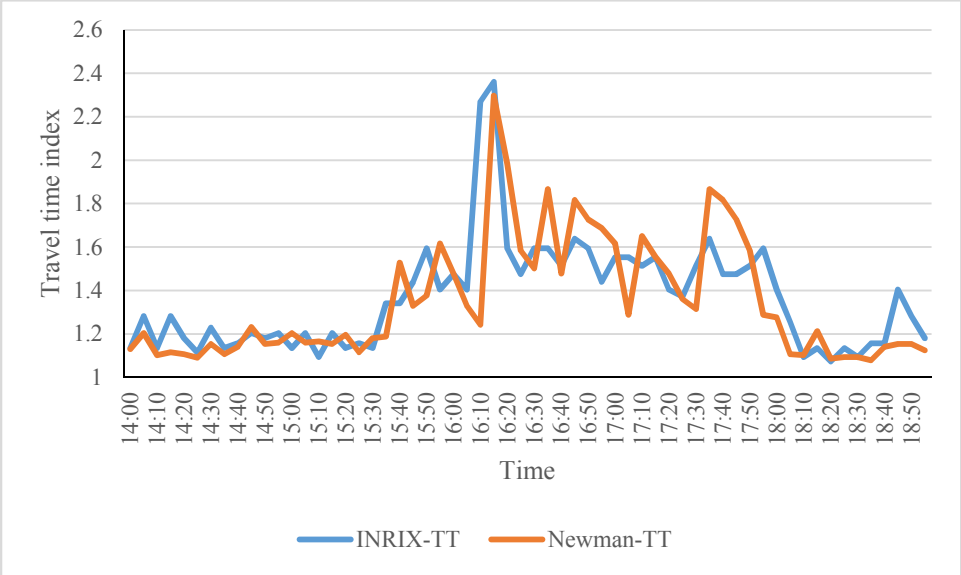


**Figure 5.14 Comparison of Model-based and INRIX Travel Time Index**

Moreover, travel times of peak hours during work zone construction period are estimated using Eq. 20. These travel times are used to derive the work zone travel time reliability indices, as in Table 5.4. Comparing the travel time reliability indices of Newman-TT and INRIX-TT, the travel time reliability indices of Newman-TT are close to INRIX-TTs. Mean travel time, standard deviation, 95$^{th}$ percentile travel and planning time index are within 10% error range.

**Table 5.4 The Reliability Indices of INRIX Travel Time and Newman Model-based Travel Time**

| | Mean (min) | Standard Deviation | 95th Percentile (min) | Planning Time Index | Buffer Time (min) | Buffer Time Index |
|---|---|---|---|---|---|---|
| Newman - TT | 8.78 | 0.86 | 10.29 | 1.17 | 1.51 | 0.17 |
| INRIX-TT | 8.55 | 0.95 | 10.53 | 1.23 | 1.98 | 0.23 |

## 5.5 Summary

In this chapter, a modified five-parameter logistic model is developed to describe the speed-density relationship. The calibrated speed-density models show that, the free flow speed and turning density are smaller when work zone presents compared to typical non-work zone conditions. Moreover, a capacity prediction method is proposed based on the relationship between free-flow speed and work zone characteristics and the logistic speed-density model. A before-and-after study is conducted to evaluate the performance of the proposed work zone capacity prediction method. The logistic model based method can predict speed-density ranges that enclose most of the scatter of the field data.

Moreover, the proposed work zone capacity estimation method is compared with the capacities estimated using WorkZoneQ software. The result shows the logistic model generates similar results as WorkZoneQ and are generally smaller than the maximum 15-min flow rate. The predicted upper bound of capacity is close to the maximum 15-min flow rate. Moreover, most of the estimated capacities using logistic model, HCM, and WorkZoneQ are located within the predicted capacity range. The work zone that has the largest free-flow speed

reduction results in the smallest capacity. The work zones that have similar free-flow speed reduction have similar capacities.

Second, based on the predicted speed-density-volume relationship, the work zone travel time and its reliability are estimated. The result shows that the Newman model-based travel time index estimation roughly followed the pattern of the INRIX travel time. Moreover, the travel time reliability indices based on Newman-TT are close to the indices based on INRIX-TT.

This chapter proposed a new method to predict speed-volume-density relationship and capacity of work zones. The proposed method can predict speed-density ranges that enclose most of the scatter of the field data. Moreover, the predicted parameters of speed-volume-density relationship are used to estimated work zone travel time and its reliability. The travel time pattern and travel time reliability indices based on Newman model are close to INRIX-TTs.

# CHAPTER 6. CONCLUSIONS AND FUTURE RESEARCH

## 6.1 Research Highlights

This dissertation addresses a series of research questions related to travel time reliability on urban freeways, including (1) design a travel time estimation method to quantify link- and corridor- level travel time and its distribution using radar sensor data; (2) develop a method to estimated link travel time reliability measures by incorporating stochastic standstill distance and time headway parameters in FRESIM car following model; and (3) develop an capacity prediction framework and a travel time reliability estimation method for work zones on freeway.

### 6.1.1 Estimating Corridor-Level Travel Time Reliability Using Radar Sensor Data

This dissertation presented a method to estimate corridor-level travel times based on data collected from roadside radar sensors, considering spatially correlated traffic conditions. Link-level and corridor-level travel time distributions are estimated using these travel time estimates and compared with the ones estimated based on probe vehicle data. The maximum likelihood estimation is used to estimate the parameters of Weibull, gamma, normal, and lognormal distributions. According to the log likelihood values, lognormal distribution is the best fit among all the tested distributions. Corridor-level travel time reliability measures are extracted from the travel time distributions. The proposed travel time estimation model can well capture the temporal pattern of travel time and its distribution.

### 6.1.2 Incorporating Standstill Distance and Time Headway Distributions in Car Following Models to Estimate Travel Time Reliability

This research presented a method to estimate travel time reliability measures by incorporating standstill distance and time headway distributions in car-following models. The method is based on simplified two-component travel time distribution. By using Monte Carlo simulation, the speed-density region under congested condition and the travel time reliability measures can be generated. Traffic flow, density, and speed data from Iowa DOT, travel time data from INRIX and VISSIM simulation are used to validate the model's estimates. The main findings include:

1) The vehicle type-specific distribution input could result in a speed-density region that better replicate real world observations, compare to the speed-density curves generated using mean standstill distance and headway parameters.
2) The speed-density region derived from the steady-state Pipes model encloses most of the field data and outperforms VISSIM simulation output.
3) Both the proposed method and VISSIM slightly overestimated the travel time reliability of the study freeway segment. The proposed method provides better estimates in a faster time, compared to VISSIM simulation.

### 6.1.3 Travel Time Reliability of Urban Freeway Work Zones

The impact of work zone on capacity is investigated in this dissertation. A method to estimate capacity and travel time of work zones is proposed. First, the speed-density relationship of work zones and non-work zone are calibrated by using the modified five-

parameter logistic model. By comparing the calibrated speed-volume-density relationships for different work zones with the non-work zone site, the work zones have similar stop-and-go speed ($V_b$) and shape parameters ($\theta_1$ and $\theta_2$) as the typical non-work zone curve. Moreover, the values of turning parameter ($\alpha$) at work zones are similar. Therefore, a capacity prediction method is proposed based on the modified five-parameter logistic model. The predicted upper bound of capacity is close to the maximum 15-min flow rate.

Moreover, by using the predicted capacity, density at capacity and free flow speed, a travel time estimation method is modified from the segment speed estimation model proposed by HCM. The estimated travel times, which are based on HCM-model, roughly followed the pattern of the INRIX travel times. The travel time reliability indices are estimated directly from the estimated travel times. The result shows that the travel time reliability indices based on HCM-TT are close to the indices based on INRIX-TT.

## 6.2 Summary of Contributions

The dissertation consists of the following main contributions:

First, the proposed travel time estimation method is based on data collected from roadside radar sensors and considering spatially correlated traffic conditions. Different from the travel time estimation methods described in Chapter 2, the proposed method considered the impact of spillback from a downstream bottleneck on target link travel time.

Second, this research proposed a stochastic modeling approach to estimate corridor travel time reliability measures. Using Dirac delta distribution to present free-flow state of two-component travel time distribution, the travel time reliability indices calculation based on two-component travel time distribution is simplified. Moreover, by incorporating stochastic

standstill distance and time headway parameters in Pipes car-following models, a computationally-efficient travel time reliability measure estimation is proposed.

Third, one of the main contributions of work zone travel time reliability problem is the incorporation of work zone characteristics into logistic speed-density model to predict the speed-volume-density relationship and capacity of work zone. Another main contribution is the work zone travel time and its reliability are estimated by applying the speed-volume-density relationship estimated by modified logistic speed-density model. This study will help traffic engineers design more appropriate traffic management strategies to avoid long periods of over-saturation.

## 6.3 Future Research

For the future research on corridor level travel time quantification problem, the impacts of lane-changing behavior and the temporal correlation on the travel time can be incorporated into the model.

Autonomous vehicle technologies are likely to be gradually implemented over time. The existing studies shows that the autonomous vehicle can improve flow string stability and reduce traffic congestion (Davis, 2004; Kesting et al., 2008). Therefore, in the future study of stochastic modeling problem of car-following model, the impact of connected and autonomous vehicle should be considered to improve the travel time reliability estimation model.

In the future study of travel time reliability problem of work zone, other types of work zones needs to be investigated. Moreover, there are some caveats of the proposed method. First, the before-and-after study is based on lane closure work zones. In the future, other types of work zones need to be investigated. Second, only free-flow speed and α are considered as

dependent variables that impact speed-density curve. Future studies should examine the impact of work zone intensity, traffic control type and road configuration on the other parameters of the logistic model.

# REFERENCES

Adeli, H., Jiang, X., 2003. Neuro-Fuzzy Logic Model for Freeway Work Zone Capacity Estimation. J. Transp. Eng. 129, 484–493. doi:10.1061/(ASCE)0733-947X(2003)129:5(484)

Ahn, S., Cassidy, M.J., Laval, J., 2004. Verification of a simplified car-following theory. Transp. Res. Part B Methodol. 38, 431–440. doi:10.1016/S0191-2615(03)00074-2

Akçelik, R., 1991. Travel time functions for transport planning purposes: Davidson's function, its time dependent form and alternative travel time function. Aust. Road Res. 21, 49–59.

Aksoy, G., Celikoglu, H.B., 2012. Modeling and distribution of link travel times: an analysis on Istanbul freeways. Proc. Ewgt 2012 - 15Th Meet. Euro Work. Gr. Transp. 54, 117–128. doi:10.1016/j.sbspro.2012.09.731

Al-Kaisy, A., Hall, F., 2003. Guidelines for Estimating Capacity at Freeway Reconstruction Zones. J. Transp. Eng. 129, 572–577. doi:10.1061/(ASCE)0733-947X(2003)129:5(572)

Al-kaisy, A., Zhou, M., Hall, F., 2000. New Insights into Freeway Capacity at Work Zones: Empirical Case Study. Transp. Res. Rec. J. Transp. Res. Board 1710, 154–160.

Benekohal, R., Kaja-Mohideen, A.-Z., Chitturi, M., 2004. Methodology for Estimating Operating Speed and Capacity in Work Zones. Transp. Res. Rec. 1883, 103–111. doi:10.3141/1883-12

Benekohal, R.F., Kaja-Mohideen, A.-Z., Chitturi, M. V., 2003. Evaluation of construction work zone operational issues: capacity , queue , and delay, in: Publication ITRC FR 00/01-4. Illinois Transportation Research Center.

Bertini, R., Malik, S., 2004. Observed Dynamic Traffic Features on Freeway Section with Merges and Diverges. Transp. Res. Rec. 1867, 25–35. doi:10.3141/1867-04

Bhouri, N., Haj-salem, H., Kauppila, J., 2013. Isolated versus coordinated ramp metering : Field evaluation results of travel time reliability and traffic impact. Transp. Res. Part C 28, 155–167. doi:10.1016/j.trc.2011.11.001

Brackstone, M., Mcdonald, M., 2007. Driver headway : How close is too close on a motorway ? Ergonomics 50, 1183–1195. doi:10.1080/00140130701318665

Brackstone, M., McDonald, M., 1999. Car-following: a historical review. Transp. Res. Part F Traffic Psychol. Behav. 2, 181–196. doi:10.1016/S1369-8478(00)00005-X

Brilon, W., Geistefeldt, J., Regler, M., 2005. Reliability of Freeway Traffic Flow: A stochastic Concept of Capacity. Proc. 16th Int. Symp. Transp. Traffic Theory 125–144.

Caceres, H., Hwang, H., He, Q., 2016. Estimating freeway route travel time distributions with consideration to time of day, inclement weather, and traffic incidents. J. Adv. Transp. 50, 967–987. doi:10.1002/atr

Cambridge Systematics, Texas Transportation Institute, 2005. Traffic Congestion and Reliability Trends and Advanced Strategies for Congestion Mitigation Federal Highway Administration.

Castillo, J.M.D., Benítez, F.G., 1995a. On the functional form of the speed-density relationship—II: Empirical investigation. Transp. Res. Part B Methodol. 29, 391–406. doi:10.1016/0191-2615(95)00009-3

Castillo, J.M.D., Benítez, F.G., 1995b. On the functional form of the speed-density relationship—I: General theory. Transp. Res. Part B Methodol. 29, 373–389. doi:10.1016/0191-2615(95)00008-2

Celikoglu, H.B., 2013a. Reconstructing freeway travel times with a simplified network flow model alternating the adopted fundamental diagram. Eur. J. Oper. Res. 228, 457–466. doi:10.1016/j.ejor.2013.02.019

Celikoglu, H.B., 2013b. Flow-based freeway travel-time estimation: A comparative evaluation within dynamic path loading. IEEE Trans. Intell. Transp. Syst. 14, 772–781. doi:10.1109/TITS.2012.2234455

Celikoglu, H.B., 2007. A dynamic network loading process with explicit delay modelling. Transp. Res. Part C Emerg. Technol. 15, 279–299. doi:10.1016/j.trc.2007.04.003

Chan, K.S., Lam, W.H.K., Tam, M.L., 2009. Real-Time Estimation of Arterial Travel Times with Spatial Travel Time Covariance Relationships. Transp. Res. Rec. J. Transp. Res. Board 102–109. doi:10.3141/2121-11

Chatterjee, I., Edara, P., Menneni, S., Sun, C., 2010. Replication of Work Zone Capacity Values in a Simulation Model. Transp. Res. Rec. J. Transp. Res. Board 2130, 138–148. doi:10.3141/2130-17

Chen, C., Skabardonis, A., Varaiya, P., 2003. Travel Time Reliability As a Measure of Service. Transp. Res. Rec. J. Transp. Res. Board 1855, 74–79.

Chootinan, P., Wong, S.C., Chen, A., 2005. A Reliability-Based Network Design Problem. J. ofAdvanced Transp. 39, 247–270.

Coifman, B., 2002. Estimating travel times and vehicle trajectories on freeways using dual loop detectors. Transp. Res. Part A Policy Pract. 36, 351–364. doi:10.1016/S0965-8564(01)00007-6

Daganzo, C.F., 1995. Properties of link travel time functions under dynamic loads. Transp. Res. Part B 29, 95–98. doi:10.1016/0191-2615(94)00026-V

Dailey, D.., 1991. Travel-time Estimation Using Cross-Correlation Techniques. Transp. Res. Part B Methodol. 27B, 97–107.

Davidson, K.B., 1978. The theoretical basis of a flow-travel time relationship for use in transportation planning. Aust. Road Res. 8, 32–35.

Davis, L.C., 2004. Effect of adaptive cruise control systems on traffic flow. Phys. Rev. E - Stat. Nonlinear, Soft Matter Phys. 69, 1–8. doi:10.1103/PhysRevE.69.066110

Deniz, O., Aksoy, G., Celikoglu, H.B., 2013. Analyzing freeway travel times within a case study: Reliability of route traversal times. IEEE Conf. Intell. Transp. Syst. Proceedings, ITSC 195–202. doi:10.1109/ITSC.2013.6728233

Dijker, T., Bovy, P.H.L., Vermijs, R.G.M.M., 1998. Car-Following Under Congested Conditions: Empirical Findings. Transp. Res. Rec. J. Transp. Res. Board 1644, 20–28. doi:10.3141/1644-03

Dong, J., Houchin, A.J., Shafieirad, N., Lu, C., Hawkins, N.R., Knickerbocker, S., 2015. VISSIM Calibration for Urban Freeways.

Dong, J., Mahmassani, H.S., 2012. Stochastic modeling of traffic flow breakdown phenomenon: Application to predicting travel time reliability. IEEE Trans. Intell. Transp. Syst. 13, 1803–1809.

Dong, J., Mahmassani, H.S., 2009. Flow Breakdown and Travel Time Reliability. Transp. Res. Rec. J. Transp. Res. Board 2124, 203–212. doi:10.3141/2124-20

Drake, J.S., Schofer, J.L., May Jr, A.D., 1967. A Statistical Analysis of Speed-Density Hypothses in Vehicular Traffic Science. Highw. Res. Rec. 112–117.

Durrani, U., Lee, C., Maoh, H., 2016. Calibrating the Wiedemann's vehicle-following model using mixed vehicle-pair interactions. Transp. Res. Part C Emerg. Technol. 67, 227–242.

Edie, L.C., 1961. Car-Following and Steady-State Theory for Noncongested Traffic. Oper. Res. 9, 66–76. doi:10.1287/opre.9.1.66

Edwards, M.B., Fontaine, M.D., 2012. Investigation of Travel Time Reliability in Work Zones with Private-Sector Data. Transp. Res. Rec. J. Transp. Res. Board 2272, 9–18. doi:10.3141/2272-02

Emam, E., AI-Deek, H., 2006. Using Real-Life Dual-Loop Detector Data to Develop New Methodology for Estimating Freeway Travel Time Reliability. Transp. Res. Rec. J. Transp. Res. Board 1959, 140–150. doi:10.3141/1959-16

Federal Size Regulations for Commercial Motor Vehicles - FHWA [WWW Document], 2004. . FHWA, U.S. Dep. Transp. URL http://ops.fhwa.dot.gov/freight/publications/size_regs_final_rpt/ (accessed 12.8.16).

Gao, Y., 2008. Calibration and Comparison of the VISSIM and INTEGRATION Microscopic Traffic Simulation Models 1–67.

Greenberg, H., 1959. An Analysis of Traffic Flow. Oper. Res. 7, 79–85. doi:10.1287/opre.7.1.79

Greenshields, B.D., 1934. A study of traffic capacity. Highw. Res. Board Proc. 14, 448–477.

Guo, F., Rakha, H., Park, S., 2010. Multistate Model for Travel Time Reliability. Transp. Res. Rec. J. Transp. Res. Board 2188, 46–54. doi:10.3141/2188-06

Hajbabaie, A., Yoem, C., Rouphail, N.M., Rasdorf, W., Schroeder, B.J., 2015. Freeway Work Zone Free-Flow Speed Prediction from Multi-State Sensor Data, in: Presented at 94th Annual Meeting of the Transportation Research Board, Washington.

Halati, A., Lieu, H., WALKER, S., 1997. CORSIM - Corridor Traffic Simulation Model. Traffic Congest. Traffic Saf. 21st Century Challenges, Innov. Oppor. 570–576.

Haseman, R.J., Wasson, J.S., Bullock, D.M., 2010. Real-Time Measurement of Travel Time Delay in Work Zones and Evaluation Metrics Using Bluetooth Probe Tracking. Transp. Res. Rec. J. Transp. Res. Board 2169, 40–53. doi:10.3141/2169-05

Heaslip, K., Kondyli, A., Arguea, D., Elefteriadou, L., Sullivan, F., 2010. Estimation of Freeway Work Zone Capacity Through Simulation and Field Data. Transp. Res. Rec. J. Transp. Res. Board 2130, 16–24. doi:10.3141/2130-03

Heaslip, K., Louisell, C., Collura, J., 2008. Driver Population Adjustment Factors for Highway Capacity Manual's Work Zone Capacity Equation, in: Presented at 87th Annual Meeting of the Transportation Research Board, Washington, DC.

Higatani, A., Kitazawa, T., Tanabe, J., Suga, Y., Sekhar, R., Asakura, Y., 2009. Empirical Analysis of Travel Time Reliability Measures in Hanshin Expressway Network. J. Intell. Transp. Syst. 13, 28–38. doi:10.1080/15472450802644454

Hoogendoorn, S.P., Bovy, P.H.L., 1998. New Estimation Technique for Vehicle- Type-Specific Headway Distributions. Transp. Res. Rec. J. Transp. Res. Board 1646, 18–28.

Houchin, A., Dong, J., Hawkins, N., Knickerbocker, S., 2015. Measurement and Analysis of Heterogenous Vehicle Following Behavior on Urban Freeways: Time Headways and Standstill Distances. IEEE Conf. Intell. Transp. Syst. Proceedings, ITSC 2015–Octob, 888–893. doi:10.1109/ITSC.2015.149

Isukapati, I.K., List, G.F., Williams, B.M., Karr, A.F., 2013. Synthesizing Route Travel Time Distributions from Segment Travel Time Distributions. Transp. Res. Rec. 71–81. doi:10.3141/2396-09

Kesting, A., Treiber, M., Schönhof, M., Helbing, D., 2008. Adaptive cruise control design for active congestion avoidance. Transp. Res. Part C Emerg. Technol. 16, 668–683.

doi:10.1016/j.trc.2007.12.004

Kim, J., Mahmassani, H., Dong, J., 2010. Likelihood and Duration of Flow Breakdown. Transp. Res. Rec. J. Transp. Res. Board 2188, 19–28. doi:10.3141/2188-03

Kim, T., Lovell, D.J., Hall, M., Paracha, J., 2000. A New Methodology to Estimate Capacity for Freeway Work Zones.

Kockelman, K., 1998. Changes in Flow-Density Relationship Due to Environmental, Vehicle, and Driver Characteristics. Transp. Res. Rec. 1644, 47–56. doi:10.3141/1644-06

Krammes, R.A., Lopez, G.O., 1994. Updated capacity values for short-term freeway work zone lane closures. Transp. Res. Rec. 49–56.

Kwon, J., Barkley, T., Hranac, R., Petty, K., Compin, N., 2011. Decomposition of Travel Time Reliability into Various Sources. Transp. Res. Rec. J. Transp. Res. Board 2229, 28–33. doi:10.3141/2229-04

Lam, W.H.K., Asce, M., Tam, M.L., Cao, X., Li, X., 2013. Modeling the Effects of Rainfall Intensity on Traffic Speed, Flow, and Density Relationships for Urban Roads. J. Transp. Eng. 4, 758–770. doi:10.1061/(ASCE)TE.1943-5436.0000544.

Lei, H., Zhou, X., List, G.F., Taylor, J., 2015. Characterizing corridor-level travel time distributions based on stochastic flows and segment capacities. Cogent Eng. 2, 990672. doi:10.1080/23311916.2014.990672

Li, R., Rose, G., Sarvi, M., 2006. Using Automatic Vehicle Identification Data to Gain Insight into Travel Time Variability and Its Causes. Transp. Res. Rec. 1945, 24–32. doi:10.3141/1945-03

Liu, H.X., Danczyk, A., 2009. Optimal sensor locations for freeway bottleneck identification. Comput. Civ. Infrastruct. Eng. 24, 535–550. doi:10.1111/j.1467-8667.2009.00614.x

M. Van Aerde & Assoc., L., 2005a. INTEGRATION © RELEASE 2.30 FOR WINDOWS: User's Guide-Volume II: Advanced Model Features INTEGRATION User's Guide Release 2.30 for Windows-Volume II ii.

M. Van Aerde & Assoc., L., 2005b. INTEGRATION © RELEASE 2.30 FOR WINDOWS: User's Guide – Volume I: Fundamental Model Features INTEGRATION User's Guide Release 2.30 -Volume I.

MacNicholas, M.J., 2011. A simple and pragmatic representation of traffic flow, in: Symposium on The Fundamental Diagram. pp. 161–177.

Makishita, H., Matsunaga, K., 2008. Differences of drivers ' reaction times according to age and mental workload. Accid. Anal. Prev. 40, 567–575. doi:10.1016/j.aap.2007.08.012

Minge, E., Peterson, S., Weinblatt, H., Coifman, B., Hoekman, E., 2012. Loop-and Length-Based Vehicle Classification, in: Publication MN/RC 2012-33. Minnesota Department of Transportation.

Modi, V., Kondyli, A., Washburn, S.S., M.ASCE, McLeod, D.S., 2014. Freeway Capacity Estimation Method for Planning Applications. J. Transp. Eng. 140, 1–9. doi:10.1061/(ASCE)TE.1943-5436.0000699.

Mori, U., Mendiburu, A., Álvarez, M., Lozano, J.A., 2015. Review of travel time estimation and forecasting for Advanced Traveller Information Systems. Transp. A Transp. Sci. 11, 119–157. doi:10.1080/23249935.2014.932469

Moses, R., Mtoi, E., McBean, H., Ruegg, S., 2013. Development of Speed Models for Improving Travel Forecasting and Highway Performance Evaluation Final Report Project No . BDK83 Task Work Order No . 977-14 by 155.

Neuhold, R., Fellendorf, M., 2014. Volume-delay functions based on stochastic capacity. Transp. Res. Rec. 2421, 93–102. doi:10.3141/2421-11

Newell, G.F., 1999. Delays caused by a queue at a freeway exit ramp. Transp. Res. Part B Methodol. 33, 337–350.

Newell, G.F., 1961. Nonlinear Effects in the Dynamics of Car Following. Oper. Res. 9, 209–229. doi:10.1287/opre.9.2.209

Nie, X., Zhang, H.M., 2005. A comparative study of some macroscopic link models used in dynamic traffic assignment. Networks Spat. Econ. 5, 89–115. doi:10.1007/s11067-005-6663-6

Oh, J.-S., Chung, Y., 2006. Calculation of Travel Time Variability from Loop Detector Data. Transp. Res. Rec. 1945, 12–23. doi:10.3141/1945-02

Park, D., Rilett, L.R., 1999. Forecasting Freeway Link Travel Times with a Multilayer Feedforward Neural Network. Comput. Civ. Infrastruct. Eng. 14, 357–367. doi:10.1111/0885-9507.00154

Park, S., Rakha, H.A., Guo, F., 2011. Multi-State Travel Time Reliability Model: Impact of Incidents on Travel Time Reliability, in: 14th International IEEE Conference on Intelligent Transportation Systems. pp. 2106–2111.

Pipes, L.A., 1953. An operational analysis of traffic dynamics. J. Appl. Phys. 24, 274–281. doi:10.1063/1.1721265

Racha, S., Chowdhury, M., Sarasua, W., Ma, Y., 2008. Analysis of work zone traffic behavior for planning applications. Transp. Plan. Technol. 31, 183–199. doi:10.1080/03081060801948175

R Development Core Team, 2011. R: A Language and Environment for Statistical Computing. Vienna,Austria: the R Foundation for Statistical Computing.

Rahmani, M., Jenelius, E., Koutsopoulos, H.N., 2013. Route travel time estimation using low-frequency floating car data. 16th Int. IEEE Conf. Intell. Transp. Syst. (ITSC 2013) 2292–2297. doi:10.1109/ITSC.2013.6728569

Rakha, H., Crowther, B., 2003. Comparison and calibration of FRESIM and INTEGRATION steady-state car-following behavior. Transp. Res. Part A Policy Pract. 37, 1–27. doi:10.1016/S0965-8564(02)00003-4

Rakha, H., Crowther, B., 2002. Comparison of Greenshields, Pipes, and Van Aerde Car-Following and Traffic Stream Models. Transp. Res. Rec. 1802, 248–262. doi:10.3141/1802-28

Richardson, A.J., 2003. Travel time variability on an urban freeway, in: 25TH CONFERENCE OF AUSTRALIAN INSTITUTES OF TRANSPORT RESEARCH (CAITR). ADELAIDE, SOUTH AUSTRALIA.

Sarasua, W., Davis, W., Chowdhury, M., Ogle, J., 2006. Estimating Interstate Highway Capacity for Short-Term Work Zone Lane Closures: Development of Methodology. Transp. Res. Rec. 1948, 45–57. doi:10.3141/1948-06

Soriguera, F., Robuste, F., 2011. Highway travel time accurate measurement and short-term prediction using multiple data sources. TRANSPORTMETRICA 7, 85–109. doi:10.1080/18128600903244651

Soriguera, F., Robusté, F., 2011. Requiem for freeway travel time estimation methods based on blind speed interpolations between point measurements. IEEE Trans. Intell. Transp. Syst. 12, 291–297.

Spiess, H., 1990. Technical Note — Conical Volume-Delay Functions. Transp. Sci. 24, 153–158.

Sumalee, A., Watling, D.P., Nakayama, S., 2006. Reliable Network Design Problem Case with Uncertain Demand and Total Travel Time Reliability. Transp. Res. Rec. J. Transp. Res. Board 81–90.

Sun, L., Zhou, J., 2005. Development of Multiregime Speed-Density Relationships by Cluster Analysis. Transp. Res. Rec. 1934, 64–71. doi:10.3141/1934-07

Susilawati, S., Student, P., Taylor, M.A.P., Somenahalli, S.V.C., 2010. Travel Time Reliability Measurement for Selected Corridors in the Adelaide Metropolitan Area. J. East. Asia Soc. Transp. Stud. 8, 86–102.

Tam, M.L., Lam, W.H.K., 2008. Using Automatic Vehicle Idenification Data for Travel Time Estimation in Hong Kong. Transportmetrica 4, 179–194. doi:10.1080/18128600808685688

Texas Transportation Institute, Cambridge System Inc., 2006. Travel Time Reliability: Making It There On Time, All The Time.

Turner, S., 1996. Advanced Techniques for Travel Time Data Collection. Transp. Res. Rec. 1551, 51–58. doi:10.3141/1551-07

Turochy, R., Smith, B., 2002. Measuring Variability in Traffic Conditions by Using Archived Traffic Data. Transp. Res. Rec. 1804, 168–172. doi:10.3141/1804-22

Underwood, R.T., 1961. Speed, volume, and density relationship: quality and theory of traffic flow, in: Yale Bureau of Highway Traffic. New Haven, Connecticut, pp. 141–188.

Van Aerde, M., Rakha, H., 1995. Multivariate calibration of single regime speed-flow-density relationships [road traffic management]. Pacific Rim TransTech Conf. 1995 Veh. Navig.

Inf. Syst. Conf. Proceedings. 6th Int. VNIS. A Ride into Futur. 334–341. doi:10.1109/VNIS.1995.518858

Van Arem, B., Van Der Vlist, M.J.M., Muste, M. (Rik., Smulders, S. a., 1997. Travel time estimation in the GERDIEN project. Int. J. Forecast. 13, 73–85. doi:10.1016/S0169-2070(96)00702-9

Vanajakshi, L.D., 2005. Estimation and prediction of travel time from loop detector data for intelligent transportation systems applications.

Vanajakshi, L.D., Williams, B.M., Rilett, L.R., 2009. Improved Flow-Based Travel Time Estimation Method from Point Detector Data for Freeways. J. Transp. Eng. 135, 26–36. doi:10.1061/(ASCE)0733-947X(2009)135:1(26)

van Lint, J., van der Zijpp, N., 2003. Improving a Travel-Time Estimation Algorithm by Using Dual Loop Detectors. Transp. Res. Rec. 1855, 41–48. doi:10.3141/1855-05

Van Lint, J.W.C., Van Zuylen, H.J., 2005. Monitoring and predicting freeway travel time reliability. Transp. Res. Rec. J. Transp. Res. Board 1917, 54–62. doi:10.3141/1917-07

Van Lint, J.W.C., Van Zuylen, H.J., Tu, H., 2008. Travel time unreliability on freeways : Why measures based on variance tell only half the story. Transp. Res. Part A Policy Pract. 42, 258–277. doi:10.1016/j.tra.2007.08.008

Vlahogianni, E.I., Karlaftis, M.G., Golias, J.C., 2014. Short-term traffic forecasting: Where we are and where we're going. Transp. Res. Part C Emerg. Technol. 43, 3–19. doi:10.1016/j.trc.2014.01.005

Wang, H., Li, J., Chen, Q., Ni, D., 2011. Logistic modeling of the equilibrium speed – density relationship. Transp. Res. Part A 45, 554–566. doi:10.1016/j.tra.2011.03.010

Wasielewski, P., 1979. Car-following Headways on Freeways Interpreted by the Semi-Poisson Headway Distribution Model. Transp. Sci. 13, 36–55. doi:10.1287/trsc.13.1.36

Wavetronix, 2013. Wavetronix SmartSensor HD User Guide [WWW Document]. URL http://www.signalcontrol.com/tech_papers/wavetronix/SS125_HD_Install Guide.pdf. (accessed 12.8.16).

Wells, T., Smaglik, E., Bullock, D., 2008. Implementation of Station Health Monitoring Procedures for ITS Sensors, Volume 1: Research Report, Publication FHWA/IN/JTRP-2006/40-1. Joint Transportation Research Program, Indiana Department of Transportation and Purdue University, West Lafayette, Indiana. doi:10.5703/1288284314233

Weng, J., Meng, Q., 2015. Incorporating work zone configuration factors into speed-flow and capacity models. J. Adv. Transp. 49, 371–384. doi:10.1002/atr

Weng, J., Meng, Q., 2013. Estimating capacity and traffic delay in work zones: An overview. Transp. Res. Part C Emerg. Technol. 35, 34–45. doi:10.1016/j.trc.2013.06.005

Weng, J., Meng, Q., 2012. Ensemble Tree Approach to Estimating Work Zone Capacity. Transp. Res. Rec. J. Transp. Res. Board 2286, 56–67. doi:10.3141/2286-07

Weng, J., Meng, Q., 2011. Decision Tree-Based Model for Estimation of Work Zone Capacity. Transp. Res. Rec. J. Transp. Res. Board 2257, 40–50. doi:10.3141/2257-05

Weng, J., Meng, Q., Fwa, T.F., 2014. Vehicle headway distribution in work zones. Transp. A Transp. Sci. 10, 285–303. doi:10.1080/23249935.2012.762564

Wong, H.-K., Sussman, J.M., 1973. Dynamic Travel Time Estimation on Highway Networks. Transp. Res. 7, 355–370.

Wu, X., Michalopoulos, P., Liu, H.X., 2010. Stochasticity of freeway operational capacity and chance-constrained ramp metering. Transp. Res. Part C Emerg. Technol. 18, 741–756.

Yang, S., Wu, Y., Yin, Z., Feng, Y., 2016. Estimating Freeway Travel Times Using the General Motors Model. Transp. Res. Rec. J. Transp. Res. Board 83–94. doi:10.3141/2594-12

Ye, F., Zhang, Y., 2009. Vehicle Type-Specific Headway Analysis Using Freeway Traffic Data. Transp. Res. Rec. J. Transp. Res. Board 2124, 222–230. doi:10.3141/2124-22

Zang, X., 2009. Forecasting of time headway distribution in merging area of urban expressway interchange based on RBF. Proc. - 2009 Int. Conf. Comput. Intell. Softw. Eng. CiSE 2009 1–4. doi:10.1109/CISE.2009.5365856

Zhang, G., Wang, Y., Wei, H., Chen, Y., 2007. Examining Headway Distribution Models with Urban Freeway Loop Event Data. Transp. Res. Rec. 1999, 141–149.

Zhang, W., 2006. Freeway Travel Time Estimation Based on Spot Speed Measurements Freeway Travel Time Estimation Based on Spot Speed Measurements. Dr. Diss. Virginia Polytech. Inst. State Univ.

Zou, Y., Zhu, X., Zhang, Y., Zeng, X., 2014. A space-time diurnal method for short-term freeway travel time prediction. Transp. Res. Part C Emerg. Technol. 43, 33–49. doi:10.1016/j.trc.2013.10.007

# APPENDIX A.

# DERIVATION OF FIRST AND SECOND CONDITION

**The first condition**

$$\frac{\partial k}{\partial V} = \theta_1 \times \frac{\partial}{\partial V}\left[\log\left[\exp\left(\frac{\log\left(\frac{V_f - V_b}{V - V_b}\right)}{\theta_2}\right) - 1\right]\right]$$

Derivation

$$\frac{\partial}{\partial V}\left[\log\left[\exp\left(\frac{\log\left(\frac{V_f-V_b}{V-V_b}\right)}{\theta_2}\right)-1\right]\right]=\frac{1}{\exp\left(\frac{\log\left(\frac{V_f-V_b}{V-V_b}\right)}{\theta_2}\right)-1}\times\frac{\partial}{\partial V}\left[\exp\left(\frac{\log\left(\frac{V_f-V_b}{V-V_b}\right)}{\theta_2}\right)-1\right]$$

$$=\frac{1}{\exp\left(\frac{\log\left(\frac{V_f-V_b}{V-V_b}\right)}{\theta_2}\right)-1}\times\frac{\partial}{\partial V}\left[\exp\left(\frac{\log\left(\frac{V_f-V_b}{V-V_b}\right)}{\theta_2}\right)\right]$$

$$=\frac{\exp\left(\frac{\log\left(\frac{V_f-V_b}{V-V_b}\right)}{\theta_2}\right)}{\theta_2\left[\exp\left(\frac{\log\left(\frac{V_f-V_b}{V-V_b}\right)}{\theta_2}\right)-1\right]}\times\frac{\partial}{\partial V}\left[\log\left(\frac{V_f-V_b}{V-V_b}\right)\right]$$

$$=-\frac{\frac{V-V_b}{V_f-V_b}\times\exp\left(\frac{\log\left(\frac{V_f-V_b}{V-V_b}\right)}{\theta_2}\right)}{\theta_2\left[\exp\left(\frac{\log\left(\frac{V_f-V_b}{V-V_b}\right)}{\theta_2}\right)-1\right]}\times\frac{\partial}{\partial V}\left[\frac{V_f-V_b}{V-V_b}\right]$$

$$=-\frac{(V-V_b)\times\exp\left(\frac{\log\left(\frac{V_f-V_b}{V-V_b}\right)}{\theta_2}\right)}{\theta_2\left[\exp\left(\frac{\log\left(\frac{V_f-V_b}{V-V_b}\right)}{\theta_2}\right)-1\right]}\times\frac{\partial}{\partial V}\left[\frac{1}{V-V_b}\right]$$

$$=-\frac{\exp\left(\frac{\log\left(\frac{V_f-V_b}{V-V_b}\right)}{\theta_2}\right)}{(V-V_b)\times\theta_2\left[\exp\left(\frac{\log\left(\frac{V_f-V_b}{V-V_b}\right)}{\theta_2}\right)-1\right]}$$

As a result,

$$\frac{\partial \mathrm{q}}{\partial \mathrm{V}} = k - \frac{\theta_1 \times \mathrm{V} \times \exp\left(\frac{\log\left(\frac{\mathrm{V_f} - \mathrm{V_b}}{\mathrm{V} - \mathrm{V_b}}\right)}{\theta_2}\right)}{(\mathrm{V} - \mathrm{V_b}) \times \theta_2 \left[\exp\left(\frac{\log\left(\frac{\mathrm{V_f} - \mathrm{V_b}}{\mathrm{V} - \mathrm{V_b}}\right)}{\theta_2}\right) - 1\right]}$$

As a result

$$\frac{\partial q}{\partial V} = k - \frac{\mathrm{V} \times \exp\left(\frac{\log\left(\frac{\mathrm{V_f} - \mathrm{V_b}}{\mathrm{V} - \mathrm{V_b}}\right)}{\theta_2}\right)}{(\mathrm{V} - \mathrm{V_b}) \times \theta_2 \left[\exp\left(\frac{\log\left(\frac{\mathrm{V_f} - \mathrm{V_b}}{\mathrm{V} - \mathrm{V_b}}\right)}{\theta_2}\right) - 1\right]} = 0$$

**The second condition**

$$\frac{\partial^2 q}{\partial V^2} = -\frac{\theta_1 \times \exp\left(\frac{\log\left(\frac{V_f - V_b}{V - V_b}\right)}{\theta_2}\right)\left[\left[\exp\left(\frac{\log\left(\frac{V_f - V_b}{V - V_b}\right)}{\theta_2}\right) - 1\right] \times \theta_2 \times (V - 2V_b) + V\right]}{[\theta_2 \times (V - V_b)]^2 \times \left[\exp\left(\frac{\log\left(\frac{V_f - V_b}{V - V_b}\right)}{\theta_2}\right) - 1\right]^2}$$

Derivation

$$\frac{\partial^2 q}{\partial V^2} = \theta_1 \times \frac{\partial}{\partial V}\left[\log\left[\exp\left(\frac{\log\left(\frac{V_f - V_b}{V - V_b}\right)}{\theta_2}\right) - 1\right]\right] - \theta_1 \times \frac{\partial}{\partial V}\left[\frac{V \times \exp\left(\frac{\log\left(\frac{V_f - V_b}{V - V_b}\right)}{\theta_2}\right)}{(V - V_b) \times \theta_2\left[\exp\left(\frac{\log\left(\frac{V_f - V_b}{V - V_b}\right)}{\theta_2}\right) - 1\right]}\right]$$

$$= -\frac{\theta_1 \times \exp\left(\frac{\log\left(\frac{V_f - V_b}{V - V_b}\right)}{\theta_2}\right)}{(V - V_b) \times \theta_2\left[\exp\left(\frac{\log\left(\frac{V_f - V_b}{V - V_b}\right)}{\theta_2}\right) - 1\right]} - \theta_1$$

$$\times \frac{\partial}{\partial V}\left[\frac{V \times \exp\left(\frac{\log\left(\frac{V_f - V_b}{V - V_b}\right)}{\theta_2}\right)}{(V - V_b) \times \theta_2\left[\exp\left(\frac{\log\left(\frac{V_f - V_b}{V - V_b}\right)}{\theta_2}\right) - 1\right]}\right]$$

$$\frac{\partial}{\partial V}\left[\frac{V \times \exp\left(\frac{\log\left(\frac{V_f - V_b}{V - V_b}\right)}{\theta_2}\right)}{(V - V_b) \times \theta_2 \left[\exp\left(\frac{\log\left(\frac{V_f - V_b}{V - V_b}\right)}{\theta_2}\right) - 1\right]}\right] = \frac{1}{\theta_2} \times \frac{\partial}{\partial V}\left[\frac{V \times \exp\left(\frac{\log\left(\frac{V_f - V_b}{V - V_b}\right)}{\theta_2}\right)}{(V - V_b) \times \left[\exp\left(\frac{\log\left(\frac{V_f - V_b}{V - V_b}\right)}{\theta_2}\right) - 1\right]}\right]$$

$$= \frac{1}{\theta_2}$$

$$\times \left[\frac{\frac{\partial}{\partial V}\left[V \times \exp\left(\frac{\log\left(\frac{V_f - V_b}{V - V_b}\right)}{\theta_2}\right)\right]}{(V - V_b) \times \left[\exp\left(\frac{\log\left(\frac{V_f - V_b}{V - V_b}\right)}{\theta_2}\right) - 1\right]}\right.$$

$$\left. - \frac{V \times \exp\left(\frac{\log\left(\frac{V_f - V_b}{V - V_b}\right)}{\theta_2}\right) \times \frac{\partial}{\partial V}\left[(V - V_b) \times \left[\exp\left(\frac{\log\left(\frac{V_f - V_b}{V - V_b}\right)}{\theta_2}\right) - 1\right]\right]}{(V - V_b)^2 \times \left[\exp\left(\frac{\log\left(\frac{V_f - V_b}{V - V_b}\right)}{\theta_2}\right) - 1\right]^2}\right]$$

$$\frac{\partial}{\partial V}\left[V \times \exp\left(\frac{\log\left(\frac{V_f - V_b}{V - V_b}\right)}{\theta_2}\right)\right] = \exp\left(\frac{\log\left(\frac{V_f - V_b}{V - V_b}\right)}{\theta_2}\right) + \frac{\partial}{\partial V}\left[\exp\left(\frac{\log\left(\frac{V_f - V_b}{V - V_b}\right)}{\theta_2}\right)\right]$$

$$= \exp\left(\frac{\log\left(\frac{V_f - V_b}{V - V_b}\right)}{\theta_2}\right) - \frac{V \times \exp\left(\frac{\log\left(\frac{V_f - V_b}{V - V_b}\right)}{\theta_2}\right)}{\theta_2 \times (V - V_b)}$$

$$\frac{\partial}{\partial V}\left[(V - V_b) \times \left[\exp\left(\frac{\log\left(\frac{V_f - V_b}{V - V_b}\right)}{\theta_2}\right) - 1\right]\right] = \left[\exp\left(\frac{\log\left(\frac{V_f - V_b}{V - V_b}\right)}{\theta_2}\right) - 1\right] - \frac{\exp\left(\frac{\log\left(\frac{V_f - V_b}{V - V_b}\right)}{\theta_2}\right)}{\theta_2}$$

As a result,

$$\frac{\partial^2 q}{\partial V^2} = \theta_1 \times \left[ -\frac{V \times \exp\left(\frac{2\log\left(\frac{V_f - V_b}{V - V_b}\right)}{\theta_2}\right)}{[\theta_2 \times (V - V_b)]^2 \times \left[\exp\left(\frac{\log\left(\frac{V_f - V_b}{V - V_b}\right)}{\theta_2}\right) - 1\right]^2} \right.$$

$$- \frac{2\exp\left(\frac{2\log\left(\frac{V_f - V_b}{V - V_b}\right)}{\theta_2}\right)}{\theta_2 \times (V - V_b) \times \left[\exp\left(\frac{\log\left(\frac{V_f - V_b}{V - V_b}\right)}{\theta_2}\right) - 1\right]}$$

$$+ \frac{V \times \exp\left(\frac{\log\left(\frac{V_f - V_b}{V - V_b}\right)}{\theta_2}\right)}{\theta_2 \times (V - V_b)^2 \times \left[\exp\left(\frac{\log\left(\frac{V_f - V_b}{V - V_b}\right)}{\theta_2}\right) - 1\right]}$$

$$\left. + \frac{V \times \exp\left(\frac{\log\left(\frac{V_f - V_b}{V - V_b}\right)}{\theta_2}\right)}{[\theta_2 \times (V - V_b)]^2 \times \left[\exp\left(\frac{\log\left(\frac{V_f - V_b}{V - V_b}\right)}{\theta_2}\right) - 1\right]} \right]$$

$$= -\frac{\theta_1 \times \exp\left(\frac{\log\left(\frac{V_f - V_b}{V - V_b}\right)}{\theta_2}\right)\left[\left[\exp\left(\frac{\log\left(\frac{V_f - V_b}{V - V_b}\right)}{\theta_2}\right) - 1\right] \times \theta_2 \times (V - 2V_b) + V\right]}{[\theta_2 \times (V - V_b)]^2 \times \left[\exp\left(\frac{\log\left(\frac{V_f - V_b}{V - V_b}\right)}{\theta_2}\right) - 1\right]^2}$$

# APPENDIX B.

# DERIVATION OF INFLECTION POINT EQUATION

$$\frac{\partial q}{\partial V} = k_c - \frac{\theta_1 \times V_c \times \exp\left(\frac{\log\left(\frac{V_f - V_b}{V_c - V_b}\right)}{\theta_2}\right)}{(V_c - V_b) \times \theta_2 \left[\exp\left(\frac{\log\left(\frac{V_f - V_b}{V_c - V_b}\right)}{\theta_2}\right) - 1\right]} = 0$$

By substituting Eq. 5 and Eq. 6 into it, we have

$$k_{IP} + \alpha\, \theta_1 \log(\theta_2) = \frac{\theta_1 \times (V_b + \frac{V_f - V_b}{(1+\theta_2^{\alpha-1})^{\theta_2}}) \times \exp\left(\frac{\log\left((1+\theta_2^{\alpha-1})^{\theta_2}\right)}{\theta_2}\right)}{\left(\frac{V_f - V_b}{(1+\theta_2^{\alpha-1})^{\theta_2}}\right) \times \theta_2 \left[\exp\left(\frac{\log((1+\theta_2^{\alpha-1})^{\theta_2})}{\theta_2}\right) - 1\right]}$$

As a result,

$$k_{IP} = \frac{\theta_1[V_b(1+\theta_2^{\alpha-1})^{\theta_2} + V_f - V_b](1+\theta_2^{\alpha-1})}{\theta_2^{\frac{1}{\alpha}}(V_f - V_b)} - \alpha\, \theta_1 \log(\theta_2)$$